Università degli Studi di Bologna

FACOLTÀ DI INGEGNERIA

Dipartimento di Ingegneria Elettrica

Current distribution in multistrand superconducting cables

Doctoral thesis

MARCO BRESCHI

University of Bologna, Bologna, Italy, 2001

Acknowledgements

This work couldn't have been realized without the valuable help of several teachers met during these years of study. I am very grateful for the continuous scientific support and stimulus given me by all the members of my research team at the Department of Electrical Engineering of the University of Bologna. I would like to acknowledge every member of the group: Prof. Francesco Negrini for having initiated me to this interesting research field, Dr. Andrea Cristofolini and Dr. Massimo Fabbri for their precious technical assistance.

A very special acknowledgment goes to Prof. Pierluigi Ribani for having patiently followed and sustained me in every step of this work.

Part of this work was developed during my stay at the MTA Group of the LHC Division of CERN, Geneva, Switzerland. I want to recall here all the members of the Group and its Leader, Dr. Peter Sievers, for the very nice and stimulating working environment found at CERN.

I express all my personal gratitude towards Dr. Luca Bottura, Section Leader MTA, for having inspired most of this work, and helped me to enter the complex world of superconducting cables and magnets.

I am grateful to Dr. Aleksander Akhmetov from LHC and the Russian Academy of Sciences for many useful suggestions on the modelling of flat Rutherford cables. I also want to acknowledge Dr. Stephan Russenschuck from LHC for having provided the field maps for the calculations and Dr. Arnaud Devred from CEA Saclay, Dr. Pierre Pugnat, Markus Haverkamp, Thomas Schreiner from LHC for many valuable discussions. The experimental data on current distribution in a two strand cable were kindly provided by Dr. Curt Schmidt from FZK, Karlsruhe.

Last but not least, I would like to thank my family for the moral and logistic support accorded me during all these years of study and all my friends for their continuous encouragement.

SUMMARY

The scope of this work is the analysis of current distribution among the strands in multistrand superconducting cables through the development of an appropriate electromagnetic model. The model must be suitable to be applied to all the main configurations of multistrand cables, and be able to describe current diffusion processes in real long cables used in magnets.

In Chapter 1 some basic information on superconducting cables and magnets is given, motivating the use of the particular configuration of multistrand cables. The operating principle of particle accelerators is briefly discussed, stressing the need for magnetic fields of a very high quality.

In Chapter 2 the problem of current distribution is described, illustrating the possible sources, and the final effects of a non-uniform current distribution among the strands of the multistrand cables. Particular attention is focused on its influence on the cable thermal stability in the case of CIC conductors and on the quality of the field generated by the cable in the case of flat Rutherford cables. An overview of the theoretical models and of the experiments concerning current distribution in multistrand superconducting cables is also presented.

In Chapter 3 an electromagnetic model based on the representation of the cable strands by means of a distributed parameters circuit model is described in detail. The results of the model are compared with those obtained with different models for the study of current distribution, in particular with the network model based on a lumped parameters circuit.

In Chapter 4 the analytical solution of the model equations is given and compared to the numerical simulations and to the simplified analytical solution found in the literature and relative to current diffusion in a 2-strand cable.

In Chapter 5 the model is applied to the analysis of experimental results on the generation and development of long current loops induced in a two-strand cable. Moreover, extensive measurements of the magnetic field in the bore of a short LHC dipole model in different powering conditions are described and analysed in detail, studying the effects of the current distribution in the cable on the field quality of the magnet.

Appendix A gives the detail on the derivation of the distributed parameters model from the Maxwell equations of electromagnetism. Appendix B deals with numerical calculation of mutual and self inductances: a general method for the calculation of the mutual inductance between conductors with circular cross sections displaced in space with any geometric configuration is developed. Appendix C derives the eigenvalues and eigenvectors of the model matrices.

LIST OF CONTENTS

LIST OF SYMBOLS

B_c	critical field
T_c	critical temperature
J_c	critical current density
ρ	radius of curvature in the particle accelerator
p	particle momentum mv
g	quadrupole field gradient
$\boldsymbol{C}_n$	complex harmonic coefficient of the multipole expansion **B**
B_n and A_n	normal and skew harmonic coefficients
s	complex co-ordinate in the coil cross sectional plane
R_0	reference radius for LHC
B	magnetic flux density
M	magnetization
J	current density
E	electric field
H	magnetic field
N	number of strands in the cable
r_i	longitudinal resistance of strand i per unit length of cable
r_{si}	longitudinal resistance of strand i per unit length of strand
$\mathbf{v}^{ext}$	vector of the external voltage source per unit length of cable
i	vector of strand currents
g	interstrand conductances matrix
r	matrix of longitudinal resistances
l	per unit length mutual inductances matrix
i_{op}	operation current of the cable
V_h	voltage of strand h

e_h	voltage difference ($V_h - V_N$)
L_1	elementary loop inductance per unit length
$\mathbf{t}_h$	unit vector tangent to the axis of strand h
$\mathbf{t}_\mathrm{c}$	unit vector tangent to the axis of the cable at x
S_h	area of the cross section of strand h
$R^c{}_{h,k}$	interstrand cross contact resistance between strand h and strand k
$R^a{}_{h,k}$	contact resistance between adjacent strands h and strand k
L_p	cable twist pitch
γ_h	angle between the unit vector $\mathbf{t}_h$ tangent to the strand axis and the unit vector $\mathbf{t}_\mathrm{c}$ tangent to the cable axis
$\mathbf{A}^{ext}$	magnetic vector potential associated with the external sources
$R_h\ (x)$	point of the strand axis corresponding to coordinate x
$P_h\ (x)$	generic point in strand h at coordinate x
G_i	set of the indexes of the strands owing to superstrand i
k_i	number of strands owing to superstrand i
$\mathbf{r}^{sup}$	matrix of longitudinal resistances relative to superstrands
$\mathbf{g}^{sup}$	contact conductances matrix relative to superstrands
$\mathbf{l}^{sup}$	mutual inductances matrix relative to superstrands
$\mathbf{i}^{sup}$	vector of the currents flowing in the superstrands
$\mathbf{b}_k$	eigenvectors of both matrices $\mathbf{g}$ and $\mathbf{l}$
U	Heaviside function
$\mathbf{\Phi}$	magnetic flux
I_{FT}	flat top current
t_{FT}	flat top time

INTRODUCTION

The design of large magnets for nuclear fusion reactors and for research in the field of particle physics requires the generation of very high magnetic fields in large volumes. The use of conventional resistive cables employing copper for the windings would require a big cooling system and would result in a very large consumption of electric power.

The discovery and development of type II or “hard” superconductors [1] has given a new possibility for the construction of these magnets. These materials carry electrical current without resistance at low temperatures also in the presence of high magnetic fields. This results in values of the power dissipated in the magnets which are several orders of magnitude smaller than in the resistive case. The most important materials of this class are superconducting alloys such as NbTi or compounds as Nb_3Sn, with critical fields at 4.2 K of 11 and 21-28 T respectively.

The superconducting materials are arranged in thin filaments which are then twisted and embedded in a matrix of normal metal, forming strands. The strands are then twisted or transposed together to build the final cable. The technical reasons for the choice of this structure of multistrand superconducting cables are outlined in section 1.3.

Several kinds of configurations have been developed starting from this basic structure. The two configurations most commonly used in technical applications are the following:

- Rutherford type cables consist of a few tens of strands, twisted together with a pitch of some centimeters and then shaped into a flat, two layer, slightly keystoned cable. The filaments are usually made of NbTi and the matrix is made of high purity copper. These cables are usually employed in accelerator magnets, where they are electrically insulated and cooled in a helium bath.

- Cable in conduit conductors (indicated as CICC's) are made of a very large number of strands which are twisted to form sub-cables in different cabling stages. The strands are then wrapped inside a stainless steel jacket and cooled by means of a forced flow of helium filling the voids between strands. This direct contact of coolant and strands strongly enhances the cable performances in terms of thermal stability to external disturbances. For this reason these cables are the preferred choice for magnets that must operate in a noisy electromagnetic and mechanical environment, where the operating conditions require a reliable and stiff design.

Magnetic fields in particle accelerator magnets are generated over a large dynamic range. At the extreme of very long time scales, superconducting dipole magnets operate with large charge up times, in the range of tens of seconds to the steady state.

In magnets for fusion applications long current ramps in the order of hundreds of seconds are needed to produce the electric field necessary for the plasma confinement.

The application of current ramps or time dependent external fields generates in the cables a variety of screening currents. Interfilament coupling currents flow inside each strand between the superconducting filaments and in the normal metal matrix. Several methods have been proposed to analyse these currents and the corresponding AC losses. The study of these currents is beyond the scope of this work.

We focus our attention on the study of the eddy currents distribution which is induced by time dependent magnetic fields in the paths formed by the contacts between the different strands of the multistrand cable. These interstrand eddy currents are superimposed to the currents flowing between the filaments inside the strands, but the approximation to study the two phenomena independently is widely accepted, because of the different time constants of the two current distributions.

A further contribution to the current imbalance between strands can result from different contact resistances of the strands to the joints at the cable ends.

The superposition of these unbalanced currents to the transport current in the strands and the heat due to the ac losses associated with these currents or to external disturbances can push the current of some strands beyond the critical value of the strand current itself, such generating a normal conducting region.

The resistive heat generated by the normal conducting material can be removed both by conduction to the neighboring parts of the conductor or by convection to the coolant. In some cases, this removal is sufficient for the conductor to recover the initial superconducting state. In other cases the conduction and convection heat fluxes propagate the normal zone over a very long part of conductor, requiring the magnet to be switched off. This is the *quench* of the magnet.

This phenomenon is particularly important during fast field ramps and limits the maximum current achievable with a multistrand cable in dynamic powering conditions. For this reason it is generally indicated as *ramp rate limitation*. A correct modeling of these phenomena can help in the choice of optimal cable parameters to avoid strong ramp rate limitations and enhance the cable stability.

Moreover, a “secondary” magnetic field varying in time and space is generated by the eddy currents induced by time dependent magnetic fields. This field component affects *directly* the magnetic field in the magnet bore of particle accelerator magnets determining a modulation of the field along the length of the magnet axis known as *magnetic field pattern.* Moreover, this field component changes in time, contributing to change the magnetization of the superconducting filaments in the strands. This *indirect* influence on strand magnetization contributes to a drift of the average field in the magnet bore during phases of constant operation current.

The field quality is a major concern for magnets used in particle accelerators, due to its influence on the beam optics. Up to now, these dynamic effects on field quality, which show a clear dependence on ramp rate and powering history of the cable, cannot be avoided. Therefore, a correct modeling of these phenomena can be useful for their compensation.

Existing network models for current distribution in Rutherford cables are characterized by a very large number of unknowns, which makes it difficult to study current distribution in real long cables used in magnets.

All these considerations result in the necessity of an electromagnetic model of current distribution, flexible enough to be applied any kind of multistrand superconducting cable, and characterized by the possibility to strongly reduce the number of unknowns, for the study of long range phenomena in real multistrand cables used in magnets. The model should also be suitable to be coupled with a thermo-hydraulic description of the refrigerating system, because of the strict coupling between electrical, thermal and hydraulic phenomena occurring in cooled superconducting cables.

The objective of this work is therefore to review the main phenomena related to current distribution in multistrand superconducting cables and to develop an electromagnetic model suited for the analysis and improved understanding of these phenomena. The results of the model will be compared with pre-existing models of current distribution, showing advantages and drawbacks of the novel approach.

The analytical solution of the equations of current diffusion in multistrand cables made of a generic number of strands will be given, and compared with the numerical results and simplified solutions found in the literature.

The model will be applied to study existing experimental results on current distribution in multistrand superconducting cables. An extensive measurement of magnetic field pattern in a superconducting dipole will also be presented in order to study the influence of the current distribution on the field quality of accelerator magnets. The possibility to apply the electromagnetic model to long cables made of some tens of strands will be demonstrated applying it to the analysis of the experimental results.

CHAPTER 1

SUPERCONDUCTIVITY: FROM MATERIALS TO PARTICLE ACCELERATORS

1. 1 SUPERCONDUCTING MATERIALS

Superconductivity is a very peculiar state of matter discovered in 1911 by Kamerlingh Onnes in the University of Leiden, Denmark [2-3]. Onnes found that below a certain very low temperature, called critical temperature T_c, the electrical resistance of a sample of mercury dropped abruptly to zero. He called this state “superconducting state”. In the following years the researches of many chemists and physicists discovered the same phenomenon in 26 metallic elements of the periodic table.

Onnes immediately understood the potential applications of his discovery, but his first attempts to build magnets with these materials were frustrated by the discovery of other limiting physical conditions to be respected in order to keep the superconducting state [4]. In particular it was found that superconductivity is possible only below a certain value of the applied magnetic field, called critical field B_c. A very peculiar magnetic phenomenon, called the Meissner effect, was observed below the critical field. In these conditions the superconducting elements showed a perfect diamagnetic behaviour, with a complete expulsion of the magnetic flux from the material. These materials are called *type I* superconductors. In these materials the critical field is too low for the application of superconducting materials to the generation of high magnetic fields.

However, in the early 1960s new superconducting alloys and compounds, like NbTi and Nb_3Sn, were discovered and studied. These materials showed a different magnetic behaviour, and were called *type II* superconductors. In these materials the complete expulsion of the magnetic flux is observed only below a small value of the applied magnetic field, generally indicated with B_{c1}. For higher values of the magnetic field the flux lines start penetrating the material, which still shows a zero DC resistance until a second critical field, called B_{c2}, is reached. When the second critical field is reached the flux is totally penetrated in the conductor and superconductivity is lost.

A third critical parameter needs to be carefully controlled when dealing with superconducting materials. This is the current density, which must be lower than a critical value J_c.

A fourth critical parameter which should not be overcome in order to keep the superconducting state is the frequency of the electromagnetic field applied to the material. The critical frequency is extremely high, around 10^{11} Hz, and it is usually not reached in practical large scale applications of superconductivity.

The three main critical parameters, temperature, field and current density, are related by an experimental correlation which can be written in the form $J_c = J_c$ (B,T). This relation is shown in Fig. 1.1 for three different superconducting materials. The critical surface J_c (B,T) defines two regions in the space: in the region included between the surface and the coordinate planes the material is superconducting, in the outer region the material is normally conducting. The most widely used materials for technical applications are NbTi and Nb_3Sn, which combine high values of all three critical parameters, as shown in Table 1.1.

In late 1986 Bednorz and Muller of the IBM research laboratory in Zurich, Switzerland, reported the observation of superconductivity in lanthanum copper oxides doped with barium or strontium at temperatures up to 38 K, above the ceiling of 30 K for the critical temperature that had been theoretically predicted almost 20 years earlier. Since then, hundreds of scientists rushed to try different compounds to see which one would give the highest T_c. These new, ceramic materials show physical and chemical properties which are very different from those of metallic superconductors. The most important ceramic superconductors for applications are YBCO (yttrium barium copper oxide), BSCCO (bismuth strontium calcium copper oxide) and HBCCO (mercury barium calcium copper oxide). Their chemical formulas and transition temperatures are shown in Table 1.2.

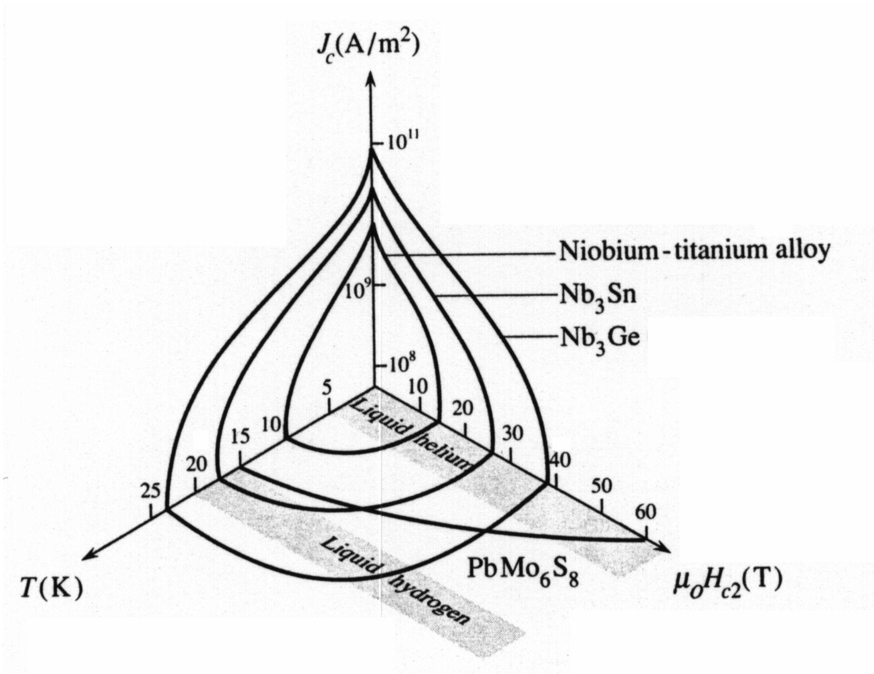

Fig. 1.1 Critical surface of some technical superconducting materials

The ceramic superconductors show the great advantage of high critical temperatures, which makes it possible to obtain proper refrigeration with liquid nitrogen, while low temperature superconductors need to be refrigerated with liquid helium, which needs a much more complex and expensive cryogenic system. Conventional low temperature superconductors are often used in magnets running at 4 K, but they lose superconductivity in high magnetic fields, typically above 6 T, although NbTi remains superconducting up 10 or 15 T. The ceramics superconductors have better performances. Bismuth strontium copper oxide (BSCCO) carries adequate currents and remains superconducting above 20 T, at 20 K. Therefore, the best way to obtain very high magnetic fields is to use ceramic superconductors at low temperatures.

On the other hand, some remarkable problems have been encountered in the application of ceramic materials to superconducting magnets. In order to wind a coil to produce a magnetic field, the first prerequisite is to make long lengths of wire from the superconducting material. Ceramic superconductors are not ductile, and are very brittle, so that the development of a reliable wire-manufacturing technique is an extremely delicate problem. Another problem is related to the granular nature of these materials. Very large currents can flow within grains, but grain boundaries impede the current flow between grains. Methods have been developed both to align grains and to provide “clean” grain boundaries, but these processing methods still need improvement.

All these technical difficulties, combined with time consuming thermal and mechanical treatments, result in very high fabrication costs. For all these considerations, at the present state low temperature superconductors are still the most used materials for large scale applications in high energy physics magnets and thermonuclear fusion magnets.

	T_c [K]	B_c [T]	J_c [kA/mm^2]
NbTi	9.3	15.0	2.0
Nb_3Sn	18.0	28.0	3.0

Table 1. Critical parameters of NbTi and Nb_3Sn

ame	*Formula*	
Yttrium barium copper oxide	$Y_1Ba_2Cu_3O_7$	92
Bismuth strontium calcium copper oxide (2223 phase)	$(Bi,Pb)_2Sr_2Ca_2Cu_3O_x$	105
Thallium barium calcium copper oxide (1223) phase	$Tl_1Ba_2Ca_2Cu_3O_y$	115
Mercury barium calcium copper oxide (1223 phase)	$Hg_1Ba_2\ Ca_2Cu_3O_y$	135

Table 2. Formulae and critical temperatures of some HTSC materials

1.2 SUPERCONDUCTING STRANDS

Superconducting materials are usually reinforced for the application in cables with additional components for structural, electrical and thermal stability reasons. In general the superconducting material is shaped to form very thin filaments, which are then embedded in a matrix of low resistivity material, forming strands. A typical cross section of a superconducting strand is shown in Fig. 1.2.

This low resistance material provides a “shunt” when a part of a superconducting filament undergoes a transition to the normal state. In this case the resistance in the superconducting material becomes orders of magnitude higher than that of the matrix material, and the matrix can rapidly conduct the heat and transfer the current of the filament to other adjacent filaments. The resistivity of the matrix should therefore be small, especially in the longitudinal direction. A typical low resistivity material used for the matrix is copper.

Technical values of the matrix resistivity for copper are about 1-2 10^{-10} Ωm. The resistivity of copper matrices is often indicated with the so called *RRR*-value (Residual Resistivity Ratio), which gives the ratio between the resistivity at 300 K and at 4 K in the absence of applied field. This value is generally about 50-200 for practical NbTi strands.

The use of the copper matrix with fine filaments was started after the first coils wound from bulk superconducting wires tripped off unpredictably at current levels much lower than the expected critical current. The reason for this behaviour was identified with the so called *flux jumps*.

The origin of flux jumps is due to the fact that the flux penetration in superconductors is associated to a small power generation, due to the resistive decay of the screening currents exceeding J_c. The power generated by the flux penetration increases the local temperature, reducing J_c, and hence inducing further flux penetration and heating. As the thermal diffusivity in the superconductor is orders of magnitude smaller than the magnetic diffusivity, the flux penetration may turn into a very fast avalanche effect, even at very slow external field variation.

A restriction to the flux motion is provided by a reduction of the filament size, which also limits the energy associated to a flux jump. The presence of a high conductivity stabiliser as the copper matrix works as a heat sink and electrical bridge around the flux jump affected zone allowing recovery in case the local temperature exceeds the critical temperature of the superconductor.

The threshold for flux jumps is about 60-80 μm filament size. Most technical superconductors are manufactured today with much smaller filaments (5-30 μm for NbTi and 2-8 μm for Nb_3Sn). However, collective interaction among filaments may give rise to flux jumps at low fields. These interactions are called “bridging” when the superconducting filaments have physical contacts through which current exchange takes place, and “proximity effects” when tunnelling of Cooper pairs occurs through the copper matrix. Both phenomena enhance the effective diameter of the filament at low magnetic fields.

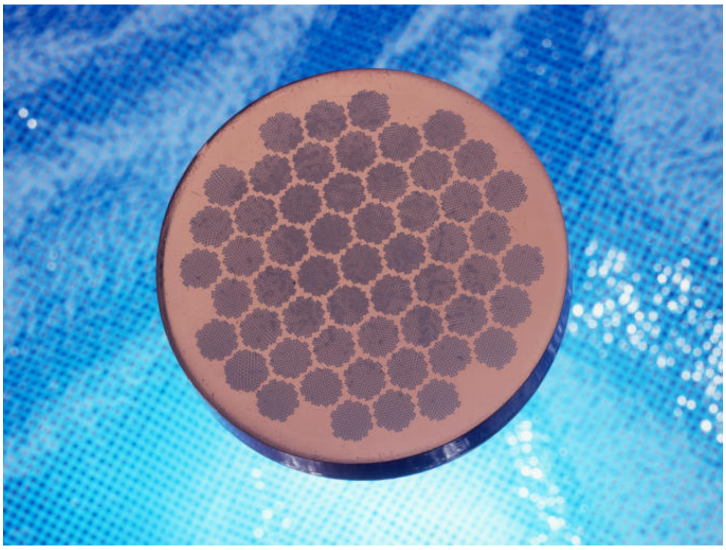

Fig. 1.2 *Cross section of a superconducting strand containing 8000 filaments of NbTi, gathered in hexagonal bundles, and embedded in a copper matrix.*

Another reason for the limitation of the filament size, at least in particle accelerator applications, is the necessity to limit field distorsions resulting from superconductor magnetisation at low field.

In the presence of an external field, in fact, persistent currents flow in the superconducting filaments shielding the interior of the filaments from the applied field. The persistent currents generate a residual field which increases increasing the filament diameter and the critical current density. At low external fields the critical current density is increased and so does the residual field due to persistent currents, resulting in a high relative field error in the bore of the magnets.

The filament uniformity, the absence of ruptures along the filament length, and the current density of the superconducting material are crucial parameters for a high overall strand critical current.

When time varying magnetic fields are applied to strands, eddy currents are induced both in the filaments and in the copper matrix. An interfilament coupling loss is associated with these currents. For this reason the filaments are in general twisted in order to reduce the area enclosed by any two filaments and therefore the interfilament coupling loss. The interfilament coupling currents exhibit time constants of 0.01 to 0.1 s and a characteristic loop length equal to the twist pitch of the filaments.

Another important parameter that must be optimized while manufacturing strands is the copper-to-superconductor ratio, which should be not too small to limit conductor heating in the case of a quench but neither too large because of the need of high overall strand current densities.

The strand coating can in some cases be essential to prevent too high interstrand currents and losses. Bare strands can be used for pure DC applications, where the coupling currents loss is not an issue. For materials like Nb_3Sn and Nb_3Al, the typical material used for the coating is Cromium.

For NbTi strands, several coatings are available, including Cr, Ni, Zn, SnAg, and PbSn.

Insulating coatings are also possible, but should be avoided as they don't allow current redistribution between neighbouring strand in the case of superconducting to normal transition of one or more strands. This can lead to a severe limitation of the cable stability to thermal disturbances.

1.3 SUPERCONDUCTING CABLES

1.3.1 Why multistrand cables?

Superconducting magnets for particle accelerators or fusion applications are often wound from multistrand superconducting cables. These cables show the following advantages as compared to single wires [5]:

- the strand to strand current redistribution in the case of localized defects or in case of quench initiation in some strands is very useful to improve the cable thermal stability
- the piece length requirement for wire manufacturing is reduced of a factor N, where N is the number of strands in the superconducting cable
- the number of turns is limited and the coil winding facilitated
- the coil inductance is limited to a value $1/N^2$ smaller than that of a similar coil wound from a single strand cable. A smaller inductance reduces the voltage requirements on the power supply to ramp up the magnets to their operating current in a given time and limits the maximum voltage to ground in case of a quench

The main drawback of using a cable is the high operating current which requires large current supplies and large current leads. The development of reliable current leads made with high temperature superconductors gives a new possibility for the construction of this technically delicate part of the system.

1.3.2 Cable cooling and insulation

In order to properly operate a superconducting cable, the conductor must be cooled below the critical temperature of the superconducting material. One way to distinguish superconducting cables is a classification based according to the cooling mode, either by forced-flow of helium, or by pool boiling.

- In forced flow conductors the helium flows in a channel which is in thermal contact with the superconductor. These cables are particularly suited for applications in which the thermal stability of the cable is a major concern, because of the direct contact between the coolant and the cable strands and the well defined flow regime which helps to know the operating conditions in detail. Among the forced-flow conductors the most interesting configuration is that of the so called “Cable in Conduit Conductors” (CICC’s). In the CICC configuration the strands are twisted in subsequent stages to form a final stage cable with interstitial voids whose area covers the 40% of the cable cross sectional area. Examples of this configuration are shown in Fig. 1.3. The cable is enclosed in a very tight stainless steel jacket, and the helium flows in the voids of the cable, so that the contact between coolant and strands is direct and characterised by a high heat transfer coefficient.
- In the cables refrigerated by pool boiling the cooling is achieved by heat exchange and natural convection from the coil winding pack to a bath of liquid helium. The thermal contact of coolant and conductor is worse than in the CIC configuration. This kind of cooling is ideally suited for magnets which operate in “persistent” mode, i.e. with a constant operating current, such as magnets for magnetic resonance imaging.

The cable insulation must satisfy some important requirements, which are listed in the following.

- a good dielectric strength at very low temperatures, around 4.2 K, and under high transverse pressure. This is also due to the fact that the dielectric strength of helium gas at 4.2 K is very low and far worse than that of liquid helium.
- the possibility to keep good mechanical properties in a wide range of temperature.

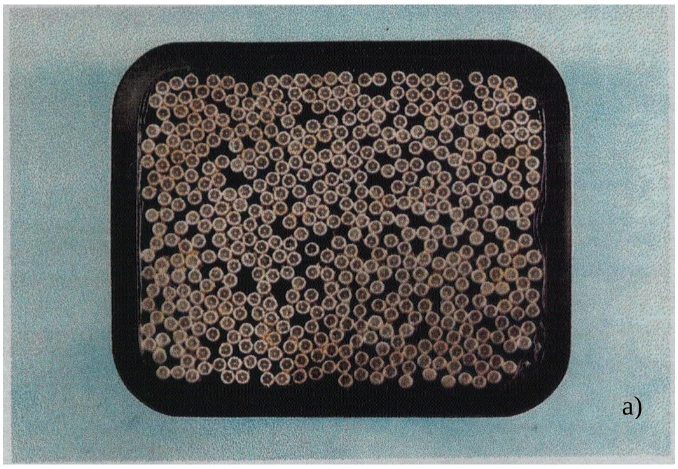
a)

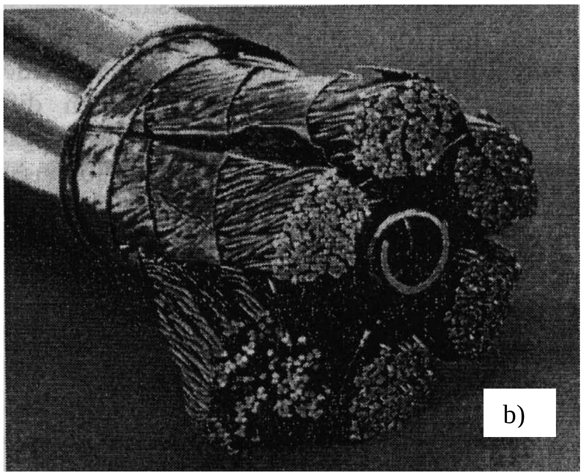
b)

Fig. 1.3. a) *Cross section of a cable in conduit conductor, showing strands enclosed in a stainless steel jacket. Helium flows in the voids between strands. b) Example of cable in conduit conductor with internal helium channel.*

- a small thickness to maximize the overall current density of the coil
- ability to withstand radiations for applications in an accelerator environment
- possibility to provide a means of bonding the coil turns together to give the coil a rigid shape and facilitate its manipulation during the subsequent steps of the magnet assembly
- a sufficient porousity to allow permeation of the helium, giving a better thermal contact with the conductor

The insulation of most NbTi cables is constituted of one or two inner layers of polyamide film, wrapped helically around the conductor, completed by an outer layer of resin-impregnated glass fiber tape (see Fig. 1.4.b). The outer layer is wrapped with a gap to set up helium cooling channels
between coil turns. The resin is of thermosetting-type and requires heat to increase cross-link density and cure into a rigid bonding agent.

As anticipated in the introduction, the coils for high field accelerator magnets are often wound from high-current Rutherford type cables. The cable is generally obtained by flattening a hollow tubular cable comprising between 20 and 40 strands. The final geometry is shown in Fig. 1.4.a. The strands are fully transposed with a twist pitch L_p. The cable cross section presents a small keystone angle which ensures a more uniform structure of the coils and facilitates the winding of the magnets.

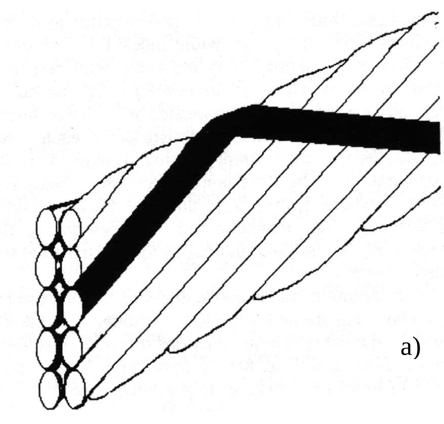
a)

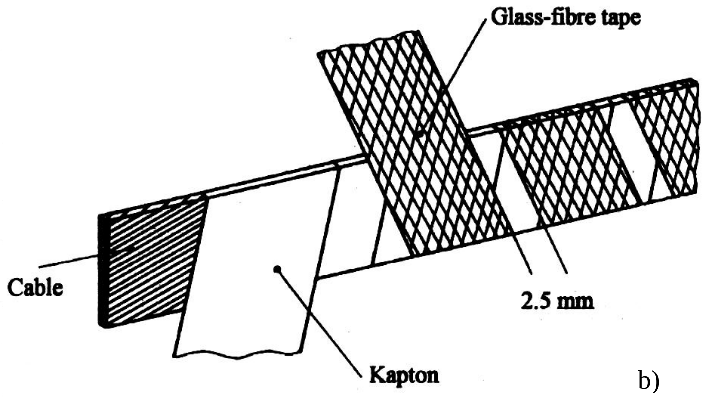

b)

Fig. 1.4. a) *Final geometry of flat Rutherford cable for LHC magnets*. b) *Insulation of a flat cable, realised with a glass-fibre tape and a kapton foil.*

A resistive barrier between the top and bottom layer of flat cables is sometimes added in order to enhance the contact resistance between strands and limit the interstrand coupling currents induced by time dependent magnetic fields.

The main parameters of the Rutherford cables used to wind dipoles in two layers (inner and outer) for the LHC (Large Hadron Collider) project at CERN (see section 1.5.3) are listed in Table 3.

	Outer layer	Inner layer
Diameter of strands (mm)	0.825	1.065
Copper/Superconductor ratio	1.9	1.6
Filament size (μm)	7	6
B_{ref} (T)	9	10
T_{ref} (K)	1.9	1.9
J_c (B_{ref}, T_{ref}) (A/mm^2)	1953.0	1433.3

***Table 3* Main parameters of flat Rutherford cables used for the LHC dipoles**

1.4 SUPERCONDUCTING MAGNETS

The possibility offered by superconducting cables to conduct high currents with low power losses is ideally suited for the construction of electromagnets. Extremely high fields (up to 20T and more) can be produced in volumes in the range from 0.01 to 1 dm^3, while fields in the range from 5 to 6 T can be produced in volumes of the order of 1 m^3.

The most typical application of superconducting magnets are listed in the following:

- Magnetic separators are devices used to capture ferromagnetic, diamagnetic, or paramagnetic particles from a streaming fluid, in order to filter impurities or to separate particles with different magnetic susceptivities. The capture capability strongly depends on the field module and on the field gradient. The choice of superconducting magnets is very competitive for the separation of very small particles, down to 1 μm of diameter, which are very difficult to capture with conventional electromagnets.
- MHD generators are devices for the magneto-fluid dynamic generation of energy. In these devices the power produced depends on the second power of the module of the magnetic induction. Superconducting

cables are necessary, because with conventional magnets the power required by the conversion cycle would be higher than the power produced.

- MRI (magnetic resonance imaging) magnets allow to obtain images with a very high resolution, used for medical diagnostics. The possibility to use the magnets in “persistent mode”, with a fixed and stable value of the operating current, leads to the required field uniformity in space and time. MRI magnets have revealed to be the most profitable investment for the superconductive technology since the 1980s.
- Nuclear fusion magnets are used to generate the magnetic field for the plasma confinement in the controlled thermonuclear fusion devices. Two main kinds of magnets are used in the tokamak configuration: the toroidal field coils which enclose the plasma ring, and pulsed transformer coils, for the poloidal field. Both kinds of coils are subject to the time dependent magnetic field generated by the transformer coils and are introduced in a very noisy electromagnetic environment, so that the preferred choice for a stable operation is to wind them with cable in conduit conductors.

1.5 PARTICLE ACCELERATORS

1.5.1 Why particle accelerators?

Particle accelerators are needed for the investigation of two very fundamental research topics, which are nowadays strictly correlated. The first is related to particle physics, and is aimed to give an answer to basic questions like “what is matter?”, “what are its basic constituents?” and “what kind of interactions exist between particles?”. The second is related to astronomy, and is aimed to recreate with high energy collisions the same conditions existing in the initial instants of the origin of universe, immediately after the “Big Bang”. The questions are the following: “how was matter at that time?”, “how did the fundamental particles coalesce to make the atoms, the stars and the galaxies we observe today?”.

By concentrating a large amount of energy into the smallest possible volume, in fact, equal numbers of particles of matter and antimatter are created from pure energy according to the equation $E = mc^2$. The energy concentrations created in modern particle accelerators correspond to the conditions prevailing less than 10^{-10} s after the Big Bang.

1.5.2 *Particle accelerators, working principle*

Two types of experiments can be realised in particle accelerators. In *fixed target* experiments the particles are accelerated and the beam is blasted against a fixed target. In *colliding-beam* experiments two counter rotating beams are blasted at each other by colliding them among themselves. The collision products are analysed in large detectors which surround the targets or the collision points. Different layers of the detectors measure different properties of the particles resulting from the collisions, while a magnetic field is needed to identify particles of opposite charges and different momentum.

Two kinds of accelerators exist, linear and circular. All particle beams start their acceleration in linear accelerators, but the need to reach very high energies would require linear accelerators of unacceptable lengths, so that the preferred solution is to counter-rotate particle beams in circular accelerators (called storage rings) until the desired energy is reached.

In any kind of accelerator there is exactly one curve - the design orbit- on which ideally all particles should move. If this design orbit is curved, as in circular accelerators, bending forces are needed. In reality, most particles of the beam will deviate slightly from the design orbit. In order to keep these deviations small on the whole way (which might be as long as 10^{11} *km in a storage ring), focusing forces are required.*

Both bending and focusing forces can be accomplished with electromagnetic fields. In modern accelerators the bending forces are provided by dipole magnets, while the focusing forces are provided by quadrupole magnets.

In order to define ideal dipole and quadrupole magnets we consider a point P *on the design orbit of the particles and a local reference frame where the (*x, y*) plane is transverse with respect to the design orbit. The* x *axis defines the horizontal direction, the* y *axis defines the vertical direction and the z axis corresponds to the direction of particle motion.*

Fig. 1.5 Lorentz force acting on a positively charged particle a) dipole field b) quadrupole field

A normal dipole magnet is a magnet which, when positioned in P*, produces within its aperture a magnetic flux density parallel to the (*x, y*) plane and such that the field components* B_x *and* B_y *satisfy the following equations:*

$$B_x = 0 \qquad \text{and} \qquad B_y = B_1 \tag{1.1}$$

a)

b)

where B_1 *is a constant. According to the Lorentz force, a charged particle travelling along the direction of the* z *axis through the aperture of such a magnet is deflected on a circular trajectory parallel to the horizontal plane. The radius of curvature* ρ *is determined by the equilibrium of Lorentz (*$F_L=qvB_1$*) and centrifugal force (*$F_c=mv^2/\rho$*) and results in:*

$$\rho = p / (q B_1) \tag{1.2}$$

where p *is the particle momentum* mv*. Equation (1.2) clearly indicates that, to maintain a constant radius of curvature as the particle is accelerated, the dipole field must be ramped up in proportion to the particle momentum.*

A normal, ideal, quadrupole magnet is designed in such a way that the field components along its aperture can be expressed in the following way:

$$B_x = g\,y \qquad \text{and} \qquad B_y = g\,x \tag{1.3}$$

where g *is a constant referred to as the* quadrupole field gradient*. A beam of positively charged particles travelling along the* z *axis is horizontally focused and vertically defocused if* g *is positive, and vertically focused and horizontally defocused if* g *is negative. The effects of dipole and quadrupole fields on a positively charged particle are shown in Fig. 1.5.*

To obtain a net focusing effect along both x *and* y *axes a pair of focusing-defocusing quadrupoles must be used. For both kinds of quadrupoles, the focal length* f *is proportional to the particle momentum [5]. This means that to maintain* f *constant while the particle beam is accelerated, the quadrupole field gradient must be ramped up in proportion to the particle momentum.*

As a consequence, for both bending and focusing purposes, the magnetic field in particle accelerator magnets is not kept constant, causing the dynamic effects on current distribution in the magnet cables discussed in this thesis.

1.5.3 CERN-*Large Hadron Collider*

CERN is the European Laboratory for Particle Physics. In this laboratory both linear and circular accelerators are installed. CERN was founded near Geneva, Switzerland, in 1954, and it is now funded by 20 European countries. More than 6000 researchers from 80 countries work in the facilities offered by this laboratory.

The largest accelerator under construction at CERN today is the Large Hadron Collider, LHC. The main goal of the LHC is finding the Higgs boson, a particle which physicists retain responsible for the mechanism how particles acquire mass. In the LHC protons and antiprotons will collide at a center of mass energy of 14 TeV. This energy is not much larger than the kinetic energy of a mosquito, but is concentrated in a volume which is 10^{12} times smaller. This is why the collimation of the particle beams is an extremely delicate technical problem.

The layout of this accelerator is shown in Fig. 1.6. The tunnel is 27 km long and is placed 100 m below the ground. The circumference is divided into 8 octants. The particles will collide in only 4 points along the ring circumference, corresponding to octants 1, 2, 5 and 8, as indicated in Fig. 1.6. The storage ring will consist of about 8400 magnets, of which 3444 will be

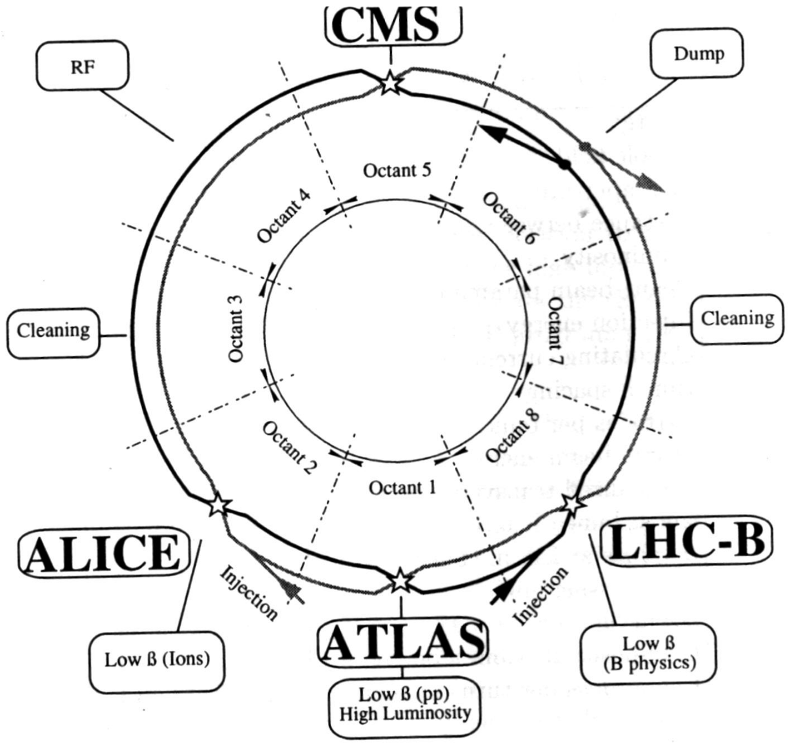

superconducting. Among the superconducting magnets there will be 1232 main dipoles, 386 main quadrupoles and other magnets for the correction of field errors.

Fig. 1.6. *Layout of the Large Hadron Collider at CERN*

1.5.4 Field quality

Accelerator magnets must provide a magnetic field of high homogeneity, better than a few parts on 10000 at a radius of 60 % of the coil diameter. An ideal dipole and quadrupole field can be generated by the current distribution shown in Fig. 1.7. An ideal dipole field is given by a cos (ϑ) current distribution while an ideal quadrupole field is obtained with a current distribution proportional to cos (2 ϑ), where ϑ is the azimuth angle [4].

The dipole and quadrupole current distributions are realized in practice by means of a discretization of the homogeneous current shells. This approximation introduces a number of field imperfections, which must be minimized and corrected. The magnetic field in the accelerator magnets is usually expressed by means of the following complex series:

$$\boldsymbol{B}(x,y) = B_y + \mathrm{i}B_x = \sum_{n=1}^{\infty} \boldsymbol{C}_n \left(\frac{\boldsymbol{s}}{R_0} \right)^{n-1}$$

(1.4)

where $\boldsymbol{s} = x + \mathrm{i}y$ is the complex co-ordinate in the (x, y) coil cross sectional plane of the magnet, R_0 is a reference radius (for LHC R_0 = 17 mm) and $\boldsymbol{C}_n$ are the so called harmonic coefficients.

The harmonic coefficients $\boldsymbol{C}_n$ can also be explicitly written as the sum of their real (referred to as *normal*) and imaginary (*skew*) parts:

$$\boldsymbol{C}_n = A_n + \mathrm{i}\, B_n$$

(1.5)

Accelerator magnets are usually produced and positioned so that they generate a pure normal or skew multipole field of order k. In a normal multipole magnet, for instance, the magnetic field has strictly y direction, implying that the *skew* part of any harmonic coefficient must be zero. However, several field errors are present in superconducting magnets, and all field harmonics have to be carefully measured and controlled. These field errors have several origins [6].

Some field errors have a *geometric* origin and result from the deviation of the placement of the conductors from the ideal current distribution giving the desired magnetic field.

Moreover, at high field significant deviation from linearity and field errors are caused by the *saturation* of the iron yoke. The geometric and saturation field contributions are reproducible, can be predicted accurately and may be largely inferred from warm measurements. These effects can also be found in normal resistive magnets.

Additional effects peculiar to superconducting magnets are caused by the known DC diamagnetic property of superconducting cables. As anticipated in Section 1.2, persistent currents flow in each filament in the cable strands, so that each filament behaves as a diamagnetic material, whose contribution to the magnetic field quality can be appreciable at low field levels.

Other effects on the field quality are associated with the superconducting properties of the cables. In particular, a *decay* of the magnetic field and field harmonics is seen during long periods of constant current excitation, followed by a rapid recovery of the initial value before the drift as soon as the current is ramped (referred to as *snapback*). These effects are due to the change in the filaments magnetization, which is also correlated to the

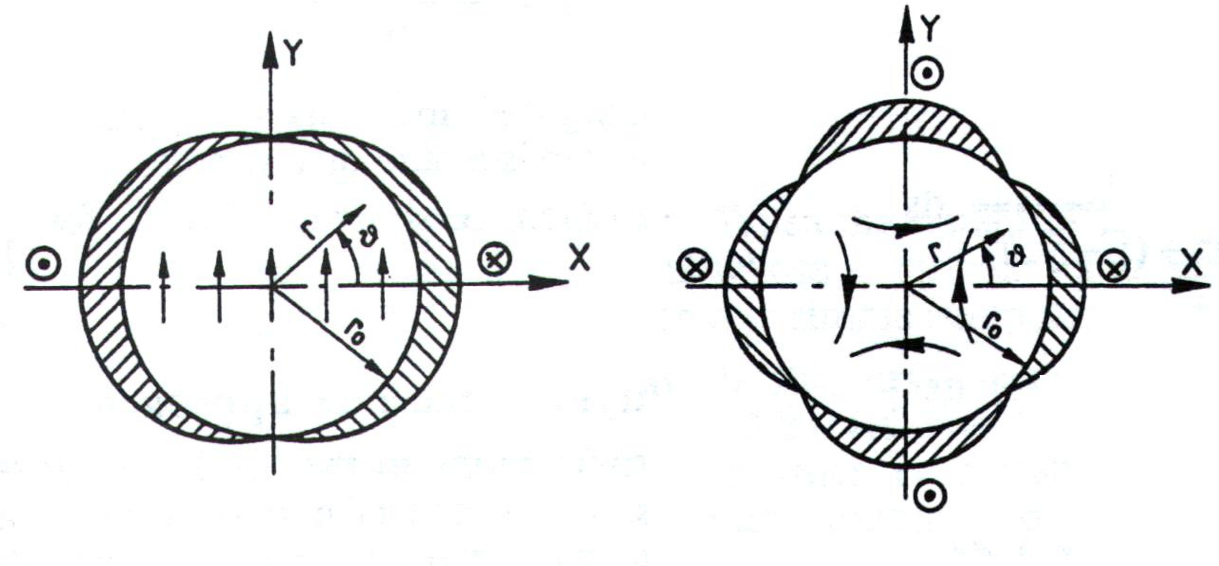

current distribution among the cable strands, as pointed out in Section 2.2.2.

Fig. 1.7 *Ideal current distribution for the generation of a dipole (a) and quadrupole (b) field. The current for the dipole field has the form* $I = I_0 \cos(\vartheta)$, *while the current for the ideal quadrupole field has the form* $I = I_0 \cos(2\vartheta)$

CHAPTER 2

CURRENT DISTRIBUTION: PROBLEM DEFINITION

2.1 SOURCES OF NON UNIFORM CURRENT DISTRIBUTIONS

Several possible sources of non uniform current distribution among the cable strands can be identified. Among them, some are effective in both AC and DC conditions, while others are only effective in AC conditions. Some possible sources of a non uniform current distribution in both stationary and dynamic conditions are listed in the following.

- Different joint resistances of the different strands at the cable terminations [1]. The cable ends can be connected through splices to other cables or through joints to the current leads. It is not technically possible to realize a perfectly identical contact between the different strands and the joints because the soldering processes cannot be so strictly controlled. However, once the statistical distribution of the different strand joint resistances is directly measured or identified, the effects on current distribution can be easily determined.
- Different strand critical properties. It is impossible to manufacture perfectly identical strands: small differences in the strand critical properties could result in some strands carrying more current than the others, in the presence of the same external conditions.

Some possible sources of non homogenous current distributions are effective only in the presence of time dependent magnetic fields. In particular long current loops can be induced between the cable strands. They are basically due to an inhomogeneous distribution of the time derivative of the magnetic flux enclosed by the various strands. The possible sources of such inhomogeneity are listed in the following:

- Strand transposition errors with respect to the background magnetic field, for which the flux linked to the loops formed by the strands cannot be fully compensated (geometrical errors)
- Differences in the strand self and mutual inductances
- *Large gradients of the magnetic flux density along the cable, even with perfectly transposed strands, which may give rise to long range coupling currents, flowing along*

the whole cable length [9]. This source of non homogeneity is considered to be more relevant in accelerator magnets than in nuclear fusion magnets.

In order to better clarify the origin and the properties of the induced circulating currents it can be useful to distinguish cables with insulated strands and cables with non insulated strands.

The situation in cables made of insulated strands can be schematized with a lumped parameters circuit model as shown in Fig. 2.1. In the circuit L_h *is the self inductance of strand* h *and* $M_{h,k}$ *is the mutual inductance between strand* h *and strand* k*, while* $\Phi_{h,k}$ *is the flux enclosed between the two strands.*

The inductive terms determine the transient circulating current, while the resistive terms determine the steady transport current. The order of the decay time constant of the induced transient circulating current is given by [7]:

$$O(\tau) \approx \frac{L-M}{R}$$

(2.1)

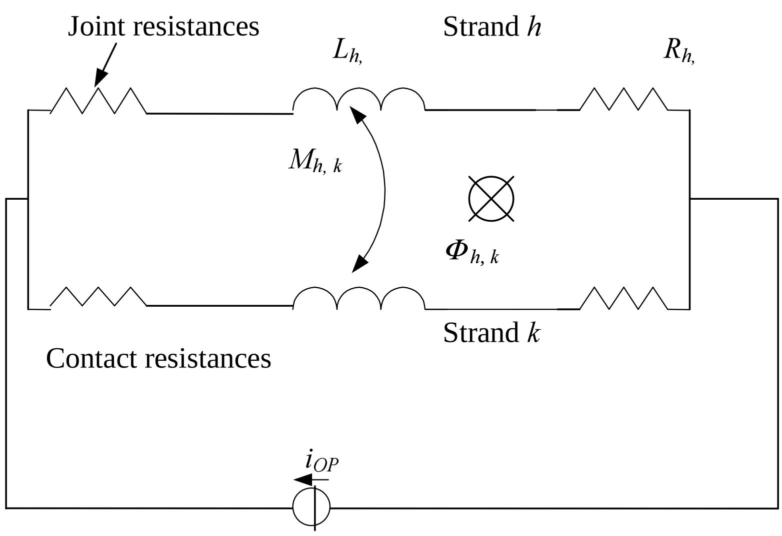

Fig. 2.1 Lumped parameters network model showing two typical insulated strands

where L*,* M*, and* R *are the typical orders of the self inductances, the mutual inductances and the joint resistances respectively. As* R *is usually very small (in the order of n**Ω**) in order to reduce the heat generation at the joints, the order of decay time constants can be very large, up to several hours. The order of magnitude of the induced circulating current is given by [7]:*

$$O\,(\Delta\, i) \approx \frac{\Phi_{sf} + \Phi_{ex}}{L - M}$$

(2.2)

where Φ_{sf} *and* Φ_{ex} *represent the magnetic flux linked to the loop due to the self field and to the external field. The induced currents can be very large when a CICC cable is exposed to a large external magnetic field, resulting in some cases in very significant current imbalances.*

In the case of non insulated strands two different types of currents can be distinguished, namely short and long range coupling currents. The short range coupling currents are often simply indicated as interstrand coupling currents (ISCCs) [27]. The long range coupling currents are often indicated as "Boundary Induced Coupling Currents" (BICC's) [27] or "Supercurrents" [10].

The short range coupling currents can be originated by a time varying magnetic field uniform along the cable axis. The loop for the interstrand coupling currents consists of two strands and a contact electrical resistance, as shown in Fig. 2.2a. Assuming that the cable is made of an integer number of half twist pitches, the short range coupling current is uniform along the cable length. If *dB/dt* is independent of time, the following equation can be written for the interstrand coupling current:

$$\dot{\Phi} = \frac{dB}{dt} = 2I_{scc}R_c + 2I_{scc}R_c$$

(2.3)

where $\dot{\Phi}$ is the time derivative of the magnetic flux linked to the loop, S is the area of the loop, I_{scc} the value of the interstrand coupling current, and R_c the resistance of each contact between strands. The value of the interstrand coupling current results in:

$$I_{scc} = \frac{1}{4R_c}\dot{\Phi}$$

(2.4)

The order of the decay time constant is given by [7]:

$$O(\tau) \approx \frac{L_1}{R_c}$$

(2.5) where L_1 is the inductance of the loop. The short range coupling currents exhibit time constants in the range from 0.01 to 1 s in typical cables. The long range coupling currents can flow along the whole cable length. Their amplitude can be orders of magnitude higher than that of the short range coupling currents.

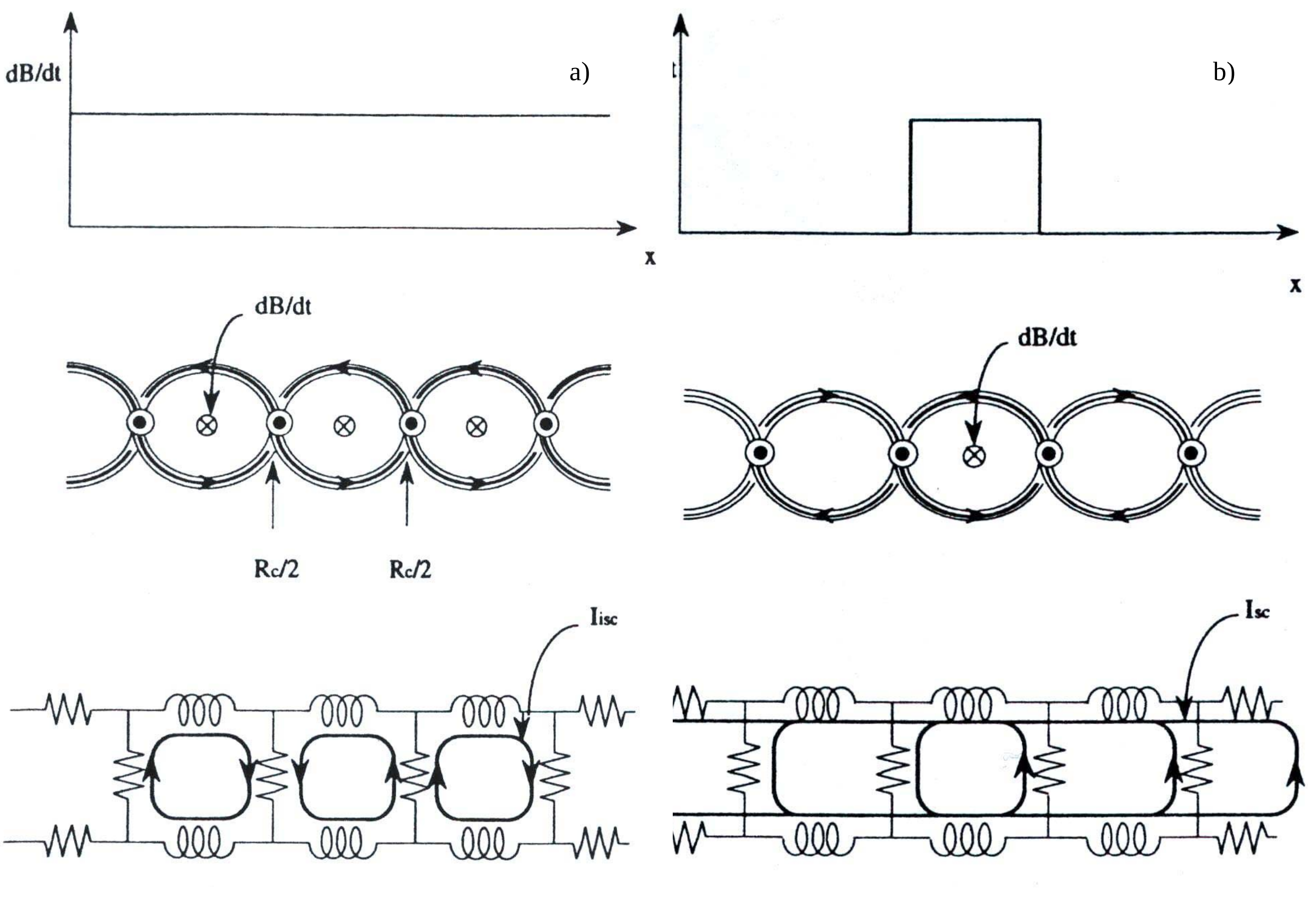

Fig. 2.2 *Schema of the loops of short (a) and long (b) range coupling currents*

The theory explaining the behaviour of this type of currents in flat Rutherford cables was developed in [10] and is briefly discussed in Section 2.3.5.

The sources listed above can lead to non homogeneous current distribution among the different strands even without the intervention of external disturbances. However, it may happen during magnet operation that a certain amount of energy is released in a portion of one or more strands by external disturbances, determining the superconducting to normal transition in this portion of the cable.

External disturbances can be due to unforeseen *increases in steady state heat input*, sudden *slipping* among cable components, *crackin*g of the insulation, *beam loss* in accelerator magnets. The energy deposition is usually very localized in time and space. Consequently, a current *redistribution* among the neighbouring strands starts, driven by the voltage of the normal zone. The redistribution takes place across the transverse contact resistance. If the strands are insulated, the current can only redistribute through the cable joints. Therefore the transverse resistance between strands is a key parameter for current re-distribution.

In systems with galvanic coupling between strands like in soldered cables the process of current redistribution is fast, the Joule heat and the associated temperature rise are small. In cables with insulated strands, the time constant, the Joule heat and the temperature rise increase with the conductor length: in a magnet system, an extension of the normal part over the whole conductor cross section and a subsequent quench are very probable.

By the point of view of thermal stability a fast current distribution given by a low contact resistance between strands is certainly very useful, as it avoids too large Joule heating in the normal zones and consequent temperature rises. On the other hand, low contact resistances can increase the circulation currents induced in the presence of time dependent magnetic fields, and enhance the AC losses related to these currents. From the above considerations, it results that the interstrand contact resistance is a key parameter that should be optimized considering both thermal stability and AC losses.

2.2 EFFECTS OF NON UNIFORM CURRENT DISTRIBUTIONS

2.2.1 *Ramp rate limitation*

The most serious consequence of extremely unbalanced current distributions is a severe limitation of the total current that multistrand cables can carry in transient conditions. As anticipated in the introduction, this effect is referred to as *ramp rate limitation*. The quench current of a coil is significantly affected by the ramp rate and the powering history [13, 8, 47].

Several sources have been identified in the previous section which can lead some strands to carry more current than the other strands. If one of these strands exceeds its critical current, while the whole cable current is still below its design critical value, a portion of this strand can turn into the normal state. From this normal region formed in one strand a quench can be originated, which can propagate along the whole cable length. In these cases the magnet must be ramped down and de-energized. This could be a *direct* mechanism leading to ramp-rate limitation.

The AC losses due to the interstrand coupling currents, and possible rapid quench and recovery events (observed in [46]) due to the fact that some strands are more charged than the others, lead some strands, in transient conditions, to work closer to the critical surface of the superconducting material. This can decrease the cable capability to recover the superconducting state after external energy depositions . This means that external energy disturbances which could be absorbed with a recovery to the superconducting state if the current distribution were uniform, can be fatal in the non uniform case. This could be an *indirect* mechanism of ramp rate limitation.

The phenomenon of ramp rate limitation is more severe in magnets for which thermal stability is a major concern, i.e. magnets for nuclear fusion applications. However, it has also been measured in magnets for particle accelerators [13].

2.2.2 *Field errors*

The magnetic field in accelerator magnets wound with Rutherford-type cables exhibits a periodic modulation along the magnet [14, 16, 17]. This *periodic pattern* has a period identical to the cable twist pitch, and shows a complex time and space dependence. Even at a constant transport current of the magnet the amplitude of the periodic field modulation may increase or decrease in time, with very long time constants. Values of the order of 100 h have been measured in some cases [35]. The field modulation persists for several hours after de-energizing the magnets.

The reason for this effect cannot be explained by flux creep in NbTi filaments. This phenomenon is due to an uneven current distribution among the strands [9]. The field modulation itself does not strongly affect the particle motion in the magnet bore. The average value of the field and field harmonics, however, strongly affects the accelerator operation. It has been shown both theoretically [28] and experimentally [29] that the average strand magnetization is affected by the field changes internal to the cable that are associated with the current redistribution.

This phenomenon is observed in accelerator magnets as a drift of the field when the transport current is held constant (*decay*). The field drift must be known and corrected precisely for accurate accelerator operation. Thus, a well established correlation and a better understanding of the current distribution as a function of the operating conditions can lead to improved correction and control algorithms.

2.3 HISTORICAL REVIEW: THEORETICAL MODELS

2.3.1 *Why modelling current distribution?*

The discovery of ramp rate limitation has shown that the thermal stability to external disturbances in multistrand cables is intimately correlated with the current distribution between the strands. It is therefore useful to spend a few words about thermal stability modelling. The aim of the analysis of cable stability is the calculation of the transient response of an initially superconducting cable to an arbitrary energy input, abstracting from the origin and the nature of the disturbance spectrum.

The main result of the analysis is the *stability margin* or *minimum quench energy (MQE)*, the maximum energy that can be deposited in the cable (over a given extension in space and time and with a given waveform) for which the transient response ends with the cable back to the superconducting state. This problem is extremely complex, as it involves coupled thermal, fluid-dynamics and electro-dynamics phenomena occurring at cryogenic temperatures, where the knowledge of non linear material properties is uncertain.

The modelling of current distribution in multistrand cables is therefore useful as it gives important information for stability studies, helping to interpret the experimental results on cable stability. Moreover, an accurate estimation of the AC losses in transient conditions is very important for the design of the cryogenic system.

As in any study which involves simulations, this kind of modelling has the remarkable advantage of studying in a very fast and cheap way a wide range of possible cable configurations, with different geometric and electric parameters. This cannot be attained easily with an experimental apparatus.

Over the years several models of current distribution in multistrand cables have been developed for different applications, at different levels of approximation and degrees of complexity. The references quoted here should be considered as typical examples of the application at the level of approximation discussed, and for obvious reasons cannot be exhaustive of the amount of work spent in the field.

2.3.2 *Network models for Rutherford Cables*

In the case of Rutherford cables several network models have been developed to study the current distribution among the strands. One of the earliest presentations of a network model was given by Morgan in 1973 [18], and assumes that the strands in one layer have electrical contacts with those in the other layer, but not between themselves. Morgan reports that "a direct application of Maxwell's equations to a flat metal-filled braid was attempted but dropped owing to the non isotropic structure of the cable". For this reason he developed a lumped-constant circuit approach. In the Morgan's model the Faraday's and Kirchoff's equations are applied to all the loops formed by two adjacent strands of one layer crossing any two adjacent strands of the other layer.

The braid is assumed to be infinitely long with uniform cross contact resistance and uniform field along the cable length, even if field variations across the cable width are allowed. In this way only N-*1 independent loops have to be solved, where* N *is the total number of strands (see Fig. 3.1). All loops include four resistances except those at the edges which have three. All crossover resistances are assumed to be the same, and all loop areas the same.*

The solution found for the cross over currents at an arbitrary position is then considered to be uniformly repeated along the cable length. Morgan's model allows to find an estimate of the power dissipated in the cable in the presence of field ramps, if the applied field is changing at a constant rate, so that the emf driving the loop currents is independent of time.

In more advanced versions of the network model [20, 27] the N-*1 loops considered by Morgan become the components of the basic units for the calculation of the current distribution (called 'columns' [20] or 'calculation bands' [26, 27]), allowing to consider longitudinal variations of the magnetic flux density along the cable length. A representation of the lumped constant circuit model described in [27] is shown in Fig. 2.4.*

A complete set of equations is written for all the columns, applying Faraday's laws to the N-*1 loops of each column. The cross over currents in each column can be calculated step by step from the knowledge of the cross over currents in the previous column [19]. The matrix approach, described in detail in [20] consists in expressing this relation in a matrix form.*

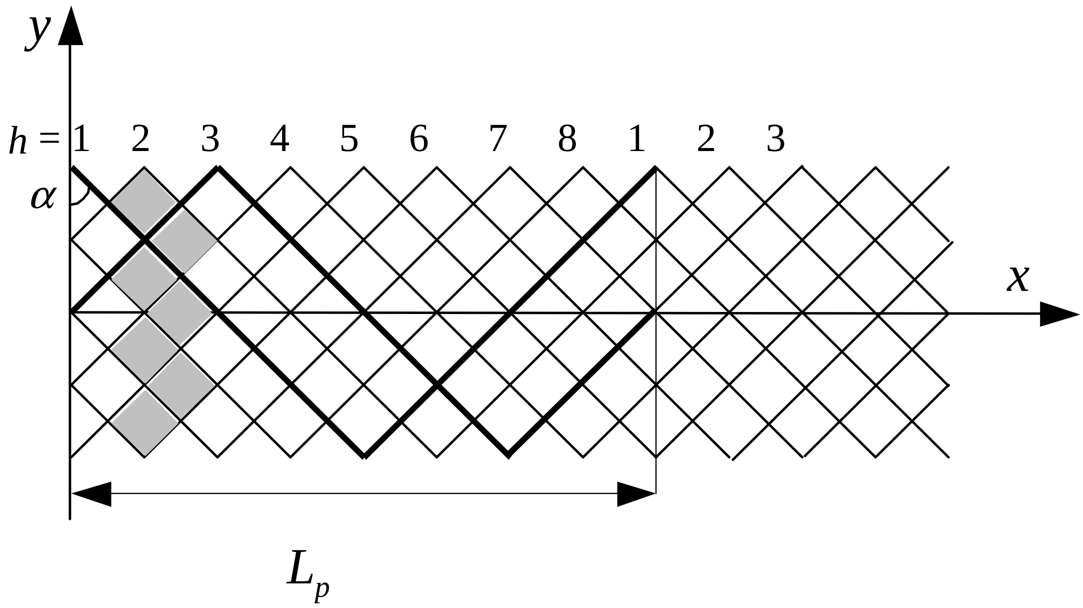

Fig. 2.3 *Top view of the idealised geometry of the strand axes of a Rutherford cable used for the distributed parameters model. The thick lines represent the strand segments of strand 1 and 3 considered for the calculation of the mutual inductances matrix along one pitch. The shaded areas represent the N-1 loops used in Morgan's network model, and as elemental calculation*

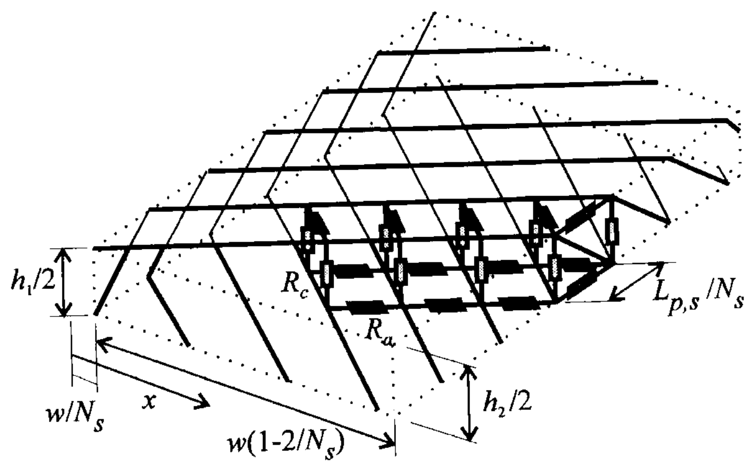

bands in the following versions of the network model.

Fig. 2.4 Network model of Rutherford cable *[27]*. The strands axes are represented by line elements, the resistances between adjacent and non adjacent strands are tinged respectively in dark and light grey.

In [19] it was shown that the Morgan's solution is only a particular solution of the general system of equations, which can be obtained imposing that the cross over currents of a certain column are all equal to the corresponding cross over currents of the previous column. Instead, a general solution of the system equations is characterized by the fact that the cross over currents of the $(k+N)^{th}$ *column are equal to those of the* k^{th} *column, where* k *is the index of the column.*

This means that the cross over currents between any two strands of the cable are the same after every twist pitch length. The remarkable consequence of this periodicity is the periodicity of the secondary field produced by the eddy currents.

The effects of sinusoidal distributions of the magnetic field applied to cable samples of finite length was analysed in [22], with the conclusion that the eddy currents distribution is pseudo-periodic if the period of the magnetic field oscillations exactly coincides with the cable twist pitch, and is periodic in the other cases.

In [27] the network model was applied to the study of the generation and development of the so called "Boundary Induced Coupling Currents" (BICC's), due to longitudinal variations of the cross contact resistances or of the magnetic field perpendicular to the broad face of the cable, obtaining a good agreement with experimental data.

The network model describes in great detail every cross contact between the strands of the two layers and permits to obtain local information about the currents flowing in every strand and in the cross contact resistances, and the power dissipated in the cable. It also permits to take into account variations of the cable parameters across the cable width. One of these possible variations is due to the fact that the cable cross section is not rectangular, but presents a slight keystone angle, which determines different pressures, and, consequently, different cross contact resistances at the two sides of the cable. Moreover the time dependent magnetic field can present a variation across the cable width.

Network models have also been used for the evaluation of power losses and for the study of cable configurations with adequate anisotropic interwire resistances aimed to ensure reduction of eddy losses without a decrease of cable stability [36, 37]. Recently the network model has been applied to an accurate study of the possible eigen-currents of a sample of a four strand cable subjected to a time dependent magnetic field [23]. The study has shown that the eigen-frequency spectrum of a N *strands cable consists of* N-*1 smooth subspectra, to each of which correspond eigen-currents with a certain type of simmetry. In each of these sub-spectra the minimum eigenfrequencies (maximum decay time constants) correspond to long slowly decaying current loops.*

The main drawback of the network model is that the number of unknowns is very high, growing quickly with the cable size. This makes it very difficult to study the problem of current distribution in real long cables made of some tens of strands used in accelerator magnets.

2.3.3 *Network models for CIC Cables*

Network models for CIC Conductors show a rather high level of complexity. This is due to the complex geometry of CIC Cables, which is not easily reproducible and in any case is strongly dependent on a complicated manufacturing process with mechanical deformation and to the very high number of strands. A remarkable problem is also the identification of the points of contact between the different strands.

Several simplified network models have been developed for the study of current distribution in cable in conduit conductors. Up to now these models have been applied to study short samples of cables made of few strands or simplified geometries of multistage cables including the final stages of the cabling process.

Fig. 2.5 *Part of a lumped parameters circuit model representing a CIC cable with two cabling stages with 1×4×6 configuration* [38].

In [38] the six petals of the final stage of a typical ITER cable have been modeled, and in a further step of analysis the two final stages of an ITER cable in a 1×4×6 configuration (see Fig. 2.5) have been implemented. In [39] a 3×3 CIC conductor model investigated experimentally in [40] was modeled via a lumped parameters network model implemented in SPICE. The network model appears to be very well suited to the analysis of this case in which the strands are insulated. In the same study the network model was applied to the study of one of the 3×4 subcables (made of 12 strands) of the 3×4×4×4 WENDELSTEIN 7-X conductor. The other 180 strands were lumped in one single branch.

Fig. 2.6. *Representation of the joint and its corresponding lumped parameters circuit model* [41].

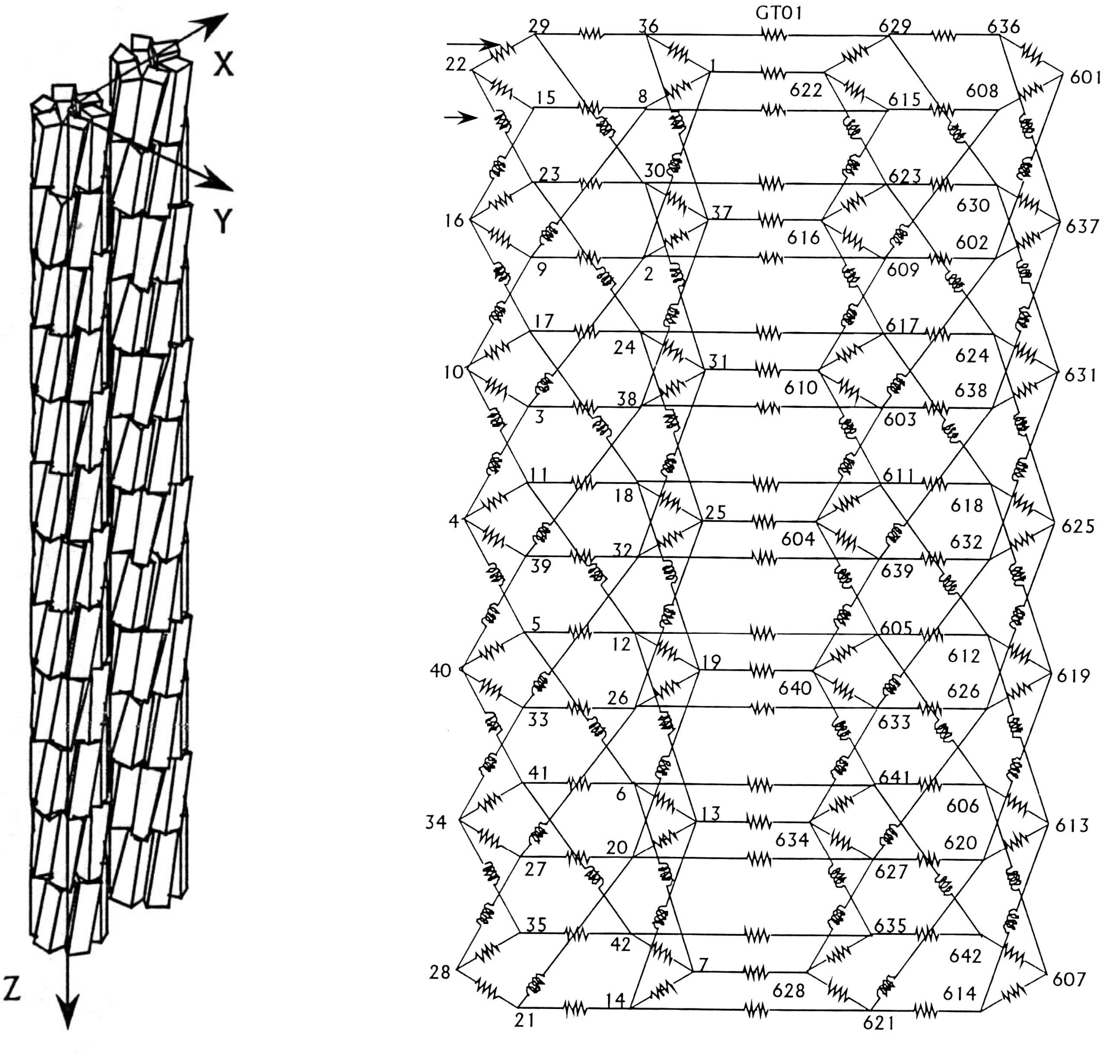

As shown in the above description, network models of CICC have the same drawback shown by the network models of Rutherford cables, as they are characterized by a very large number of unknowns, making it very difficult to study current distribution in very long cables.

Artificial simplifications can be eventually made in the modeling of these extremely complex structures. Particular scaling laws can be developed for long cable lengths using well defined parameter variations, but this operation is not straightforward, due to the non linear dependencies of the time constants on the cable length. Moreover, the lumped parameters circuits are strongly dependent on the particular cable configuration studied, as every contact between strands must be in principle represented.

A network model has also been developed for the description of current distribution at the joints between cables [41]. This kind of model is very well suited for the analysis of joints, because the joint length is not exceedingly large, and even a detailed model describing all contacts between strands can be handled.

The description of the effects of the cable joints should be somehow included in a complete analysis of current distribution in multistrand superconducting cables, as it may significantly affect the overall cable behaviour. However, a simplified modeling of the cable joints can also be attained through appropriate choices of the model parameters at the cable ends in distributed parameters circuit models [59].

2.3.4 *The field model*

The problem of current distribution in multistrand supercondcuting cables has also been tackled with a continuum model directly based on field theory [44]. In the frame of this model the cable is viewed as a continuum with anisotropic conductivity, obeying Maxwell’s equations. The current density at each point in the cable is defined as an average over the currents in a fundamental volume element surrounding the point considered, where the volume is large enough so that the resulting current density is a smooth function of the position. The volume element can have any convenient shape.

The case of circular cables made of twisted strands can be studied applying the results of the analysis of circular strands made of twisted filaments [43].

In the case of a flat Rutherford cables two different values of conductivity can be defined, corresponding to two different directions. One direction is perpendicular to the strands and parallel to the broad face of the cable, the other is perpendicular to the broad face of the cable. In the frame of this model, the currents flowing along the cable can be viewed as a sum of three terms, corresponding to two terms in the directions mentioned above and an additional term corresponding to the direction parallel to the strand axis.

Once the current density and the electric field are evaluated in a given volume element from the solution of the Maxwell equations, the general expression of the eddy current loss per cycle can be applied [44]:

$$Q_e = \int_V dV \oint_{cycle} dt \, (\mathbf{J} \cdot \mathbf{E} + \mathbf{H} \cdot \mathbf{M}) \tag{2.6}$$

where **M** is the magnetization due to local eddy currents circulating within the volume element, **J** is the eddy current density averaged over the volume element, **E** and **H** are the Maxwell electric and magnetic fields.

The contribution of power loss in the crossover contacts between the strands of the two layers can be shown to be a generalization of the results obtained by Morgan [18].

An additional loss term corresponding to currents flowing down one edge of the cable and back along the other edge can be added to the term corresponding to the currents flowing along the upper and lower face of the cable already considered in the model.

The field model can give a very elegant and quick estimation of the eddy losses due to the coupling currents induced in Rutherford cables or in cable in conduit conductors in the case of an uniform time dependent magnetic field applied perpendicular to the broad face of the cable. In the model presented in [44] the electric field component parallel to the strand axis is taken equal to zero, considering the strand in a perfectly superconducting state. In principle the field model can be generalized to the study of any time and space varying magnetic field, and to the introduction of a non-linear **E-J** relation in the direction parallel to the strand axis.

However, this model requires the assumption that a relatively high density of electrical contacts between the strands exists.

2.3.5 *The theory of "supercurrents"*

As anticipated in Section 2.1, one of the possible sources of non uniform current distributions is a longitudinal variation of the time derivative of the magnetic field perpendicular to the broad face of the cable. Let's consider a 2-strand cable of length $2w$, much longer than the cable twist pitch L_P. The two strands have two contacts per pitch and the cable is exposed to a time dependent magnetic field as shown in Fig. 2.2b. In general a finite number of loops can be exposed to the time dependent magnetic field. Let's consider the simple case in which only one loop, half twist pitch, is exposed to *dB/dt*.

If $w = N_l L_P$ the parallel resistance seen on either side of the cable central loop is equal to:

$$R_w = \frac{R_c}{N_l}$$

(2.7)

If *dB/dt* is time independent, a steady state solution for the value of the supercurrent in the middle of the cable can be easily found as:

$$I_{sc} = i_1 = N_l \frac{\dot{\Phi}}{2R_c}$$

(2.8)

where $\dot{\Phi}$ is the time derivative of the magnetic flux linked to the loop. Comparing eq. (2.8) and (2.4) we note that the magnitude of the supercurrents is much larger than that of the short range coupling currents, the ratio depending on the cable length. As cables can be as long as many thousands of twist pitches this ratio can be very high. The order of the longest decay time constant of the supercurrent is given by:

$$O(\tau) \approx \frac{L_w}{R_w} = \frac{N_l \; L_w}{R_c} \approx \frac{N_l^2 \; L_1}{R_c}$$

(2.9)

where L_w is the inductance relative to the length w. Typical decay time constants are in the range from 10 to 10^5 s in practical cables.

The supercurrents strongly contribute to the ramp rate limitation found in superconducting magnets [11].

The theory developed in [10] allows the evaluation of time dependent supercurrents in a simple-two strand cable and of steady state *"supercurrents" in cables made by a generic number of strands. The exact equations for the time dependent supercurrents in a two strand cable are derived in Section 4.2.*

The approach adopted in [10] for the calculation of the steady state supercurrents was to compute the total flux linked to two generic strands as the product of the area of the elementary loop formed by the two strands and the local value of the magnetic flux density. The steady state current in each strand can then be calculated considering the N-*1 contributions given by the driving voltages induced in the loops formed by the strand considered and all the others. If the magnetic flux density change is applied to more than one loop a superposition of the effects of the different loops is calculated and the final currents in the strands are found.*

2.4 HISTORICAL REVIEW: EXPERIMENTS

The experimental activity on current distribution and redistribution is not yet enough extensive for a correct interpretation of all the phenomena involved in these processes. However, since the middle of the 90's, several experiments have been carried out focussing on both current distribution and its coupling with the cable thermal stability.

Two fundamental methods have been used for the measurements of current distribution in multistrand cables: *direct* and *indirect* [45].

In *direct* methods special sensors are associated to each strand of the cable and the current in the strand is directly measured. The possible sensors that can be used are listed in the following:

- Hall Sensors are rather simple and their signals are directly proportional to the local value of the field. In order to obtain signals proportional to the current in a particular strand the effect of the currents flowing in the other strands must be suppressed through appropriate calibration procedures. They are especially suited for the measurement of slow current changes due to long range induced current loops.
- Pick up coils should be placed around the strand in order not to be affected by the neighbouring strands. Their signal is directly proportional to the derivative of the current, which must be integrated for the

knowledge of the currents in the strands. They are especially suited for the measurement of fast current changes, but have low sensitivity for slow processes.

The *direct* methods show the great advantage to provide direct data about current non-uniformity, but require the preparation of special cables or special sample models. Moreover the installation of current sensors may change the cable structure modifying the system to be measured. Finally these methods are practically unfeasible for cables made of more than some tens of strands.

Indirect methods are based on the measurement of the magnetic field in several points around the complete cable. The measurements can be performed once again with Hall sensors or pick-up coils. By solving an inverse electromagnetic problem, the current distribution processes inside the cable can be inferred. This part of the method contains a remarkable margin of uncertainty which should be reduced as much as possible through appropriate calibrations to understand the meaning of the measured data. Indirect methods do not disturb the cable structure, and may be used in real environments, inside or near superconducting magnets, without any limitation in the total number of strands in the cable.

We list in the following some of the experiments on current distribution found in the literature which were performed with different cable configurations.

2.4.1 *Experiments on a 2-strand cable*

An experiment on current distribution was performed on a two-strand cable in order to validate the theory of supercurrents originated by longitudinal variations of the time derivative of the magnetic flux linked to the strands. A 4.7 m long cable twisted with a pitch of 10 mm. was soldered with Sn(50%)In. In the middle of the cable, and over a length of approximately half a twist pitch (5 mm), a loop with a cross section of approximately 70 mm^2 was formed between the strands. The cable was wound into a test coil, with the loop placed in the coil center, normal to the coil axis, as shown in Fig. 2.7.

The coil was then placed in a background AC vertical field. The AC field caused a variation of the flux linked with the loop in the center of the sample, inducing currents in opposite directions in the two superconducting strands. These supercurrents could flow along the whole cable length, closing through the solder between the two strands.

The supercurrent circulating in the center of the sample was measured by means of a Hall plate placed in the loop. Different cycles of the external field were performed, with field ramps alternated with constant field phases.

2.4.2 *Experiments on triplex cables*

Several experiments on current distribution on triplex cables have been realized, aimed to the understanding of the coupling of current redistribution processes and cable thermal stability to thermal disturbances [48-51].

Fig. 2.7 *Experimental apparatus used for the measurement of "supercurrents" induced by the time dependent field in the loop formed by the two strands*

In this kind of experiments a heat pulse was applied to a short part of one strand, and the minimum quench energy and the temporal evolution of the strand current during the quench or recovery process were measured. The experimental results showed that when the ratio between the transport current and the critical current is large, the MQE against a local disturbance almost equals the MQE of the single strand. When the ratio of the overall I_{op}/I_c is less than 0.4, the MQE against a local disturbance is much larger than that of the single strand. In this small I_{op}/I_c region, when a heat pulse whose energy is slightly less than the MQE is applied, current redistribution is observed during the recovery process. This means that the stability against local disturbance is improved by the current redistribution only when the ratio I_{op}/I_c is less than a threshold value, dependent on the thermal contact conductance

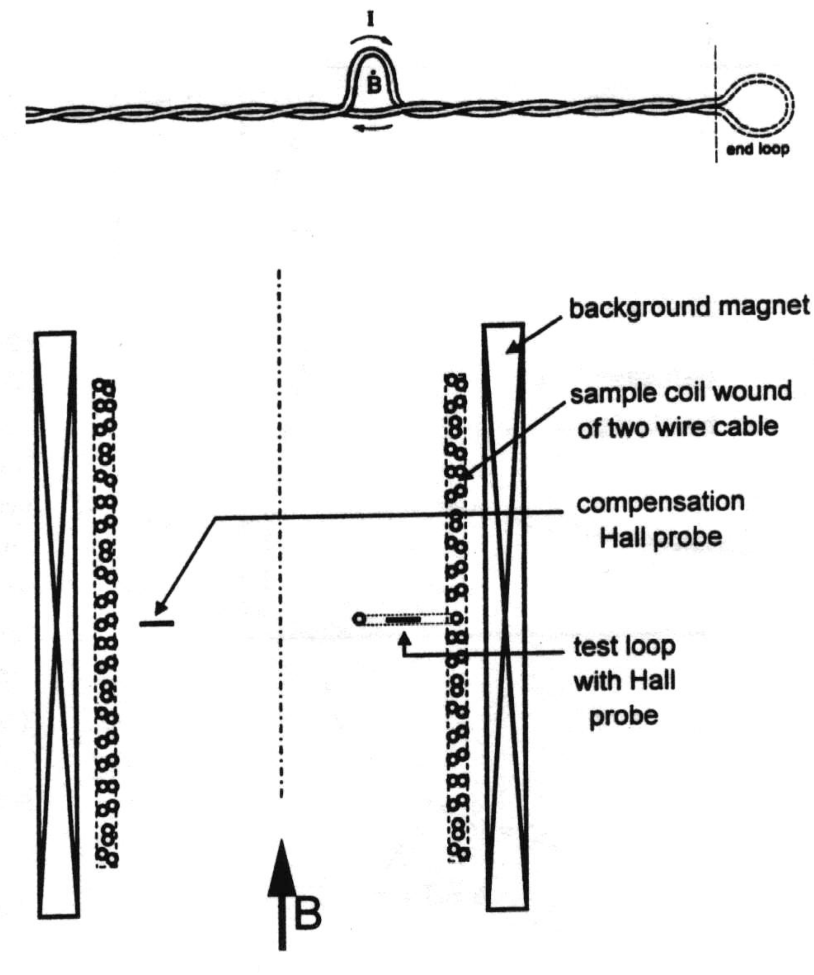

between the strands.

Other experiments [52-54] have shown the influence of different strand configurations on the cable stability to thermal disturbances. In particular the use of different materials for the strands matrices has been investigated [52], with the result that some improvements of triplex cable stability to thermal disturbances can be obtained with Cu matrix either than CuNi matrix because of the high heat conduction and low Joule heating of the Cu matrix.

Moreover, the influence of the number of initially quenched strands on the quench properties of the cable was studied initiating the quench in one, two or three strands of the cable. In the case of quenching two strands simultaneously, the current which redistributes to the neighbouring strand is 4 times larger than when only one strand is initially quenched, with the result of a lower cable stability.

2.4.2 *Experiments on CIC cables*

Several experiments have also been performed for the study of current distribution and redistribution phenomena in CIC cables made of more than three strands. In some of these experiments the current non-uniformity in cables wound with insulated strands was studied in AC conditions with cables made of copper strands [55] and usual superconducting strands [56]. These experiments clearly showed that current distribution in DC conditions or at very low frequency operation (in the frequency region up to 0.1 Hz) is only determined by the joint resistances of the strands. The influence of the different inductances of the insulated strands is dominant in the determination of the current distribution above 1 hz.

Between these two regions a third intermediate region was identified, in which the current distribution is influenced by both resistances and inductances. Even very small differences in the values of inductances can generate large current imbalances. It is not yet clear why the inductance imbalance and the corresponding current imbalance is generated in symmetrically assembled strands.

An extensive measurement of current distribution in a 12 strand Nb_3Sn CIC conductor was performed in order to study the phenomenon of ramp rate limitation [46]. The experiments were performed measuring the current in each of the 12 strands during current or field ramps. Very severe inhomogeneities of the current distribution were found during field ramps. After a current ramp currents in strands were observed to vary from 0.28 up to 3.7 of the average level independent of di_{op}/dt and of the final current level. This effect was caused by uneven joint resistances.

Immediately before quenches the individual strand currents within a triplet were observed to differ by as much as an order of magnitude. Moreover, quench-recovery events of some strands were observed during field ramps with a constant operation current. These events are responsible for a extra heat release inside the conduit, which can favour the premature quench of the cable during a ramping field experiment.

An interesting result obtained with direct measuring on this 12 strand cable wound from four triplets is that the nucleation of a normal zone in a single strand determines a current redistribution in which the current distributes into two adjacent strands in the same triplet as the quenched strand, with small influence on the currents in the other strands.

Experiments on large scale CICC's were also performed. These experiments showed that increased AC losses are observed during the excitation of CICC coils which can be attributed to induced coupling currents [58].

The dominant influence of the joint resistances on current distribution was suggested in a steady state analysis of non-uniform current distribution in short 4 m samples of 40-50 kA multistage cables [8]. Many of the conductor samples tested quenched at current levels much lower than expected from the performance of individual strands. This was supposed to be due to the short length available for current transfer and to the non-uniformity of joint resistances.

The tests performed suggested that the severe current non uniformities happen within large petals among the different strands, either than among the different large petals of the last cabling stages.

Cables wound adding some copper strands showed more premature quenches than cables with all superconducting strands, due to the larger differences between the low joint resistances in the cables containing copper strands.

Transient effects in pulsed mode operation in short 3.5 m samples and long 140 m single layer coils were widely analysed in [59]. The analysis was based on a time dependent coupled electrical-thermal model applied to a range of Nb_3Sn conductors with 1000 strands and revealed that current non uniformity gives a little degradation of stability to local thermal disturbances, even when the non uniformity is very severe. The current redistribution times calculated for short samples range from several tens to several hundreds of seconds. For long

140 m conductors redistribution times increase to 3000 s for the lower cabling stages and to more than 10000 s for the final substage.

2.4.2 *Experiments on Rutherford cables*

An experiment on current distribution in a 1.3 m flat Rutherford cable was described in [27]. The cable was exposed to a small local field change in order to measure the consequent "Boundary Induced Coupling Currents" generated during field sweeps. The experiment was aimed to study the decay of the induced currents as a function of time and their propagation velocity along the cable length, comparing the results with the lumped parameters network model for Rutherford cables [27].

Other experiments were conducted on short samples of Rutherford cables made of 3 and 11 strands, in order to observe the current redistribution among the strands in two different situations [21]. In the first configuration only one strand was connected with the external power supply, and the current entered and exited the cable from the same strand while the rest of the cable served as a shunt. In the second configuration the current entered the cable through a strand and got out through the rest of the cable. The analysis of the time constants of the current redistribution after current ramps demonstrated that the largest time constant is proportional to the square of the length of the sample, as predicted by theoretical models [20].

Extensive measurement campaigns were also conducted in order to evaluate the AC losses and interstrand resistances of Rutherford cables [60, 61].

CHAPTER 3

THE THEORETICAL MODEL

INTRODUCTION

In this Chapter an electromagnetic model for the study of current distribution is described. The model is based on a distributed parameters circuit, and is described by a set of partial differential equations, which are suitable to be coupled with a complete thermo hydraulic description of the refrigerating system [31].

This model is aimed to find a synthesis between two different kinds of models previously developed for the study of current distribution and described in Chapter 2.

On one hand, the model starts from the development of the theory of supercurrents [10], which allows to calculate time dependent supercurrents in a simple-two strand cable and steady state "supercurrents" in cables made of a generic number of strands.

The model presented here intends to extend this theory to the study of time dependent supercurrents in cables made of N strands, considering the mutual dynamic interactions between the strand currents. A simplified modelling of this situation was proposed in [24], where a single strand was considered and all the rest of the cable is lumped in another idealised strand, with which the current exchange takes place. An equivalent inductance of the strand and of all the rest of the cable, as well as an equivalent conductance between these two elements is evaluated, and the equation of current diffusion between the strand and the rest of the cable is then solved. The model presented here contains instead a complete representation of the cable.

On the other hand the model is based on the achievements obtained by the development of different network models for current distribution in Rutherford cables [19-27] and cable in conduit conductors [8, 38]. As pointed out in Chapter 2 these network models are peculiar to the configuration chosen and are difficult to apply to long cables, because of the very high number of unknowns.

The model presented here intends to be suited for a correct modeling of both Rutherford cables and cable in conduit conductors, by means of an appropriate calculation of the model parameters.

It is therefore important to show that this model reduces to the equations found in [10] when a 2 strand cable is considered, and is consistent with the network models of both Rutherford cables and cable in conduit conductors in the evaluation of the strand currents. In Chapter 3 these features of the model are demonstrated.

In order to do this the model is presented and the equations reported in [10] are derived, showing the relations between the parameters of the two models.

Moreover the model is applied to study the generation and development of the long range coupling currents (BICC's), induced in Rutherford cables by longitudinal variations of the time derivative of the magnetic field perpendicular to the cable face. A comparison of the results obtained with the present model and the commonly used network model for Rutherford cables is shown, stressing the reduction of the unknowns obtained with the present model.

In addition to that the current redistribution after quench of one strand in a simple triplex cable is analysed. The results are compared with those obtained with a lumped parameters network model of the same cable.

Finally another interesting feature of the model is demonstrated, i.e. the possibility to simplify the analysis of complex situations in which long cables with many strands have to be studied introducing equivalent "superstrands". This simplification allows a further reduction of the number of unknowns without affecting in a relevant way the final results.

3.1 DISTRIBUTED PARAMETERS CIRCUIT MODEL

3.1.1 Model equations

The model assumes that each strand carries a current distributed in a uniform way in its cross section, neglecting the influence of interfilament coupling currents flowing inside each strand between different superconducting filaments. We also assume that the current transfer between different strands happens along the length of the cable in a continuous manner. Under these assumptions we can derive approximate equations governing the current distribution in the cable.

To do so, we consider a superconducting cable made by N strands, and we examine the elemental length dx. Over this length the strands have parallel resistances $R_i = r_i\, dx$, (i=1, N), where r_i are the longitudinal resistances per unit length of cable (zero if the strand is in the superconducting state). The self inductances of the strands are indicated with $L_{ii} = l_{ii}\, dx$ where l_{ii} $(i=1,N)$ are artificial parameters which we temporarily introduce. In the final equations only differences between these parameters appear, which have the physical meaning of per unit length induction coefficients. Finally, each strand can have an external voltage source $V^{ext}_i = v^{ext}_i\, dx$, that can be originated, for instance, by changes of the magnetic field flux due to external sources linked to a couple of strands. This idealised situation is represented schematically in Fig. 3.1

The strands have initial currents i_i and voltages V_i at the coordinate x. Over an elemental length dx the currents will change by di_i because of the current transfer through the interstrand contact resistances $R_{hk} = 1/(g_{hk}\, dx)$, where g_{hk} is the interstrand conductance per unit length. Similarly the voltages will drop by dV_h due to the parallel resistance, inductance and the voltage source.

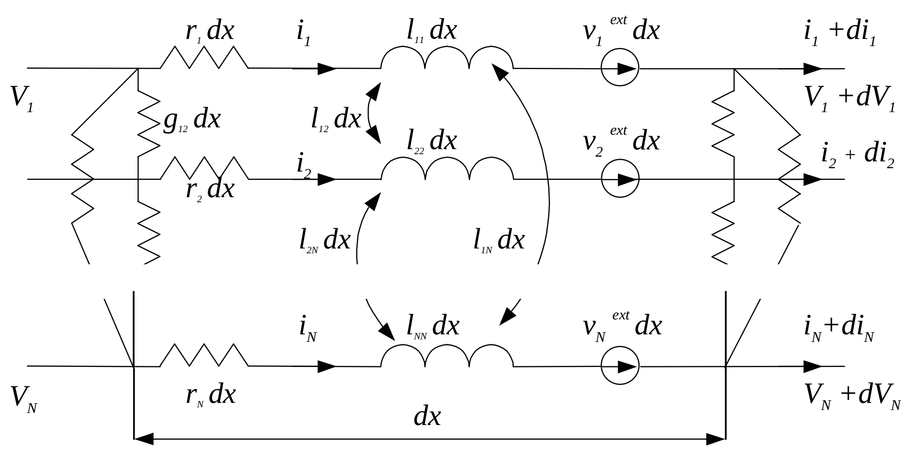

Fig. 3.1 *The distributed parameters circuit model*

Applying the Kirchhoff's current law to the N nodes, we obtain the following N dependent equations for the current variations:

$$\begin{cases} di_1 = -\left(g_{12} + g_{13} + ...g_{1N}\right) dx\, V_1 + g_{12}\, dx\, V_2 + g_{13}\ dx\, V_3 .... + g_{1N}\ dx\, V_N \\ di_2 = +g_{21}\ dx\, V_1 - \left(g_{21} + g_{23} + ...g_{2N}\right) dx\, V_2 + g_{23}\ dx\, V_3 ... \quad ..... \quad + g_{2N}\ dx\, V_N \\ di_N = +g_{N1}\ dx\, V_1 + g_{N2}\ dx\, V_2 + g_{N3}\ dx\, V_3 .. \quad . - \left(g_{N1} + g_{N2} + ...g_{N\,N-1}\right) dx\, V_N \end{cases}$$

(3.1)

where V_h is the voltage of strand h at position x.

Applying the Kirchhoff's voltage law to evaluate the voltage drops along the elemental mesh identified, and neglecting the inductive coupling for all sections, but for the one of length dx located at x, we obtain the following equations:

$$dV_h = v_h^{ext} dx - i_h r_h dx - \sum_{k=1}^{N} l_{hk} dx \frac{\partial i_k}{\partial t} \qquad h = 1,\ N$$

(3.2)

In addition, the solution is subject to a condition that expresses the conservation of the total operation current i_{op} in the cable cross section. We can write this condition as:

$$\sum_{h=1}^{N} i_h = i_{op}$$

(3.3)

that must hold at any point in time and space. The equations above can be conveniently put in the following matrix form to ease the further algebra:

$$\frac{\partial\ \mathbf{v}}{\partial\ x} = -\mathbf{ri} - \mathbf{l}\frac{\partial \mathbf{i}}{\partial t} + \mathbf{v}^{ext}$$

(3.4a)

$$\frac{\partial \mathbf{i}}{\partial x} = \mathbf{g}\ \mathbf{v}$$

(3.4b)

where we have defined the following vectors and matrices:

$$\mathbf{v} = \begin{bmatrix} V_1 \\ V_2 \\ \vdots \\ V_N \end{bmatrix} \qquad \mathbf{i} = \begin{bmatrix} i_1 \\ i_2 \\ \vdots \\ i_N \end{bmatrix} \qquad \mathbf{v}^{ext} = \begin{bmatrix} v_1^{ext} \\ v_2^{ext} \\ \vdots \\ v_N^{ext} \end{bmatrix}$$

(3.5a)

$$\mathbf{r} = \begin{bmatrix} r_1 & 0 & \cdots & 0 \\ 0 & r_2 & \cdots & 0 \\ \vdots & & & \\ 0 & 0 & \cdots & r_N \end{bmatrix} \quad \mathbf{l} = \begin{bmatrix} l_{11} & l_{12} & \cdots & l_{1N} \\ l_{21} & l_{22} & \cdots & l_{2N} \\ \vdots & & & \\ l_{N1} & l_{N2} & \cdots & l_{NN} \end{bmatrix} \quad \mathbf{g} = \begin{bmatrix} -\sum\limits_{\substack{k=2 \\ k\neq 1}}^{N} g_{1k} & g_{12} & \cdots & g_{1N} \\ g_{21} & -\sum\limits_{\substack{k=1 \\ k\neq 2}}^{N} g_{2k} & \cdots & g_{2N} \\ \vdots & & & \\ g_{N1} & g_{N2} & \cdots & -\sum\limits_{\substack{k=1 \\ k\neq N}}^{N} g_{Nk} \end{bmatrix}$$

(3.5b)

If we calculate the space derivative of equation (3.4b) assuming that the interstrand conductances are uniform along the cable axis, so that the spatial derivative of the interstrand conductances matrix **g** *is nil, we obtain the following differential equations for the currents in the strands:*

$$\mathbf{gl}\frac{\partial \mathbf{i}}{\partial t} + \frac{\partial^2 \mathbf{i}}{\partial x^2} + \mathbf{gri} - \mathbf{gv}^{ext} = 0$$

(3.6)

These are parabolic differential equations that describe the processes of current diffusion along the cable. The N equations in system (3.6) are linearly dependent, due to the application of the Kirchhoff's current law to all the nodes of the distributed circuit in the elemental mesh of length dx. However we can arbitrarily consider N-1 equations for the currents in the first N-1 strands and couple them to equation (3.3). In this way we obtain a complete set of N independent partial differential equations for the currents in the strands at any time and position:

$$\begin{cases} (gl)_{1,1}\dfrac{\partial i_1}{\partial t}+\cdots+(gl)_{1,N}\dfrac{\partial i_N}{\partial t}+(gr)_{1,1}\ i_1+\cdots+(gr)_{1,N}\ i_N+\dfrac{\partial^2 i_1}{\partial x^2}-(gv)_1^{ext}=0 \\ (gl)_{2,1}\dfrac{\partial i_1}{\partial t}+\cdots+(gl)_{2,N}\dfrac{\partial i_N}{\partial t}+(gr)_{2,1}\ i_1+\cdots+(gr)_{2,N}\ i_N+\dfrac{\partial^2 i_2}{\partial x^2}-(gv)_2^{ext}=0 \\ \vdots \\ (gl)_{N-1,1}\dfrac{\partial i_1}{\partial t}+\cdots+(gl)_{N-1,N}\dfrac{\partial i_N}{\partial t}+(gr)_{N-11}\ i_1+\cdots+(gr)_{N-1,N}\ i_N+\dfrac{\partial^2 i_{N-1}}{\partial x^2}-(gv)_{N-1}^{ext}=0 \\ \sum\limits_{h=1}^{N} i_h = i_{op} \end{cases}$$

(3.7)

where we indicate with $(gl)_{i,j}$ the element i, j of the result of the matrix product **gl**.

A more accurate description of the meaning of the system parameters can be found in Appendix A.

These equations are in general not linear because the strand resistance depends on the current flowing in the strands, so that an appropriate model for the strand behaviour has to be chosen. Finally the appropriate length for the smearing of the system parameters (resistance, inductance and external voltage) has to be chosen. As multistrand superconducting cables have an intrinsic periodicity related to the twist pitch, good choices of the length for the smearing of electric parameters are appropriate multiples or fractions of the pitch. Once the parameters for matrices **g** and **l** are experimentally evaluated or calculated, the finite element method can be applied to solve system (3.7).

3.1.2 Initial conditions

In order to solve system (3.7) by means of the finite element method it is necessary to fix the initial current distribution among the cable strands. The only physical situation in which a clear condition on strand currents can be set is at zero total current before any current ramp, when the following initial conditions hold:

$$i_h\ (x,0) = 0 \qquad h = 1, N$$

(3.8)

A simple way to obtain this condition with a real magnet is to make it quench, so that the long “memory” of persistent currents flowing in the strands can be erased. In other cases, after a sufficiently long time from the last operation current variation, a simply resistive current distribution is established between the strands. As a starting point for the calculations, it can be assumed that the initial current distribution is uniform, i. e.:

$$i_h\ (x,0) = \frac{i_{op}(0)}{N} \qquad h = 1, N$$

(3.9)

3.1.3 Boundary conditions

The choice of the correct boundary conditions is quite delicate. In fact, in order to correctly model the connection of a multistrand superconducting cable to another cable through a termination or to a current lead through a joint, it would be necessary to have a complete description of the whole system (joint + cable + joint). However, two reasonable choices of boundary conditions can be identified, which describe different properties of the actual cable end surfaces.

If we consider the end surfaces to be equipotential, we can write:

$$v_h\ (x,0) = v_{h+1}\ (x,0) \qquad h = 1, N-1 \quad x = 0,\ x = L$$

(3.10)

This condition implies that the voltage differences between all the strands and strand N are nil:

$$e_h\ (x,0) = 0 \qquad h = 1, N-1 \quad x = 0,\ x = L$$

(3.11)

where we have defined:

$$e_h\ (x,t) = v_h\ (x,t) - v_n\ (x,t)$$

(3.12)

Applying the method of analysis based on nodes potentials, we can write system (3.4b) in terms of the voltage differences e_h (h= 1, N), obtaining a set of N-1 independent equations:

$$\begin{cases} -\dfrac{\partial i_1}{\partial x} = \left(g_{12} + g_{13} + ...g_{1N}\right) e_1 - g_{12}e_2 .... - g_{1N-1}e_{N-1} \\ -\dfrac{\partial i_2}{\partial x} = -g_{12}e_1 + \left(g_{21} + g_{23} + ...g_{2N}\right) e_2 .... - g_{2N-1}e_{N-1} \\ \vdots \\ -\dfrac{\partial i_{N-1}}{\partial x} = -g_{1\,N-1}e_1 - g_{2\,N-1}\,e_2 ... + \left(g_{1N-1} + g_{2N-1} + ...g_{N\,N-1}\right) e_{N-1} \end{cases}$$

(3.13)

The possibility to invert system (3.13) guarantees that a condition equivalent to (3.10) can be written for the space derivatives of the longitudinal currents in the strands:

$$\frac{\partial i_h}{\partial x} = 0 \quad h = 1, N-1 \quad x = 0,\, x = L$$

(3.14)

As the operation current is only a function of time, from equation (3.3) it can be deduced that the condition (3.14) holds for the N^{th} strand as well, so that the complete boundary conditions in the equipotential end surfaces case can be written as:

$$\frac{\partial i_h}{\partial x} = 0 \quad h = 1, N \quad x = 0,\, x = L$$

(3.15)

Another possibility is to assume that the current distribution is uniform at the cable ends, imposing the following boundary conditions:

$$i_h(x,\, t) = \frac{i_{op}(t)}{N} \quad h = 1, N \quad x = 0,\, x = L$$

(3.16)

Different kinds of boundaries can in principle be described with an accurate choice of the model parameters at the cable ends.

3.1.4 Equations of current diffusion in a 2 strand cable

The theory of "supercurrents" in a cable made of two strands was developed in [9, 10]. In that formulation of the problem the contribution of external voltage sources is taken into account in the evaluation of the current distribution at the end of a field ramp. During the constant field phase the external flux linked to the loops formed by the two strands is nil, and the free diffusion of "supercurrents" along the cable is studied.

In the present model the effect of the external field is directly inserted in the model equations. The equations reported in [10] can be found as a particular case of the general system (3.6). In fact, considering equations (3.6) for a two strands cable in the absence of an external voltage source, we obtain:

$$\begin{cases} \dfrac{\partial^2 i_1}{\partial x^2} = g_{12} l_{11} \dfrac{\partial i_1}{\partial t} + g_{12} l_{12} \dfrac{\partial i_2}{\partial t} - g_{12} l_{22} \dfrac{\partial i_2}{\partial t} - g_{12} l_{12} \dfrac{\partial i_1}{\partial t} \\ \dfrac{\partial^2 i_2}{\partial x^2} = -g_{12} l_{11} \dfrac{\partial i_1}{\partial t} - g_{12} l_{12} \dfrac{\partial i_2}{\partial t} + g_{12} l_{22} \dfrac{\partial i_2}{\partial t} + g_{12} l_{12} \dfrac{\partial i_1}{\partial t} \end{cases}$$

(3.17)

If the parameters l_{11} and l_{22} are equal, as in the case considered in [10], we can write:

$$\begin{cases} \dfrac{\partial^2 i_1}{\partial x^2} = g(l-m)\dfrac{\partial i_1}{\partial t} - g(l-m)\dfrac{\partial i_2}{\partial t} \\ \dfrac{\partial^2 i_2}{\partial x^2} = g(l-m)\dfrac{\partial i_2}{\partial t} - g(l-m)\dfrac{\partial i_1}{\partial t} \end{cases}$$

(3.18)

where $l = l_{11} = l_{22}$ is the common parameter representing self inductance, $m = l_{12} = l_{21}$ the mutual inductance, and $g = g_{12} = g_{21}$ the interstrand conductance.

In the case of a transport current equal to zero, we can write $i_1 = -i_2$, so that equation (3.18) gives:

$$\begin{cases} \dfrac{\partial^2 i_1}{\partial x^2} = 2g(l-m)\dfrac{\partial i_1}{\partial t} \\ \dfrac{\partial^2 i_2}{\partial x^2} = 2g(l-m)\dfrac{\partial i_2}{\partial t} \end{cases}$$

(3.19)

The corresponding equation for the free current diffusion in the two strands cable without transport current reported in [10] is written in the following form:

$$\frac{\partial^2 I}{\partial x^2} = L_1 G_1 \frac{\partial I}{\partial t}$$

(3.20)

where I is either current i_1 or i_2, G_1 is the interstrand conductance (indicated with g in the present model) and L_1 the elementary loop inductance per unit length.

We still have to show that the loop inductance L_1 reported in [10] is equal to the parameter 2 (l-m) of equation (3.19).

Considering the definition of the loop inductance in the hypothesis of an uniform current distribution inside each strand, we can write:

$$L_1 = \frac{1}{d}\frac{\mu_0}{4\pi}\int_\tau\int_\tau \frac{\mathbf{f}(P)\cdot\mathbf{f}(Q)}{r_{PQ}} d\tau_p \, d\tau_Q$$

(3.21)

where τ is the volume occupied by the two strands forming the loop, and d the length of the loop along the cable axis. The vector **f** is defined as follows:

$$\mathbf{f}\,(P) = \frac{\mathbf{t}\,(P)}{S}$$

(3.22)

where **t** is the unit vector tangent to the strand, and S is the area of the cross section. The integral (3.21) can be divided into four parts, corresponding to the integration over the volumes τ_1 and τ_2 occupied by strand 1 and strand 2:

$$L_1 = \frac{1}{d}\frac{\mu_0}{4\pi}\left(\begin{array}{l} \int\limits_{\tau_1}\int\limits_{\tau_1} \frac{\mathbf{f}_1(P)\cdot\mathbf{f}_1(Q)}{r_{PQ}} d\tau_P\, d\tau_Q + \int\limits_{\tau_1}\int\limits_{\tau_2} \frac{\mathbf{f}_1(P)\cdot\mathbf{f}_2(Q)}{r_{PQ}} d\tau_P\, d\tau_Q + \\ \int\limits_{\tau_2}\int\limits_{\tau_1} \frac{\mathbf{f}_2(P)\cdot\mathbf{f}_1(Q)}{r_{PQ}} d\tau_P\, d\tau_Q + \int\limits_{\tau_2}\int\limits_{\tau_2} \frac{\mathbf{f}_2(P)\cdot\mathbf{f}_2(Q)}{r_{PQ}} d\tau_P\, d\tau_Q \end{array} \right)$$

(3.23)

Defining the per unit length parameters as follows:

$$l_{11} = \frac{1}{d}\frac{\mu_0}{4\pi}\int\limits_{\tau_1}\int\limits_{\tau_1} \frac{\mathbf{f}_1(P)\cdot\mathbf{f}_1(Q)}{r_{PQ}} d\tau_P d\tau_Q \quad l_{12} = \frac{1}{d}\frac{\mu_0}{4\pi}\int\limits_{\tau_1}\int\limits_{\tau_2} \frac{\mathbf{f}_1(P)\cdot\mathbf{f}_2(Q)}{r_{PQ}} d\tau_P d\tau_Q$$
$$l_{21} = \frac{1}{d}\frac{\mu_0}{4\pi}\int\limits_{\tau_2}\int\limits_{\tau_1} \frac{\mathbf{f}_2(P)\cdot\mathbf{f}_1(Q')}{r_{PQ}} d\tau_P d\tau_Q \quad l_{22} = \frac{1}{d}\frac{\mu_0}{4\pi}\int\limits_{\tau_1}\int\limits_{\tau_1} \frac{\mathbf{f}_2(P)\cdot\mathbf{f}_2(Q)}{r_{PQ}} d\tau_P d\tau_Q$$

(3.24)

we can finally write:

$$L_1 = l_{11} - l_{12} + l_{22} - l_{21} = 2\,(l - m)$$

(3.25)

3.2 MODEL PARAMETERS

3.2.1 Contact conductances per unit length

Rutherford cables

In order to define the smeared interstrand conductances, we consider that each strand crosses every other strand in two points per twist pitch. Indicating with $R^c_{h,k}$ the interstrand cross contact resistance between strand h

and strand k, and with L_p the cable twist pitch, the cross contact conductance per unit length is given by the following expression:

$$g^c_{h,k} = \frac{2}{L_p\, R^c_{h,k}}$$

(3.26)

The description of the cross contact resistance between strands given by the network model is closer to the physical reality of the cross contacts than that given by the distributed parameters model, while a better representation of the contact between adjacent strands is given by the present model.

However, in order to make comparisons with the network model, and to consistently calculate the interstrand adjacent conductances, we consider that in the most advanced versions of the network model [20, 27], a lumped contact resistance $R^a_{h,k}$ is inserted between two adjacent strands at the same positions in which they have cross contacts with the strands of the other layer. Every strand crosses all the other strands in two points per twist pitch, so that a total of 2 (N-1) lumped resistances are inserted along a twist pitch between each pair of adjacent strands. The equivalent adjacent conductance per unit length results in:

$$g^a_{h,k} = \frac{2\,(N-1)}{R^a_{h,k}\, L_p}$$

(3.27)

Cable in conduit conductors

The smeared interstrand conductance between strand h *and* k *can be defined in the same way as in Rutherford cables, summing all the contact conductances along a certain smearing length and dividing by the length itself. An appropriate length for the smearing can be the twist pitch of the last cabling stage, which we simply indicate with* L_p. *The contact conductance results in:*

$$g_{h,k} = \frac{1}{L_p} \sum_{i=1}^{N^c_{h,k}} \frac{1}{R^i_{h,k}}$$

(3.28)

where $R^i_{h,k}$ *is the* i^{th} *contact resistance between strand* h *and* k *along the twist pitch considered and* $N^c_{h,k}$ *is the total number of contacts between strand* h *and* k *along the length considered. It may happen that some strands have no contacts along the final twist pitch of multi-stage cable in conduit conductor, resulting in a nil contact conductance.*

If the contact along two strands is continuous, like in a two-strand cable, or in a triplex cable, the smeared interstrand conductance is coincident with the continuous conductance along the length of the triplet.

This way to calculate smeared interstrand conductances is very well suited for the evaluation of long range coupling currents, neglecting an accurate description of the influence of short range coupling currents.

3.2.2 Mutual inductances matrix

The evaluation of the coefficients of the mutual inductances matrix was done numerically. A code for the calculation of mutual and self inductances between conductors with circular cross-section having any geometric disposition in space was developed, considering either the possibility to have an analytical expression of the trajectory of the strands axes, or to know the coordinates of a sufficient number of points along the strands axes, allowing to reconstruct the strands axes by means of spline interpolation.

The code was applied to the calculation of induction coefficients for both flat Rutherford cables and simple cable in conduit conductors.

The numerical procedures and some results of these calculations are reported in Appendix B.

3.2.3 Longitudinal resistance

The strand longitudinal resistance is in general dependent on the magnetic flux density **B**, on the temperature T, and on the current flowing in the strand. Once an appropriate model for the longitudinal resistance per unit length of the strand $r_{s,h}$ is known, the longitudinal resistance per unit length of cable r_h can be calculated according to Equation (A.19) as follows:

$$r_h(x) = \frac{r_{s,h}}{\cos(\gamma_h)}$$

(3.29)

where γ_h is the angle between the unit vector $\mathbf{t}_h(x)$ tangent to the axis of strand h at x, and the unit vector $\mathbf{t}_c(x)$ tangent to the axis of the cable at x.

3.2.4 External voltage

The external voltage per unit length can be defined in the following way (see Appendix A):

$$v_h^{ext}(x,t) = -\frac{\partial \mathbf{A}^{ext}}{\partial t}(R_h(x),t) \cdot \mathbf{t}_h(x) \frac{1}{\cos(\gamma_h)}$$

(3.30)

where $\mathbf{A}^{ext}$ is the magnetic vector potential associated with the external sources, and $R_h(x)$ is the point of the strand axis corresponding to coordinate x (see Fig. A.1). This definition guarantees that the integral effect of the difference $v^{ext}{}_h$ - $v^{ext}{}_k$ along any loop formed by two generic strands h and k provides a driving force equivalent to the time derivative of the magnetic flux due to the external sources linked to the loop.

A simple expression for the external voltage in the case of Rutherford cables can be found when the magnetic flux density is orthogonal to the broad face of the cable (see Fig. 2.3). In this case we can write:

$$\mathbf{B}^{ext} = B(x,t)\,\mathbf{k}$$

(3.31)

where $\mathbf{k}$ is the unit vector of the z axis, perpendicular to the broad face of the cable.

The external field is related to the external vector potential through the following relation:

$$\mathbf{B}^{ext} = \nabla \times \mathbf{A}^{ext}$$

(3.32)

Choosing a coordinate system as in Fig. 2.3, we can write the cartesian components of equation (3.32):

$$\begin{cases} B^{ext}{}_x = 0 \\ B^{ext}{}_y = 0 \\ B^{ext}{}_z = B(x,t) \end{cases} \Rightarrow \begin{cases} \dfrac{\partial A^{ext}{}_z}{\partial y} - \dfrac{\partial A^{ext}{}_y}{\partial z} = 0 \\ \dfrac{\partial A^{ext}{}_x}{\partial z} - \dfrac{\partial A^{ext}{}_z}{\partial x} = 0 \\ \dfrac{\partial A^{ext}{}_y}{\partial x} - \dfrac{\partial A^{ext}{}_x}{\partial y} = B(x,t) \end{cases}$$

(3.33)

A possible choice for the divergence of the vector potential is the Coulomb gauge:

$$\frac{\partial A^{ext}{}_x}{\partial x} + \frac{\partial A^{ext}{}_y}{\partial y} + \frac{\partial A^{ext}{}_z}{\partial z} = 0$$

(3.34)

The following expression of the vector potential of the external field satisfies both (3.33) and (3.34):

$$\begin{cases} A^{ext}{}_x = -B(x,t)\, y \\ A^{ext}{}_y = 0 \\ A^{ext}{}_z = 0 \end{cases} \tag{3.35}$$

We can then write:

$$\mathbf{A}^{ext} = A^{ext}{}_x \ \mathbf{i}$$

(3.36)

From the general definition (3.30), and considering that for the particular geometry of Rutherford cables $\cos(\gamma_h) = \sin(\alpha)$ (with α indicated in Fig. 2.3), we obtain:

$$v_h^{ext}\ (x) = -\frac{\partial A_x^{ext}}{\partial t} \sin(\alpha) \frac{1}{\sin(\alpha)} = y_h(x) \frac{\partial B^{ext}}{\partial t}(x,t)$$

(3.37)

3.3 COMPARISON WITH THE NETWORK MODEL: RUTHERFORD CABLES

We have applied the model to the evaluation of currents induced by longitudinal variations of the external field perpendicular to the broad face of the cable. A comparison between the results obtained with the continuum and the network model illustrated in [27] is shown in Fig. 3.2 in the case of a simple step variation of the magnetic field along the cable axis. As far as possible the same conditions as in [27] have been used for the simulations.

The cable considered is a 16 strands cable, with $R^c_{h,k}$ = 1 μΩ, $R^a_{h,k}$ = 10 μΩ for every h and k and L_P = 100 mm. The cable is exposed to a time dependent magnetic field perpendicular to its broad face. The field is equal to 0 for $x < L/2$ and increases with a rate of 0.01 T/s for $x > L/2$. It was assumed in [27] that the strand can be characterized by a constant and uniform longitudinal effective strand resistivity. For the sake of comparison, we have introduced a uniform and constant longitudinal resistance per unit length r_h, and we have evaluated the strand currents at the final steady state for two different values of r_h, equal to 1.54 10^{-8} Ω/m and 1.54 10^{-11} Ω/m. These values have been calculated according to equation (3.29).

In the case reported in Fig. 3.2 the short range coupling currents due to the uniform field applied at the right of $x = L/2$ are superimposed to the main long range coupling currents due to the field variation at $x = L/2$. It can be noticed that the qualitative behaviour of the BICC's obtained with the two models is very similar in both the current distribution regimes shown.

Only a quantitative difference in the range 5-20% on the maximum amplitude of the BICC's is found. This could be due to the slightly different description of the geometry of the cable made in the two models. The present model in fact is based on the simple geometry illustrated in Fig. 2.3, with a discontinuous jump of the strands from one layer to the other. In the model described in [27] instead, the strands go from one layer to the other via short side cylinders (see Fig. 2.4).

In the evaluation of the short range coupling currents, instead, the two models strongly differ. In fact, the amplitude of these currents obtained with the continuum model is about half of that obtained through the network model. This is due to the smearing of the system parameters performed in the continuum model and can be confirmed by an analytical calculation of the short range coupling currents in the simple case of a two strand cable made of an integer number of pitches to which an uniform time dependent magnetic field is applied (see par. 3.6).

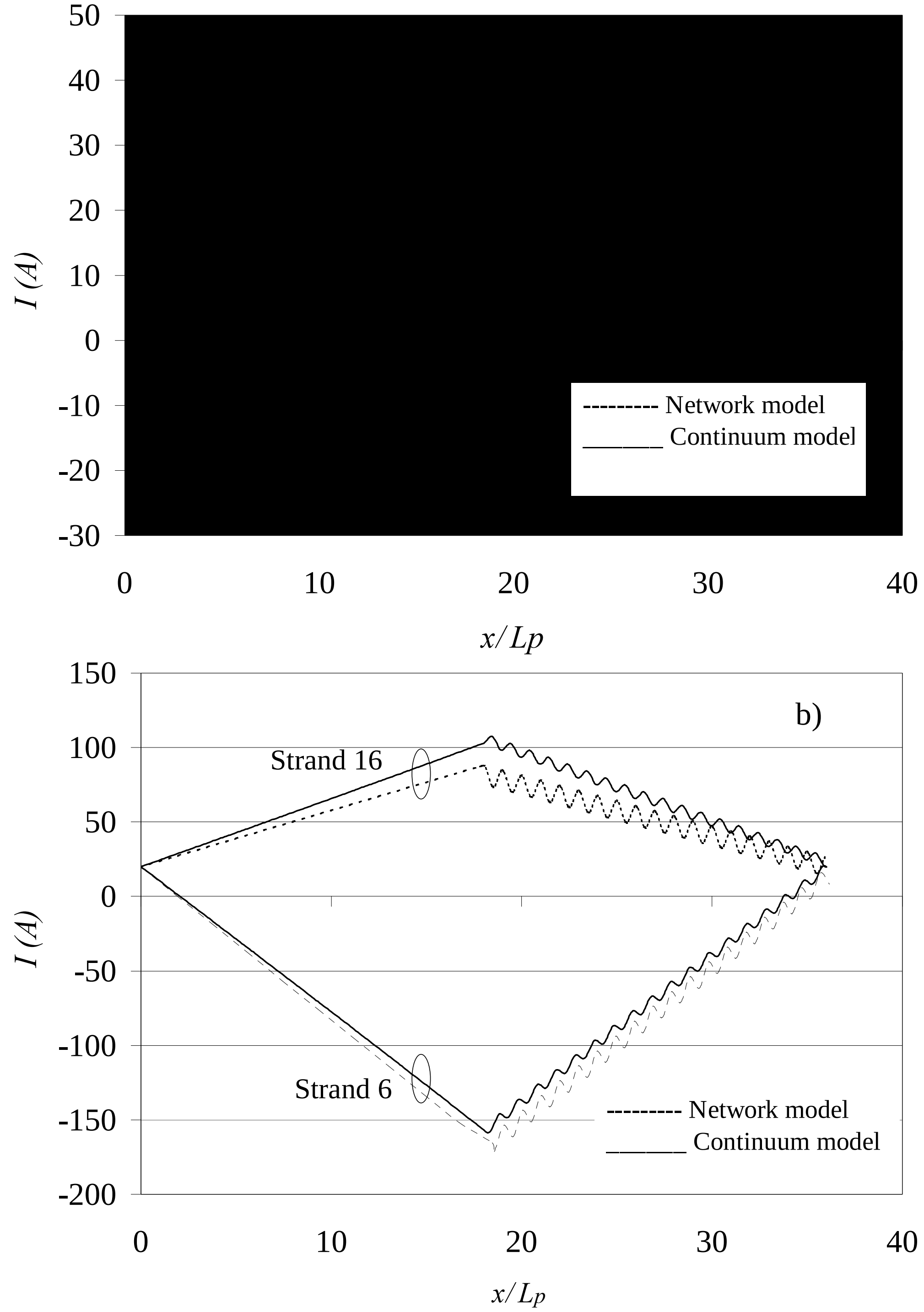

Fig. 3.2 *Comparison between network and continuum model: behaviour of Boundary Induced Coupling Currents in a 16 strands Rutherford cable at the regime condition in the case of a step-like spatial distribution of the magnetic flux density perpendicular to the broad face of the cable. a) $r_h = 1.54\ 10^{-8}$ Ω/m b) $r_h = 1.54\ 10^{-11}$ Ω/m.*

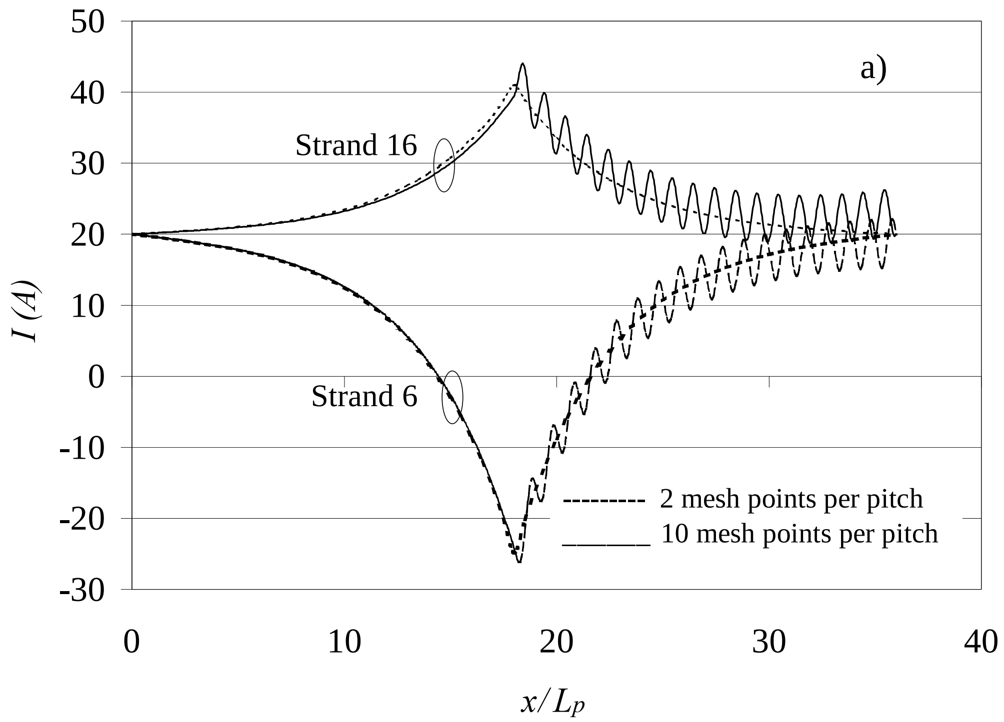

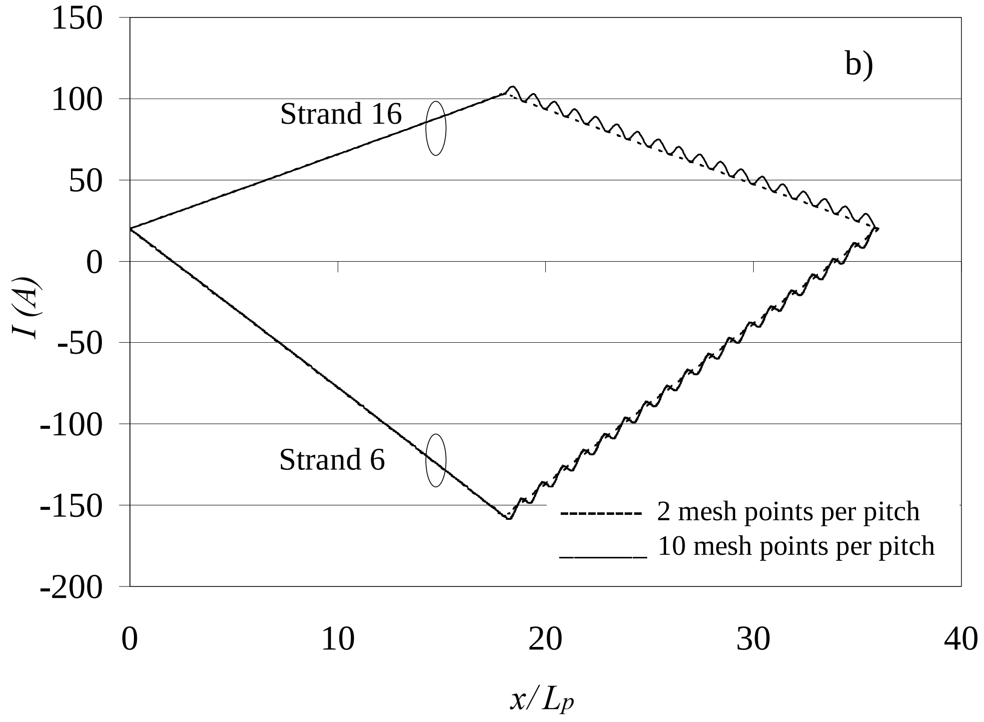

Fig. 3.3 *Comparison between two different calculations performed with the continuum model in the same cases reported in Fig. 3.2. The two calculations are performed with a different number of mesh points per pitch, showing that the main BICC's can be well described with only two mesh points per pitch.*

Our aim in this comparison is to model correctly the behaviour of the long range coupling currents, neglecting the influence of the short range coupling currents. For this reason we have tried to find the minimum number of mesh points needed for a correct evaluation of the long range BICC's. We have found that with 2 mesh points per pitch the main BICC's can be very well approximated for the case-study previously described (see Fig. 3.3). If the longitudinal variations of the time derivative of the field were less sharp, appropriate meshing strategies could lead to even larger meshes.

Considering that in the network model there are (5N-3) unknowns per calculation band [27], and N bands per pitch, we end up with a total of (5N-3)·N unknowns per pitch. In the actual implementation of the continuum model a point collocation method [70] has been used for the numerical solution of system (3.7), with two gaussian points per elemental mesh. This results in a total of 2$M_P N$ unknowns per pitch, where M_P is the number of mesh points per pitch. The ratio of the number of unknowns per pitch of cable in the two models is then equal to:

$$\Re = \frac{5\,(N-3)}{2\,M_P}$$

(3.38)

In the case reported in Fig. 3.4 $\Re$ is approximately equal to 16. This leads to a remarkable computational advantage, which allows the application of the distributed parameters model to the study of real long Rutherford cables operating in accelerator magnets, as shown in Section 5.3.

3.4 COMPARISON WITH THE NETWORK MODEL: CIC CONDUCTORS

We have implemented a network model for the study of current distribution in short samples of simple cable in conduit conductors, in order to evaluate the consistence of the distributed parameters model, and the equivalence of the two models in simple cases.

In particular, we have simulated the current redistribution after quench of one strand in a short sample of a triplex cable (Fig. 3.4). The cable is 1m. long, and is composed of three strands wound helicoidally along a straight axis, with a twist pitch L_p equal to 2.5 cm. The lumped parameters network model is illustrated schematically in Fig. 3.5. The model is applicable to a generic number of strands and to a generic time varying operation current. The model has been implemented both in SPICE and with a Fortran programme obtaining a good agreement between the two codes.

The network model has been implemented in two different ways. In a first implementation (N1) the cable is divided into 40 sectors having the same length as the cable twist pitch. In the second implementation (N2) the cable is divided into 80 sectors having the same length as half of the cable twist pitch.

The mutual inductance between sector i of strand h and sector j of strand k is indicated with $L_{h,\ i,\ k,\ j}$ as shown in Fig. 3.5 for the first two sectors of two generic strands. The self inductance $L_{h,\ i}$ of sector i of strand h is indicated with $L_{h,\ i,\ h,\ i}$. Both self and mutual inductances have been calculated numerically as explained in Appendix B, eq. (B.2). The self inductance of the first sector of strand 1 and the mutual inductances between this sector and adjacent sectors of the same strand, ($L_{1,\ 1,\ 1,\ i}$ with i = 1, 20 in model (N1)), is plotted in Fig. 3.6a versus the distance d = (i-1) L_P/2 of these sectors from sector 1.

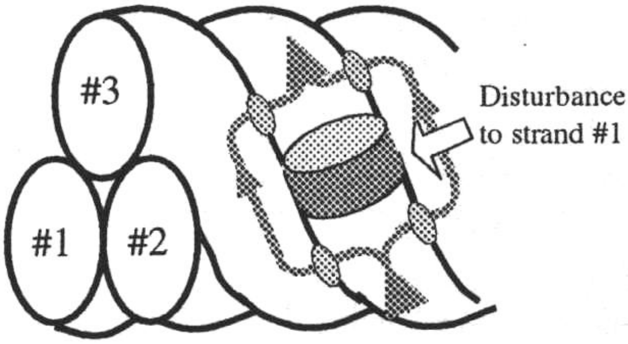

Fig. 3.4 *Quench in a sector of one strand of a triplex cable*

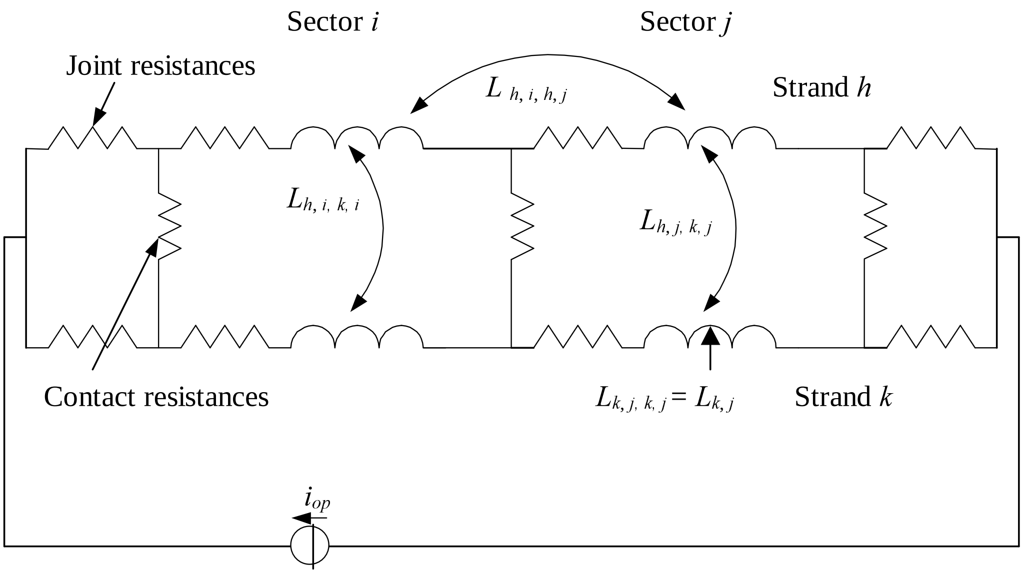

Fig. 3.5 *Lumped parameters network model showing two sectors of two typical strands*

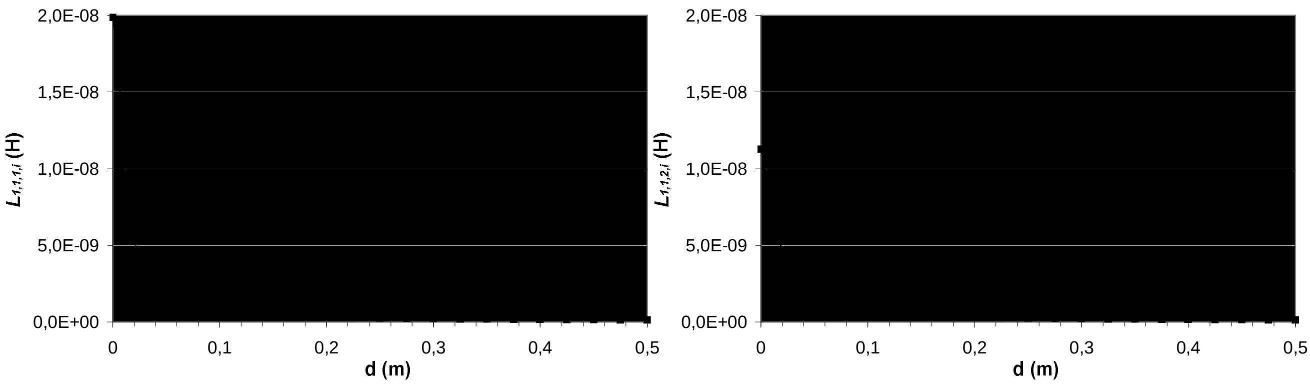

Fig. 3.6 *Dependence of the mutual inductance between strand sectors on the distance along the cable axis. a) Mutual inductances between sectors of the same strand $L_{1,1,1,i}$ b) Mutual inductances between sectors of two different strands $L_{1,1,2,i}$*

The mutual inductances among the first sector of strand 1 and different sectors of strand 2 ($L_{1,\ 1,\ 2,\ i}$ with i = 1, 40) are plotted in Fig. 3.6b versus the distance d of these sectors from sector 1 of strand 1. We can notice that the mutual inductance between different strand sectors obviously decreases with the distance, but in principle the mutual inductances between all the different strand sectors of the cable should be considered. For this reason we have performed simulations with the network model both keeping the mutual inductances among all the strand sectors (N1a-N2a), and neglecting the mutual inductances between strand sectors corresponding to different positions along the cable length, i.e. setting $L_{h,\ i,\ k,\ j} = 0$ if $i \neq j$ (N1b-N2b).

The effect of different joint resistances on the current distributions can be taken into account. However, the joint resistances have been taken all equal to zero, for a simple comparison with the distributed parameters model associated with the boundary conditions (3.15), which describe equipotential cable end surfaces.

The distributed parameters circuit model has been implemented in two different ways (D1 and D2), distributing the contact resistances and the mutual inductances along two different smearing lengths, L_P and $L_P / 2$. It is important, in order to show the consistence of the distributed parameters model, that the results of the current re-distribution among the different strands are not influenced significantly by the choice of the smearing length. The values of mutual and self inductances for the distributed parameters model are reported in Table 3.1.

Smearing length	L_P	$L_P/2$
Self inductances $l_{11} = l_{22} = l_{33}$ (μH)	0.79	0.67
Mutual inductances $l_{12} = l_{21} = l_{13} = l_{31} = l_{23} = l_{32}$ (μH)	0.45	0.33

Table 3.*1 Mutual induction coefficients for matrix* ***l*** *with two different smearing lengths*

Strand diameter	1 mm
Cabling pitch	25 mm
Cable length	1 m
Initial time of the external disturbance	T=1 ms
Final time of the external disturbance	T=2 ms
Final resistance of the quenched strand	$0.5 \cdot 10^{-3}$ Ω/m
Joint resistance	0 Ω

Operation current	1000 A

Table 3.*2 Simulation of current redistribution in a triplex cable after quench in one strand: data*

The parameters chosen for the simulations of redistribution after quench are shown in Table 3.2. The quenched zone is 5 cm. long and is placed in the middle of strand 1. The quench is simulated by means of a sudden increase of the strand longitudinal resistance in the quenched zone arising to the value of the normal matrix resistance which is in parallel to the superconducting filaments. The operation current is kept constant during the simulations at the value of 1000 A.

The space and time dependence of the current in the quenched strand calculated with the distributed parameters model (D1) is shown in Fig. 3.7. It can be noticed that the length of the region from which the strand curent is deviated to other strands increases in time. We have performed several simulations with different contact conductances, in the range 10^5 – 10^7 S/m, confirming that the typical redistribution times and the width of the quenched zone decrese with increasing the contact conductances, as shown in [62] with simplified analytical calculations.

The data reported in the following have to be considered as examples of many tests performed to verify the agreement of the different models.

3.4.1.Distributed parameters model (D1) versus distributed parameters model (D2)

A comparison between the currents in the strands 1 and 3 calculated with the distributed parameters models D1 and D2 is presented in Fig. 3.8. The curves are very close. A very good agreement between the two models is found, both considering time and space dependence of the strand currents. This result confirms the consistence of the distributed parameters model and the possibility to smear the distributed parameters along different lengths.

3.4.2 Distributed parameters model (*D1*) versus lumped parameters (*N1b*)

The comparison between strand currents found with the distributed parameters model and the lumped parameters model are in good agreement for both space and time dependence, as shown in Fig. 3.9.

The same type of agreement, in many different situations and between all the three strand currents in space and time, has been obtained between the lumped parameters model made of 40 sectors and the lumped parameters model made of 80 sectors, both considered in the version which does not include the mutual inductances between far strand sectors.

As a conclusion, the two distributed parameters models behave identically to the two lumped parameters models which neglect inductances between far strand sectors. In addition we found that with these four models the two non quenched strands carried exactly the same currents in every situation.

3.4.3 Distributed parameters model *(D2)* versus complete lumped parameters model *(N2a*)

Some small deviation from this agreement is found when considering lumped network models including all the mutual inductances between the strand sectors (N1a and N2a). A comparison between the complete network model (N2a) and the distributed parameters model D2 is shown in Fig. 3.10. The basic features and behaviour of the currents are identical. Only a small difference in the amplitude of the current in the non quenched strand is found. In particular, it is found that the current in the two non quenched strands calculated with model N2a is not exactly the same, due to a long range coupling current flowing all along the two strands and closing at the joint resistances. The currents in the two non quenched strands along the cable length are shown in Fig. 3.11, for the case of joint resistances all equal to zero. The amplitude of this long range current is strongly reduced with increasing the joint resistance.

Beside this small difference (about 2% of the total strand current), the agreement between the distributed parameters models and the network models including all the mutual inductances is satisfactory, giving therefore confidence in the application of the distributed parameters model to more complex situations.

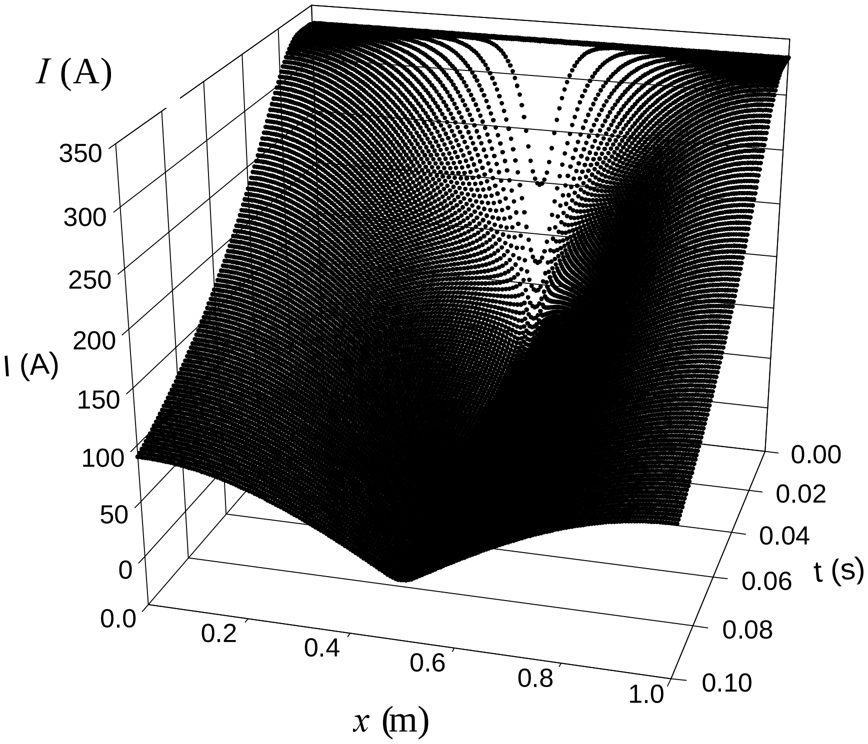

Fig. 3.7 *Space and time dependence of the current in the quenched strand*

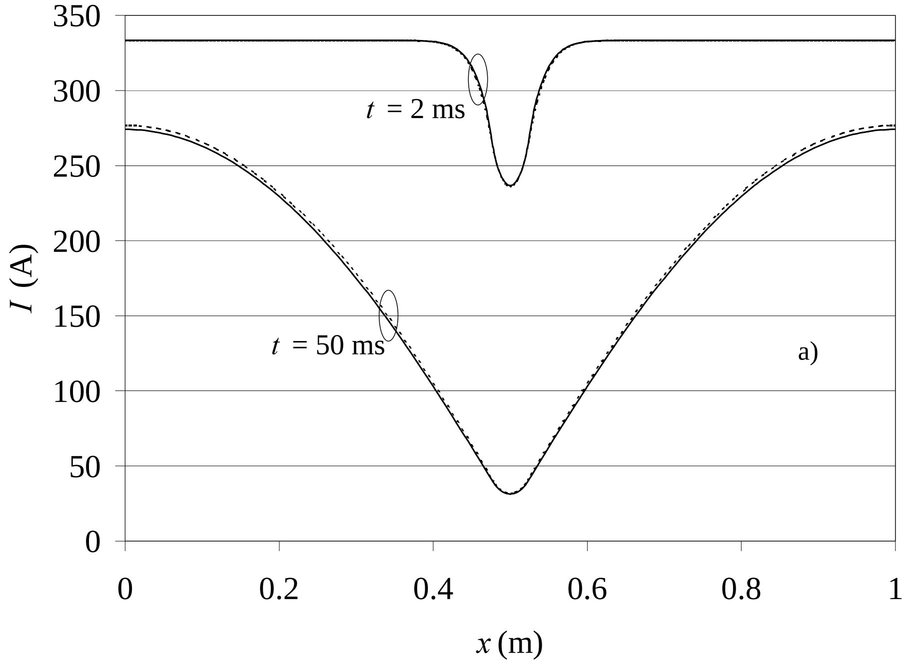

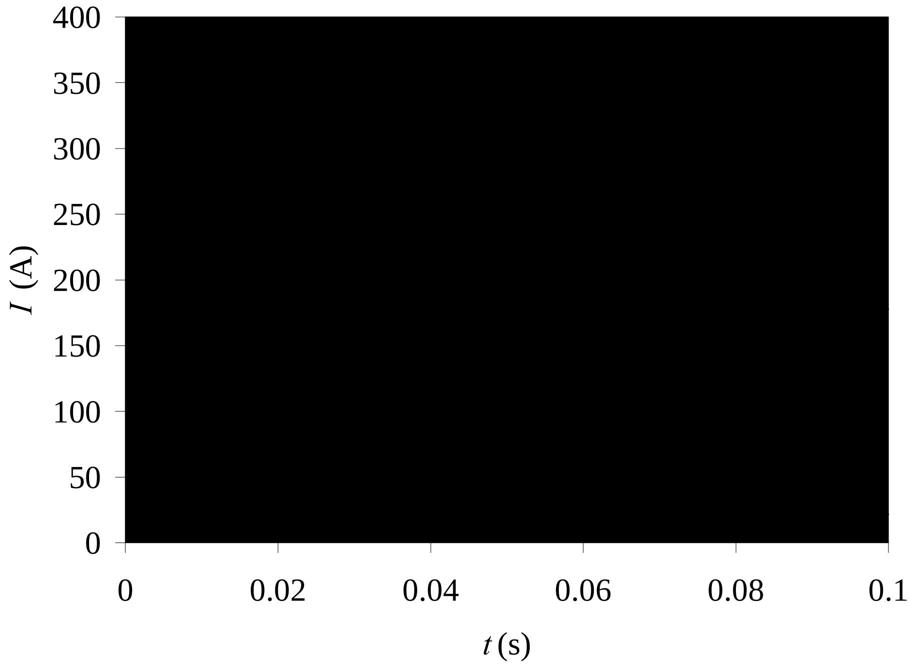

Fig. 3.8 *Comparison between distributed parameters model with smearing length equal to 1 pitch (dotted lines) and half a pitch (solid lines). Current in the quenched strand a) Space dependence at two different times b) Time dependence in two different positions*

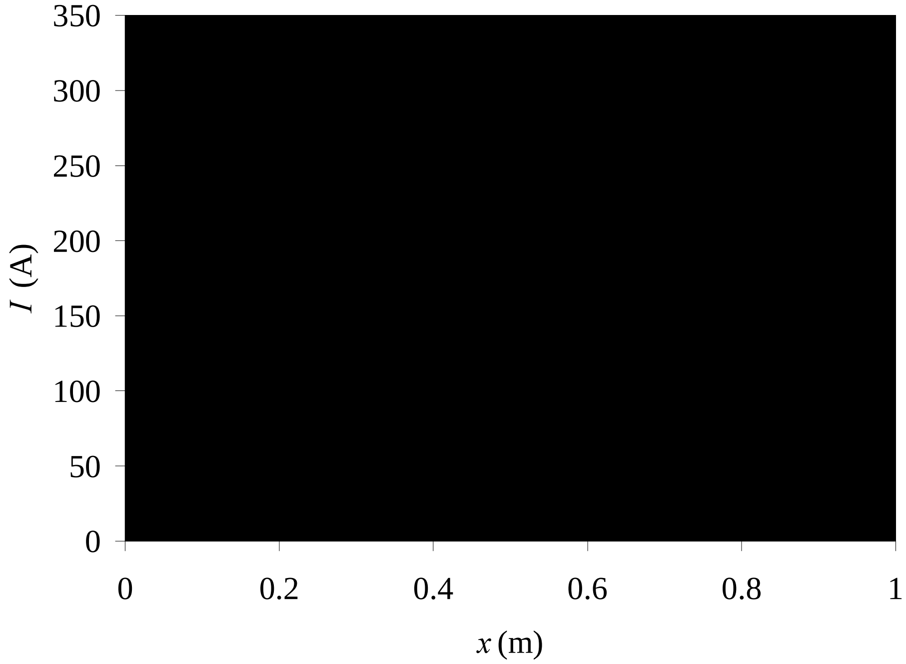

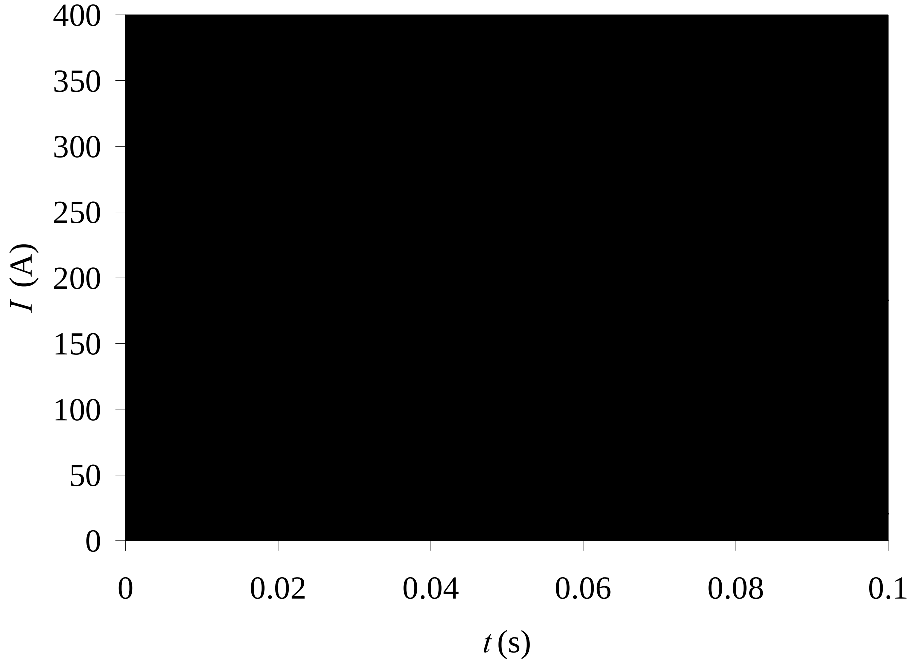

Fig. 3.9 *Comparison between distributed parameters model with smearing length equal to 1 twist pitch (dotted line) and lumped parameters model N1b (40 sectors, without mutual inductances between far strand sectors). Current in the quenched strand a) Space dependence at two different times b) Time dependence in two different positions.*

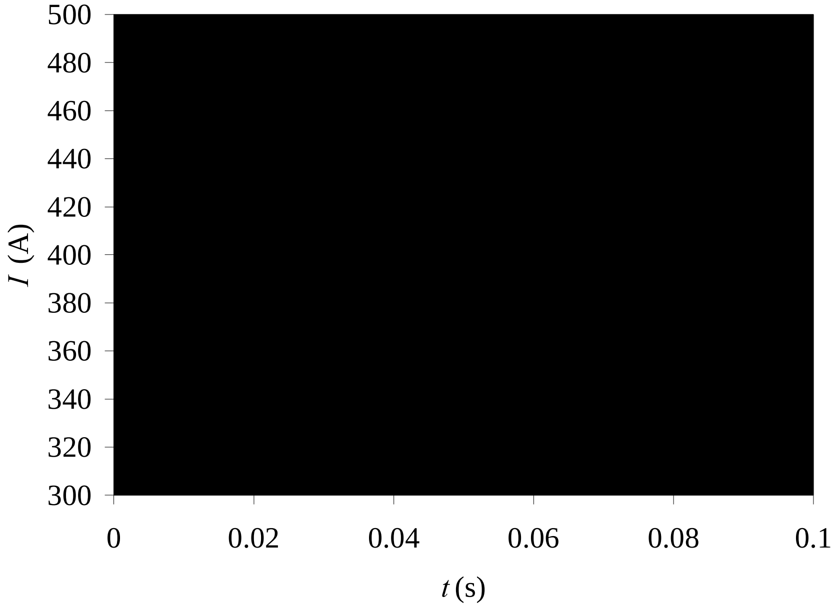

Fig. 3.10 *Comparison between distributed parameters model D2 (dotted line) and the lumped parameters model (solid line) including all mutual inductances between strand sectors (N2a). Current in the non-quenched strand 2 vs time from quench initiation.*

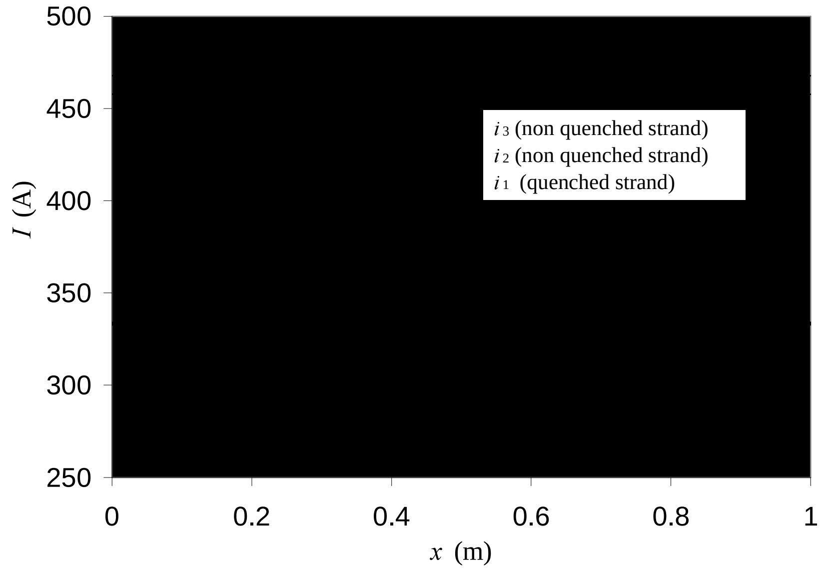

Fig. 3.11 *Currents obtained with the complete lumped parameters network model. After 50 ms from the quench initiation, a difference in the current of the non quenched strands is observed corresponding to a long current loop flowing between the two strands along the whole cable length. At t = 50 ms the current in the quenched strand is low and is not reported.*

3.5 EQUIVALENT "SUPERSTRANDS"

We have shown in Section 3.3 that the distributed parameters model allows a remarkable reduction of the number of unknowns of the problem of current distribution. A further reduction of the number of unknowns of the problem can be obtained by introducing equivalent "superstrands". These "superstrands" are made assembling a certain number of strands of the cable and defining the appropriate parameters for the solution of the equations of current diffusion in these equivalent "superstrands".

Let the N strands of the cable be divided in g_s groups of strands which we call "superstrands". Each strand in the superstrand carries the same current, equal to the total current in the superstrand divided by the number of strands in the superstrand. Each group can be represented by means of a set G_i of k_i integer numbers representing the indexes of the strands owing to superstrand i.

In order to define the equivalent per unit length longitudinal resistances the value of the parallel resistance between the strands in each superstrand can be taken:

$$\frac{1}{r_i^{sup}} = \sum_{h \in G_i} \frac{1}{r_h}$$

(3.39)

where r_i^{sup} is the longitudinal resistance of the superstrand i. If all the strands in the superstrand have r_h equal to zero also r_i^{sup} must be taken equal to zero.

In order to define contact conductances between superstrands, all the possible transverse paths between two generic superstrands must be considered, summing up the corresponding conductances. The contact conductance $g_{i,j}^{sup}$ between superstrand i and superstrand j can be calculated as follows:

$$g_{i,j}^{sup} = \frac{1}{2} \sum_{h \in G_i} \sum_{l \in G_j} g_{h,l}$$

(3.40)

Considering for example superstrand 1 made of strands (1, 2), and superstrand 2 made of strands (3, 4), the contact conductance between superstrand 1 and superstrand 2 can be calculated as:

$$g_{1,2}^{sup} = g_{1,3} + g_{2,3} + g_{1,4} + g_{2,4} \qquad (3.41)$$

A correct choice of the strands owing to a superstrand can be made taking strands which follow a close path along the cable length, so that the vector potential of the external field is approximately equal for all strands. The best way to build superstrands in the case of Rutherford cables is to take adjacent strands, so that if the strands are numbered as in Fig. 2.3, the strands in each superstrand have consecutive indexes. In this case a fast way to calculate an equivalent external voltage is to take the average external voltage of the strands in each superstrand.

The external voltage can be calculated as follows:

$$v_i^{ext\,sup} = \frac{1}{k_i} \sum_{h \in G_i} v_h^{ext}$$

(3.42)

where $v_i^{ext\,sup}$ is the external voltage relative to superstrand *i*.

Finally, if the original matrix **l** for the complete cable has been calculated or measured, the equivalent mutual inductances matrix relative to superstrands, $\mathbf{l}^{sup}$, can be evaluated considering that the two cables, made of strands or superstrands, must have the same energy per unit length associated to the currents flowing in either strands or superstrands. In order to impose this condition, we can write the following equation:

$$\frac{1}{2}\mathbf{i}^{sup^T}\mathbf{l}^{sup}\mathbf{i}^{sup} = \frac{1}{2}\mathbf{i}^T\mathbf{l}\,\mathbf{i}$$

(3.43)

where $\mathbf{i}^{sup}$ is the vector of the currents flowing in the equivalent superstrands.

As an example we calculate the values of matrix $\mathbf{l}^{sup}$ in the case of a cable made of four strands and divided into two superstrands of index 1 and 2 made of strands (1, 2) and (3, 4) respectively. The following conditions have to be imposed:

$$
\begin{bmatrix} i_1^{sup} & i_2^{sup} \end{bmatrix} \begin{pmatrix} l_{11}^{sup} & l_{12}^{sup} \\ l_{21}^{sup} & l_{22}^{sup} \end{pmatrix} \begin{bmatrix} i_1^{sup} \\ i_2^{sup} \end{bmatrix} = \begin{bmatrix} i_1 & i_2 & i_3 & i_4 \end{bmatrix} \begin{pmatrix} l_{11} & l_{12} & l_{13} & l_{14} \\ l_{21} & l_{22} & l_{23} & l_{24} \\ l_{31} & l_{32} & l_{33} & l_{34} \\ l_{41} & l_{42} & l_{43} & l_{44} \end{pmatrix} \begin{bmatrix} i_1 \\ i_2 \\ i_3 \\ i_4 \end{bmatrix}
$$

$$\Downarrow$$

$$
\begin{bmatrix} 2i_1 & 2i_3 \end{bmatrix} \begin{pmatrix} l_{11}^{sup} & l_{12}^{sup} \\ l_{21}^{sup} & l_{22}^{sup} \end{pmatrix} \begin{bmatrix} 2i_1 \\ 2i_3 \end{bmatrix} = \begin{bmatrix} i_1 & i_1 & i_3 & i_3 \end{bmatrix} \begin{pmatrix} l_{11} & l_{12} & l_{13} & l_{14} \\ l_{21} & l_{22} & l_{23} & l_{24} \\ l_{31} & l_{32} & l_{33} & l_{34} \\ l_{41} & l_{42} & l_{43} & l_{44} \end{pmatrix} \begin{bmatrix} i_1 \\ i_1 \\ i_3 \\ i_3 \end{bmatrix}
$$

(3.44)

We obtain the following values for matrix $\mathbf{l}^{sup}$:

$$
\begin{aligned}
l_{11}^{sup} &= \frac{1}{4}\left(l_{11} + l_{12} + l_{21} + l_{22}\right) \\
l_{12}^{sup} &= \frac{1}{4}\left(l_{13} + l_{14} + l_{23} + l_{24}\right) \\
l_{21}^{sup} &= \frac{1}{4}\left(l_{31} + l_{32} + l_{41} + l_{42}\right) \\
l_{22}^{sup} &= \frac{1}{4}\left(l_{33} + l_{34} + l_{43} + l_{44}\right)
\end{aligned}
$$

(3.45)

All the new parameters can be directly inserted in the same equations used for the strands. We have applied this procedure in several cases obtaining a good approximation of the behaviour of the current distribution in the real cable. We report in Fig. 3.12 and 3.13 the description of the BICC's in the same case study already reported in Fig. 3.2. The original cable is a Rutherford cable made of 16 strands, while the equivalent cable is made of 8 superstrands defined as above. It can be noticed that the current in the superstrands (which has been divided by two for the sake of comparison) is included between the values of the currents of the two strands represented by the superstrand. This is true both in time (see Fig. 3.12a, 3.13a) and in space (see Fig. 3.12b, 3.13b).

The possibility of analysis through superstrands offered by the distributed parameters model contributes to a further remarkable reduction of the number of unknowns when studying very long cables.

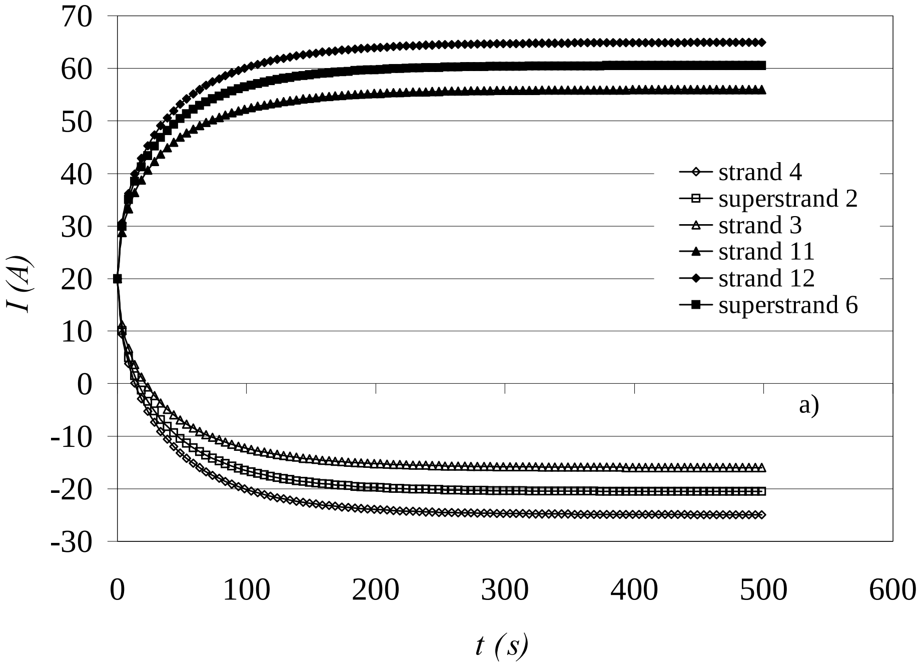

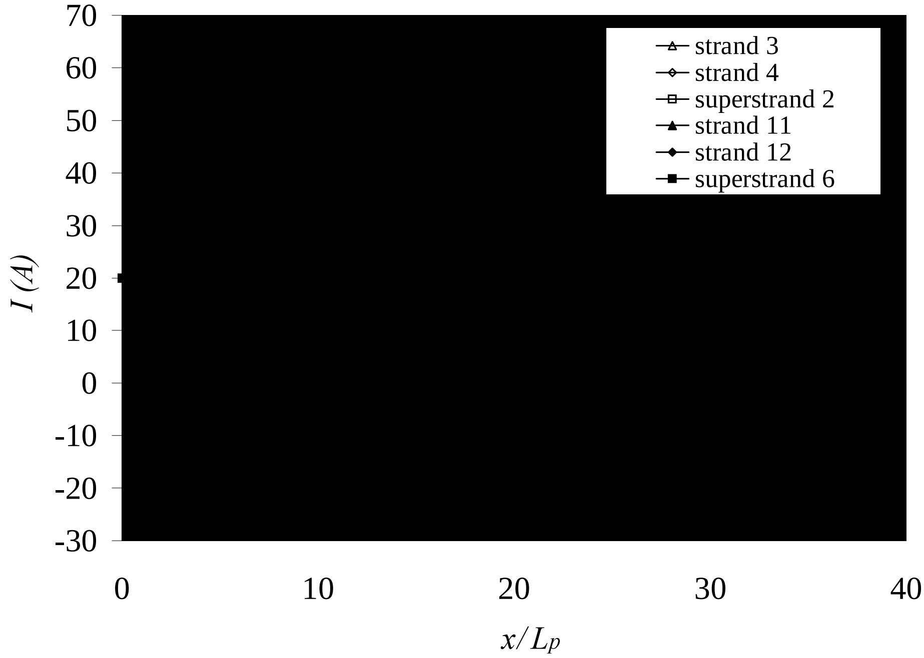

Fig. 3.12 *Dependence on time (a) and space (b) of BICC's induced in the strands of a 16 strands Rutherford cable and in the superstrands of a 8-superstrands simplified Rutherford cable. Superstrand 2 contains strands 3 and 4 while Superstrand 6 contains strands 11 and 12. The currents are calculated in the same case reported in Fig. 3.2.a.*

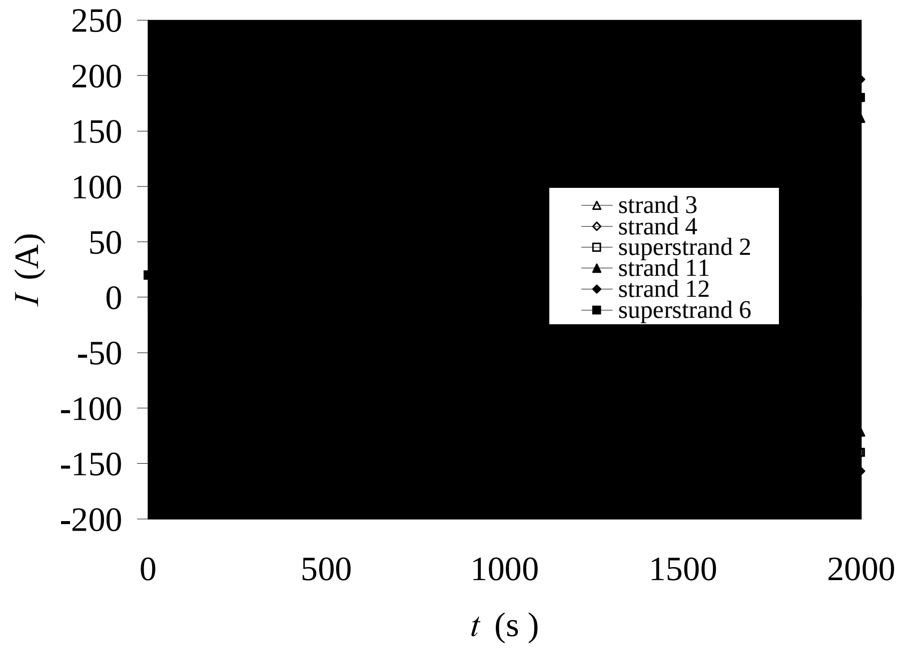

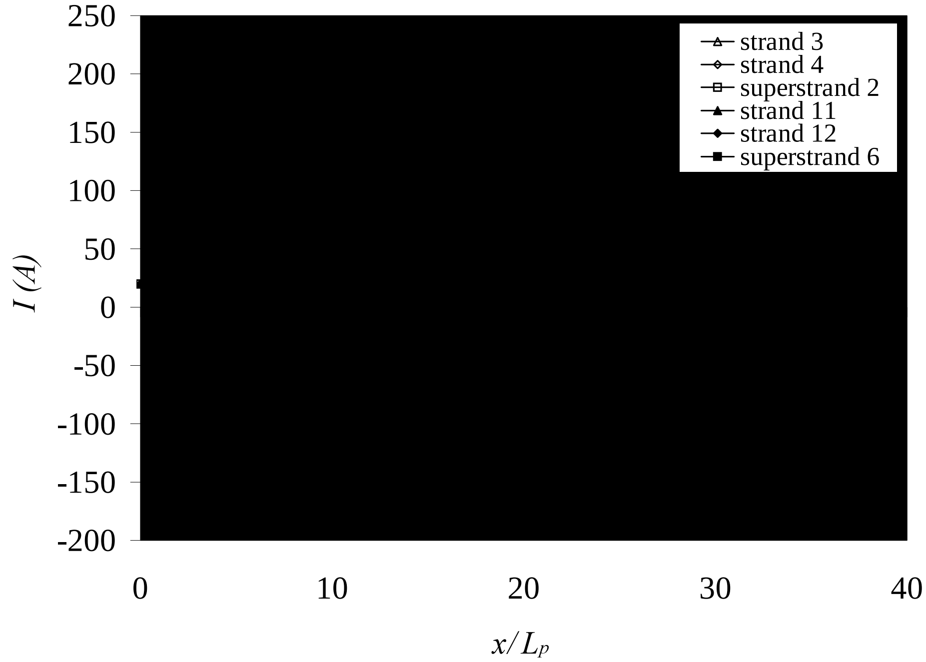

Fig. 3.13 *Dependence on time (a) and space (b) of BICC's induced in the strands of a 16 strands Rutherford cable and in the superstrands of a 8-superstrands simplified Rutherford cable. Superstrand 2 contains strands 3 and 4 while Superstrand 6 contains strands 11 and 12. The currents are calculated in the same case reported in Fig. 3.2.b.*

3.6 COMPARISON BETWEEN NETWORK AND DISTRIBUTED PARAMETERS MODEL: 2-STRAND CABLE SUBJECT TO A UNIFORM FIELD RAMP

In order to show the difference between the distributed parameters model with uniform **g** matrix and the network model in the evaluation of the short range coupling currents, we consider the simple case of a two strand-cable subject to a uniform time dependent external field. In this situation an alternate flux, changing sign every half twist pitch, is applied along the cable length in the loops formed by the two strands. We indicate with A_l the area of the loops formed between the two strands.

We can write:

$$A = \delta \; p/2$$

(3.46)

where δ is the width of the loop in the case of a loop of rectangular shape or another characteristic dimension.

If the strands are in the perfectly superconducting state, and the regime condition is considered, equations (3.4.a) and (3.4.b) can be written as follows:

$$\frac{\partial \; v}{\partial \; x} = v^{ext}$$

(3.47)

$$\frac{\partial \; i}{\partial \; x} = g\,v$$

(3.48)

which give:

$$\frac{\partial^2 i}{\partial x^2} = g v^{ext}$$

(3.49)

For a simple, analytical solution we calculate the value of a uniform v^{ext} applied along half of a cable twist pitch:

$$v^{ext} = -\frac{\dot{\phi}}{L_P/2} = -\dot{B}\delta$$

(3.50)

The following boundary conditions can be associated to Eq. (3.50), due to the inversion of the current flowing in each strand in longitudinal direction every half twist pitch:

$$
\begin{aligned}
&i(0) = 0 \\
&i(L_P / 2) = 0
\end{aligned}
$$

(3.51)

The integration of Eq. (3.50) with the boundary conditions (3.51) gives:

$$i(x) = g\dot{B}\delta\left(x\frac{L_P}{4} - \frac{x^2}{2}\right)$$

(3.52)

Substituting in (3.52) the smeared value of g obtained by the knowledge of the cross contact resistance (see Eq. (3.26)):

$$g = \frac{2}{L_P R_c}$$

(3.53)

we obtain:

$$i(x) = \frac{2}{L_P R_c}\dot{B}\delta\left(x\frac{L_P}{4} - \frac{x^2}{2}\right)$$

(3.54)

which is a parabolic curve with a maximum in $x = p/4$.

The value of this maximum is:

$$i\left(\frac{L_P}{4}\right) = \frac{1}{16R_c}L_P\dot{B}\delta$$

(3.55)

This current shape is the same along the whole cable length with an alternated sign due to the change of sign of the magnetic flux.

Solving the same problem of current distribution in a 2-strand cable subject to a uniform field ramp by means of the network model, we obtain an uniform value of current in the strands, which changes sign every half twist pitch along the cable length. This value can be obtained considering that in a loop between two strands the time derivative of the flux must be equal to the sum of the voltage drops across the cross contact resistances.

Indicating with I the absolute value of the current in each strand calculated with the network model, and imposing the boundary conditions $i_1 = i_2 = I = 0$ at the cable ends, we obtain the following solution:

$$
\begin{aligned}
&i_1 = -I \qquad && kL_P \le x \le \left(k + \frac{1}{2}\right) L_P \\
&i_1 = +I \qquad && \left(k + \frac{1}{2}\right) L_P \le x \le (k+1) L_P \qquad\qquad k = 0,1,2,3..... \\
&i_2 = -i_1 &&
\end{aligned}
$$

(3.56)

The absolute value of the current through the contact resistances is equal to the variation of the longitudinal current in any of the two strands crossing with the other strand:

$$i_{12} = \Delta i = 2I$$

(3.57)

Applying the Faraday's law to a generic loop, we obtain:

$$4IR_c = -\dot{\phi} \Rightarrow I = -\frac{\dot{\phi}}{4R_c}$$

(3.58)

We show in Fig. 3.14 a comparison between the strand currents calculated by means of the two network model and the distributed parameters model in this simple case.

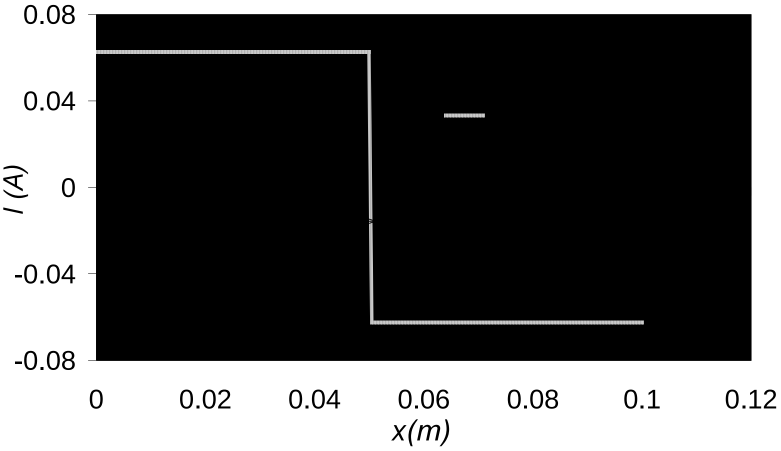

Fig. 3.14 *Comparison between the current in the strands of a 2 strands cable, with* $R_c = 20\ 10^{-6}\ \Omega$*, db/dt=0.01 T/s,* L_P*=100 mm,* δ*=10 mm*

The voltage difference between the two strands along the cable length can be obtained by means of Eq. (3.48):

$$v = \frac{1}{g}\frac{\partial i}{\partial x} = \dot{B}\delta\left(\frac{p}{4} - x\right)$$

(3.59)

The power dissipated in half pitch can be calculated with the distributed parameters model by means of the following integral:

$$P_{dis}^{distributed} = \int_0^{p/2} v(x)\, i_{12}(x)\, dx = \int_0^{p/2} g v^2(x) dx = \frac{1}{48R_c}\dot{B}^2\delta^2 L_P{}^2$$

(3.60)

The power per twist pitch of cable calculated with the network model is equal to:

$$P_{dis}^{network} = R_c(2I)^2 = \frac{1}{16R_c}\dot{B}^2\delta^2 L_P{}^2$$

(3.61)

The following ratio of the power dissipated per twist pitch of cable calculated with the two models can be found in this situation:

$$\frac{P_{dis}^{network}}{P_{dis}^{distributed}} = 3$$

(3.62)

It appears clearly from these calculations that if the distributed parameters model in the form with uniform interstrand conductances (Equations 3.6) is used for the evaluation of long range strand currents, a suitable model for the evaluation of the power dissipated by the short range coupling currents must be introduced for a complete calculation of ac losses.

However, as we will show in the next paragraph, the distributed parameters model can be generalized to the study of multistrand superconducting cables without any assumption on the interstrand conductances matrix.

3.7 GENERALIZATION OF THE DISTRIBUTED PARAMETERS MODEL

Interstrand conductances in mulstistrand superconducting cables depend on several factors, including the level of oxidation of bare strands, the size of the contact surfaces, the soldering of the cable, the presence of resistive barriers, the matrix material and the pressure applied transversely on the cable.

If some of these factors vary along the cable length, the matrix of interstrand conductances **g** is not uniform along the cable length, and equations (3.6) cannot be applied. It is however possible to generalize the distributed parameters model to study cables with non uniform interstrand conductances along the cable length.

In order to do this we consider the voltage differences of any strand from strand *N* defined in (3.12), and we rewrite system (3.13) in the following form:

$$\mathbf{e}^* = [\mathbf{g}^*]^{-1} \frac{\partial\, \mathbf{i}^*}{\partial\, x}$$

(3.63)

where we have defined the following vectors and matrices:

$$\mathbf{e}^* = \begin{bmatrix} e_1 \\ e_1 \\ \vdots \\ e_{N-1} \end{bmatrix} \qquad \mathbf{g}^* = \begin{bmatrix} -\sum_{\substack{k=2 \\ k\neq 1}}^{N} g_{1k} & g_{12} & \cdots & g_{1N} \\ g_{21} & -\sum_{\substack{k=1 \\ k\neq 2}}^{N} g_{2k} & \cdots & g_{2N} \\ \vdots & & & \\ g_{N-1,1} & g_{N-1,2} & \cdots & -\sum_{\substack{k=1 \\ k\neq N-1}}^{N} g_{N-1k} \end{bmatrix} \qquad i^* = \begin{bmatrix} i_1 \\ i_1 \\ \vdots \\ i_{N-1} \end{bmatrix}$$

(3.64)

It can be shown that matrix **g*** is always invertible, allowing to write system (3.63).

Considering system (3.4.a) and subtracting the last equation to all the first N-1 equations, we obtain:

$$\frac{\partial\, \mathbf{e}}{\partial\, x} = -\mathbf{r}^{**}\,\mathbf{i} - \mathbf{l}^{**}\,\frac{\partial\, \mathbf{i}}{\partial\, t} + \mathbf{e}^{ext}$$

(3.65)

where **i** was defined in (3.5.a) and we have introduced the following vectors and matrices:

$$\mathbf{e} = \begin{bmatrix} e_1 \\ e_1 \\ \vdots \\ e_{N-1} \\ 0 \end{bmatrix} \qquad \mathbf{e}^{ext} = \begin{bmatrix} v_1^{\ ext} - v_N^{\ ext} \\ v_2^{\ ext} - v_N^{\ ext} \\ \vdots \\ v_{N-1}^{\ ext} - v_N^{\ ext} \\ 0 \end{bmatrix}$$

(3.66.a)

$$\mathbf{r}^{**} = \begin{bmatrix} r_1 & 0 & \cdots & -r_N \\ 0 & r_1 & \cdots & -r_N \\ \vdots & & & \\ 0 & 0 & \cdots r_{N-1} & -r_N \\ 0 & 0 & & 0 \end{bmatrix} \quad \mathbf{l}^{**} = \begin{bmatrix} l_{1,1} - l_{N,1} & l_{1,2} - l_{N,2} & l_{1,N} - l_{N,N} \\ l_{2,1} - l_{N,1} & l_{2,2} - l_{N,2} & l_{2,N} - l_{N,N} \\ \vdots & & \\ l_{N-1,1} - l_{N,1} & l_{N-1,1} - l_{N,2} & l_{N-1,N} - l_{N,N} \\ 0 & 0 & 0 \end{bmatrix}$$

(3.66.b)

Eliminating the last identity in (3.65), and introducing (3.63) in (3.65) we obtain the following system:

$$\frac{\partial}{\partial x}\left(\hat{\mathbf{c}}\frac{\partial \mathbf{i}}{\partial x}\right)=-\hat{\mathbf{r}}\,\mathbf{i}-\hat{\mathbf{l}}\,\frac{\partial \mathbf{i}}{\partial t}+\hat{\mathbf{e}}^{ext}$$

(3.67)

where matrix $\hat{\mathbf{c}}$ is obtained adding a column made of 0 to matrix $[\mathbf{g}^*]^{-1}$ while matrices $\hat{\mathbf{r}}$ and $\hat{\mathbf{l}}$ and vector $\hat{\mathbf{e}}^{ext}$ are defined as follows:

$$\hat{\mathbf{r}}=\begin{bmatrix} r_1 & 0 & \cdots & -r_N \\ 0 & r_1 & \cdots & -r_N \\ \vdots & & & \\ 0 & 0 & \cdots r_{N-1} & -r_N \end{bmatrix} \hat{\mathbf{l}}=\begin{bmatrix} l_{1,1}-l_{N,1} & l_{1,2}-l_{N,2} & l_{1,N}-l_{N,N} \\ l_{2,1}-l_{N,1} & l_{2,2}-l_{N,2} & l_{2,N}-l_{N,N} \\ \vdots & & \\ l_{N-1,1}-l_{N,1} & l_{N-1,1}-l_{N,2} & l_{N-1,N}-l_{N,N} \end{bmatrix} \hat{\mathbf{e}}^{ext}=\begin{bmatrix} v_1{}^{ext}-v_N{}^{ext} \\ v_2{}^{ext}-v_N{}^{ext} \\ \vdots \\ v_{N-1}{}^{ext}-v_N{}^{ext} \end{bmatrix}$$

(3.68)

Finally we need to add to system (3.67) the law of conservation of the total operation current at any time and position:

$$\sum_{h=1}^{N} i_h = i_{op}$$

(3.69)

Equations (3.67) and (3.69) represent the extension of the distributed parameters model to the analysis of cables with variable tranverse conductances and are in a form that is well suited for the coupling with a complete thermal and fluid-dynamic description of the refrigeration system, as shown in [74].

CHAPTER 4

THE ANALYTICAL SOLUTION

INTRODUCTION

An important advantage of the description of current distribution phenomena by means of partial differential equations is the possibility to determine an analytical solution of the problem equations [65]. The analytical solution can be useful for the validation of numerical codes, and for fast parametric studies on current distribution and redistribution phenomena.

The study of current distribution and redistribution phenomena by means of the analytical solution of the equations of current diffusion in a 2-strand cable has been already carried on in several works [10, 59, 73]. In particular, Turck [73] analysed current sharing between two non-insulated coupled superconducting wires with different joint resistances, with and without superficial oxides. The equilibrium current sharing imposed at the input by the boundary conditions propagates axially along the composite to produce equal current redistribution. This propagation is achieved with a magnetic diffusivity dependent on the interstrand contact resistance and on the mutual coupling between the strands. Moreover, the analytical solution was applied to study the current redistribution in the presence of a faulty wire or of a short circuit between strands.

In [6] the analytical solution of the equation of current distribution in a 2-strand cable was used for the study of long range "supercurrents" induced by longitudinal variations of the time derivative of the magnetic field applied perpendicular to the cable face. The evaluation of the strand currents in the presence of a generic current cycle was obtained by considering two different analytical solutions of the equation of current diffusion in the presence of field ramps (forced diffusion), and during constant field phases (free diffusion). The final currents in the two strands were then evaluated by a superposition of the effects of different ramps and constant field phases.

In Chapter 4 the analytical solution of the equations of current diffusion for cables made of a generic number of strands is given and compared to the numerical solution in both transient conditions and steady state. It is also shown that the general solution reduces to the solution given in [10] when a two-strand cable is considered.

4.1 THE ANALYTICAL SOLUTION FOR CABLES WITH SYMMETRIC STRANDS

A necessary condition for the evaluation of the analytical solution is the determination of the eigenvalues and eigenvectors of matrices **g** and **l** appearing in system (3.6).

In Appendix C it is shown that when Rutherford cables or simple cable in conduit conductors are considered, it is possible to determine in a simple way the eigenvalues and eigenvectors of matrices **g** and **l**. The equations of system (3.6) are reported in the following with a particular choice of the boundary conditions:

$$\begin{cases} \mathbf{gl}\dfrac{\partial \mathbf{i}}{\partial t}(x,t)+\mathbf{gri}(x,t)+\dfrac{\partial^2 \mathbf{i}}{\partial x^2}(x,t)=\mathbf{gv}^{ext}(x,t) \\ i_i(x=0,t)=i_i(x=L,t)=\dfrac{i_{op}(t)}{N} \qquad \text{with } i=1, N \\ \mathbf{i}\,(x,t=0)=\mathbf{i}^{(0)}(x) \end{cases}$$

(4.1)

We consider the simple case in which all the strand longitudinal resistances are equal to a given value r (if the strands are in the superconducting state r = 0) so that matrix **r** can be written as r **I** where **I** is the unit matrix. Matrices **l** and **g** are defined as in (3.5.b). The boundary conditions can be written as follows:

$$\mathbf{i}\,(x=0,t)=\mathbf{i}\,(x=L,t)=\frac{i_{op}(t)}{\sqrt{N}}\mathbf{b}_0$$

(4.2)

where $\mathbf{b}_0$ is one of the eigenvectors of both matrices **g** and **l** and is defined in Appendix C, eq. (C.11).

We define the current variations from the uniform current distribution as:

$$\delta\,\mathbf{i}\,(x,t)=\mathbf{i}\,(x,t)-\frac{i_{op}\,(t)}{\sqrt{N}}\mathbf{b}_0$$

(4.3)

and rewrite system (4.1), considering that $\mathbf{gl}\,\mathbf{b}_0 = \mathbf{g}\,\lambda_0\,\mathbf{b}_0 = \gamma_0\,\lambda_0\,\mathbf{b}_0 = 0$:

$$
\begin{cases}
\mathbf{g}\,\mathbf{l}\dfrac{\partial\delta\,\mathbf{i}}{\partial t}(x,t)+\mathbf{g}\,\mathbf{r}\delta\,\mathbf{i}(x,t)+\dfrac{\partial^2\delta\,\mathbf{i}}{\partial x^2}(x,t)=\mathbf{g}\,\mathbf{v}^{ext}(x,t)\\
\delta\,\mathbf{i}\,(x=0,t)=\delta\,\mathbf{i}\,(x=L,t)=0\\
\delta\,\mathbf{i}(x,t=0)=\mathbf{i}^{(0)}(x)-\dfrac{i_{op}(t=0)}{\sqrt{N}}\mathbf{b}_0
\end{cases}
$$

(4.4)

Using the trigonometric base, orthogonal in [0. L], $\{\sin(n\pi x/L)\}_n$, with $n\in\mathbb{N}$, the following series developments can be defined:

$$
\mathbf{F}(x,t)=\sum_{n=1}^{\infty}\mathbf{F}_n(t)\sin\left(\frac{n\pi\,x}{L}\right)\Leftrightarrow\ \mathbf{F}_n(t)=\frac{2}{L}\int_0^L\mathbf{F}(\xi,t)\sin\left(\frac{n\pi\xi}{L}\right)d\xi
$$

(4.5)

and the system (4.1) can be redefined as follows:

$$
\begin{cases}
\mathbf{gl}\dfrac{d\delta\,\mathbf{i}_n}{dt}(t)+\mathbf{gr}\delta\,\mathbf{i}_n(t)-\left(\dfrac{n\pi}{L}\right)^2\delta\,\mathbf{i}_n(t)=\mathbf{g}\mathbf{v}^{ext}{}_n(t)\\
\delta\,\mathbf{i}_n(t=0)=\mathbf{i}_n^{(0)}-\dfrac{I(t=0)}{\sqrt{N}}\mathbf{b}_0\,\dfrac{2}{n\pi}\left[1-(-1)^n\right]
\end{cases}
$$

(4.6)

Using the base $\mathbf{b}_k$, with $k = p, p-1, \ldots, 1, 0, -1, \ldots -(p-1)$, defined in (C.11) we can write:

$$
\delta\,\mathbf{i}_n(t)=\sum_{k=-(p-1)}^{p}\mathbf{b}_k\eta_{n,k}(t)\Leftrightarrow\eta_{n,k}(t)=\mathbf{b}_k^T\delta\,\mathbf{i}_n(t)\qquad\mathbf{v}^{ext}{}_n(t)=\sum_{k=-(p-1)}^{p}\mathbf{b}_k\nu_{n,k}(t)\Leftrightarrow\nu_{n,k}(t)=\mathbf{b}_k^T\mathbf{v}^{ext}{}_n(t)
$$

and the problem (4.6) can be redefined in the following way:

$$
\begin{cases}
\gamma_k\lambda_k\dfrac{d\eta_{n,k}}{dt}(t)+\gamma_k r\,\eta_{n,k}(t)-\left(\dfrac{n\pi}{L}\right)^2\eta_{n,k}(t)=\gamma_k\nu_{n,k}(t)\\
\eta_{n,k}(t=0)=\mathbf{b}_k^T\mathbf{i}_n^{(0)}
\end{cases}
\text{with } k=p,p-1,\ \ ,1,-1,\ldots-(p-1)\qquad(4.7)
$$

It is worth remarking that $k \neq 0$, because $\eta_{n,0} = 0$ as a consequence of $\mathbf{b}_0^T \delta \, \mathbf{i}(x,t) = 0$. Problem (4.7) can be solved directly:

$$\begin{cases} \lambda_k \dfrac{d\eta_{n,k}}{dt} + \left[r - \dfrac{1}{\gamma_k} \left(\dfrac{n\pi}{L} \right)^2 \right] \eta_{n,k} = \nu_{n,k}(t) \\ \eta_{n,k}(t=0) = \mathbf{b}_k^T \mathbf{i}_n^{(0)} \end{cases} \Rightarrow$$

$$\eta_{n,k}(t) = \left(\mathbf{b}_k^T \mathbf{i}_n^{(0)} \right) e^{\frac{-t}{\lambda_k}\left[r - \frac{1}{\gamma_k}\left(\frac{n\pi}{L} \right)^2 \right]} + \frac{1}{\lambda_k} \int_0^t \nu_{n,k}(\tau) e^{\frac{-(t-\tau)}{\lambda_k}\left[r - \frac{1}{\gamma_k}\left(\frac{n\pi}{L} \right)^2 \right]} d\tau$$

(4.8)

The solution can then be written as follows:

$$\mathbf{i}(x,t) = \frac{i_{op}(t)}{\sqrt{N}} \mathbf{b}_0 + \sum_{\substack{k=-(p-1) \\ k \neq 0}}^{p} \mathbf{b}_k \sum_{n=1}^{\infty} \eta_{n,k}(t) \, sin\left(\frac{n\pi x}{L} \right) \Rightarrow$$

$$\mathbf{i}(x,t) = \frac{i_{op}(t)}{\sqrt{N}} \mathbf{b}_0 + \sum_{\substack{k=-(p-1) \\ k \neq 0}}^{p} \mathbf{b}_k \sum_{n=1}^{\infty} \left(\mathbf{b}_k^T \mathbf{i}_n^{(0)} \right) e^{\frac{-t}{\lambda_k}\left[r - \frac{1}{\gamma_k}\left(\frac{n\pi}{L} \right)^2 \right]} sin\left(\frac{n\pi x}{L} \right) +$$

$$\Rightarrow$$

$$+ \int_0^t d\tau \sum_{\substack{k=-(p-1) \\ k \neq 0}}^{p} \frac{\mathbf{b}_k}{\lambda_k} \sum_{n=1}^{\infty} \left(\mathbf{b}_k^T \mathbf{v}^{ext}{}_n(\tau) \right) e^{\frac{-(t-\tau)}{\lambda_k}\left[r - \frac{1}{\gamma_k}\left(\frac{n\pi}{L} \right)^2 \right]} sin\left(\frac{n\pi x}{L} \right)$$

$$\mathbf{i}(x,t) = \frac{i_{op}(t)}{\sqrt{N}} \mathbf{b}_0 + \frac{2}{L} \int_0^L d\xi \sum_{\substack{k=-(p-1) \\ k \neq 0}}^{p} \mathbf{b}_k \left(\mathbf{b}_k^T \mathbf{i}^{(0)}(\xi) \right) \sum_{n=1}^{\infty} e^{\frac{-t}{\lambda_k}\left[r - \frac{1}{\gamma_k}\left(\frac{n\pi}{L} \right)^2 \right]} sin\left(\frac{n\pi x}{L} \right) sin\left(\frac{n\pi\xi}{L} \right) +$$

$$\Rightarrow$$

$$+ \frac{2}{L} \int_0^L d\xi \int_0^t d\tau \sum_{\substack{k=-(p-1) \\ k \neq 0}}^{p} \frac{\mathbf{b}_k}{\lambda_k} \left(\mathbf{b}_k^T \mathbf{v}^{ext}(\xi,\tau) \right) \sum_{n=1}^{\infty} e^{\frac{-(t-\tau)}{\lambda_k}\left[r - \frac{1}{\gamma_k}\left(\frac{n\pi}{L} \right)^2 \right]} sin\left(\frac{n\pi x}{L} \right) sin\left(\frac{n\pi\xi}{L} \right)$$

$$\mathbf{i}\,(x,t)=\frac{i_{op}(t)}{\sqrt{N}}\mathbf{b}_0+\frac{2}{L}\int_0^L d\xi\sum_{\substack{k=-(p-1)\\k\neq 0}}^{p}\mathbf{b}_k\left(\mathbf{b}_k^T\mathbf{i}^{(0)}(\xi)\right)\Gamma_k(x,\xi,t)+$$
$$+\frac{2}{L}\int_0^L d\xi\int_0^t d\tau\sum_{\substack{k=-(p-1)\\k\neq 0}}^{p}\frac{\mathbf{b}_k}{\lambda_k}\left(\mathbf{b}_k^T\mathbf{v}^{ext}(\xi,\tau)\right)\Gamma_k(x,\xi,t-\tau)$$

(4.9)

Considering that $\sin(\omega_1)\sin(\omega_2)=\frac{1}{2}[\cos(\omega_1-\omega_2)-\cos(\omega_1+\omega_2)]$ and the definition of the elliptic function ϑ_3 [52]: $\vartheta_3(u,q)=1+2\sum_{n=1}^{\infty}q^{n^2}\cos 2nu$, the Green functions Γ_k can be written as:

$$\Gamma_k(x,\xi;t)=\sum_{n=1}^{\infty}e^{\frac{-t}{\lambda_k}\left[r-\frac{1}{\gamma_k}\left(\frac{n\pi}{L}\right)^2\right]}\sin\left(\frac{n\pi x}{L}\right)\sin\left(\frac{n\pi\xi}{L}\right)=$$
$$=\frac{e^{\frac{-rt}{\lambda_k}}}{2}\sum_{n=1}^{\infty}e^{\frac{tn^2}{\lambda_k\gamma_k}\left(\frac{\pi}{L}\right)^2}\cos\left(\frac{n\pi(x-\xi)}{L}\right)-\frac{e^{\frac{-rt}{\lambda_k}}}{2}\sum_{n=1}^{\infty}e^{\frac{tn^2}{\lambda_k\gamma_k}\left(\frac{\pi}{L}\right)^2}\cos\left(\frac{n\pi(x+\xi)}{L}\right)$$
$$=\frac{e^{\frac{-rt}{\lambda_k}}}{4}\left[\vartheta_3\left(\pi\frac{x-\xi}{2L},e^{\frac{t}{\lambda_k\gamma_k}\left(\frac{\pi}{L}\right)^2}\right)-\vartheta_3\left(\pi\frac{x+\xi}{2L},e^{\frac{t}{\lambda_k\gamma_k}\left(\frac{\pi}{L}\right)^2}\right)\right]$$

(4.10)

with $k=p,\ p-1,\ \ldots,\ 1,\ -1,\ \ldots\ -(p-1)$. The Green matrices are then expressed by:

$$\mathbf{K}^{(0)}(x,\xi,t)=\sum_{\substack{k=-(p-1)\\k\neq 0}}^{p}\Gamma_k(x,\xi,t)\mathbf{b}_k\mathbf{b}_k^T \qquad \mathbf{K}(x,\xi,t)=\sum_{\substack{k=-(p-1)\\k\neq 0}}^{p}\Gamma_k(x,\xi,t)\frac{\mathbf{b}_k\mathbf{b}_k^T}{\lambda_k}$$

(4.11) and the final solution of problem (4.1) can be written as:

$$\boxed{\mathbf{i}(x,t)=\frac{i_{op}(t)}{\sqrt{N}}\mathbf{b}_0+\frac{2}{L}\int_0^L d\xi\ \mathbf{K}^{(0)}(x,\xi,t)\ \mathbf{i}^{(0)}(\xi)+\frac{2}{L}\int_0^L d\xi\int_0^t d\tau\ \mathbf{K}(x,\xi,t-\tau)\mathbf{v}^{ext}(\xi,\tau)}$$

(4.12)

It is worth noting that solution (4.12) is invariant to the addition of terms proportional to $\mathbf{b}_0$ to the source terms $\mathbf{i}^{(0)}(x)$ and $\mathbf{v}^{ext}(x,\ t)$. We can write, in fact:

$$\mathbf{K}^{(0)}(x,\xi)\left\{\mathbf{i}^{(0)}(\xi)+\hat{i}(\xi)\,\mathbf{b}_0\right\}=\mathbf{K}^{(0)}(x,\xi)\mathbf{i}^{(0)}(\xi)+\hat{v}(\xi)\mathbf{K}^{(0)}(x,\xi)\,\mathbf{b}_0=\mathbf{K}^{(0)}(x,\xi)\mathbf{i}^{(0)}\,(\xi)$$

$$\mathbf{K}(x,\xi,\tau)\left\{\mathbf{v}^{ext}(\xi,\tau)+\hat{v}(\xi,\tau)\,\mathbf{b}_0\right\}=$$

$$=\mathbf{K}(x,\xi,\tau)\,\mathbf{v}^{ext}(\xi,\tau)+\hat{v}(\xi,\tau)\mathbf{K}(x,\xi,\tau)\,\mathbf{b}_0=\mathbf{K}(x,\xi,\tau)\mathbf{v}^{ext}(\xi,\tau)$$

(4.13)

This means that the solution does not change if we substitute $\delta\mathbf{i}^{(0)}(x)$ to $\mathbf{i}^{(0)}(x)$ in the first integral of (4.12) or changing the voltage reference.

The integration of the kernels $\mathbf{K}^{(0)}$ and $\mathbf{K}$ can cause convergence problems, as the function Γ_k tends to the Dirac δ distribution, when t tends to zero:

$$\lim_{t\to 0}\Gamma_k(x,\xi;t)=\sum_{n=1}^{\infty}\sin\left(\frac{n\pi x}{L}\right)\sin\left(\frac{n\pi\xi}{L}\right)=\frac{L}{2}\delta(x-\xi)$$

(4.14)

It is therefore advantageous, if $\mathbf{i}^{(0)}(x)$ and $\mathbf{v}^{ext}(x,\ t)$ are derivable with respect to x, to refer to the following equivalent form of the solution, obtained by means of an integration per parts. Let's define function $\underline{\Gamma}_k$ as follows:

$$\underline{\Gamma}_k(x,\xi;t)=\int_0^{\xi}\Gamma_k(x,\xi';t)\,d\xi'=2L\sum_{n=1}^{\infty}\frac{e^{\frac{-t}{\lambda_k}\left[r-\frac{1}{\gamma_k}\left(\frac{n\pi}{L}\right)^2\right]}}{n\pi}\sin\left(\frac{n\pi x}{L}\right)\sin^2\left(\frac{n\pi\xi}{2L}\right)$$

(4.15)

with $k = p,\ p-1, \ldots, 1, -1, \ldots -(p-1)$; and new integration kernels $\underline{\mathbf{K}}^{(0)}$ e $\underline{\mathbf{K}}$ as:

$$\underline{\mathbf{K}}^{(0)}(x,\xi,t)=\sum_{\substack{k=-(p-1)\\k\neq 0}}^{p}\underline{\Gamma}_k(x,\xi,t)\;\mathbf{b}_k\mathbf{b}_k^T \qquad \underline{\mathbf{K}}(x,\xi,t)=\sum_{\substack{k=-(p-1)\\k\neq 0}}^{p}\underline{\Gamma}_k(x,\xi,t)\frac{\mathbf{b}_k\mathbf{b}_k^T}{\lambda_k}$$

(4.16)

The solution of problem (4.1) can then be written as:

$$\mathbf{i}\,(x,t)=\frac{i_{op}(t)}{\sqrt{N}}\,\mathbf{b}_0+\frac{2}{L}\int_0^L d\xi\,\frac{\partial}{\partial\xi}\,\underline{\mathbf{K}}^{(0)}(x,\xi,t)\,\mathbf{i}^{(0)}(\xi)+\frac{2}{L}\int_0^L d\xi\int_0^t d\tau\,\frac{\partial}{\partial\xi}\,\underline{\mathbf{K}}(x,\xi,t-\tau)\,\mathbf{v}^{ext}(\xi,\tau)=$$

$$=\frac{i_{op}(t)}{\sqrt{N}}\,\mathbf{b}_0+\left\{\frac{2}{L}\underline{\mathbf{K}}^{(0)}(x,\xi,t)\,\mathbf{i}^{(0)}(\xi)\right\}_{\xi=0}^{\xi=L}-\frac{2}{L}\int_0^L d\xi\,\left[\underline{\mathbf{K}}^{(0)}(x,\xi,t)\right]\frac{\partial\,\mathbf{i}^{(0)}}{\partial\xi}(\xi)+$$

$$+\frac{2}{L}\left\{\int_0^t d\tau\,\underline{\mathbf{K}}(x,\xi,t-\tau)\mathbf{v}^{ext}(\xi,\tau)\right\}_{\xi=0}^{\xi=L}-\frac{2}{L}\int_0^L d\xi\int_0^t d\tau\,\left[\underline{\mathbf{K}}(x,\xi,t-\tau)\right]\,\frac{\partial\mathbf{v}^{ext}}{\partial\xi}(\xi,\tau)$$

(4.17)

and finally:

$$\mathbf{i}\,(x,t)=\frac{i_{op}(t)}{\sqrt{N}}\mathbf{b}_0+\frac{2}{L}\underline{\mathbf{K}}^{(0)}(x,L,t)\,\mathbf{i}^{(0)}(L)-\frac{2}{L}\int_0^L d\xi\,\underline{\mathbf{K}}^{(0)}(x,\xi,t)\frac{\partial\,\mathbf{i}^{(0)}}{\partial\xi}(\xi)+$$

$$+\frac{2}{L}\int_0^t d\tau\,\underline{\mathbf{K}}(x,L,t-\tau)\mathbf{v}^{ext}(L,\tau)-\frac{2}{L}\int_0^L d\xi\int_0^t d\tau\,\underline{\mathbf{K}}(x,\xi,t-\tau)\frac{\partial\mathbf{v}^{ext}}{\partial\xi}(\xi,\tau)$$

(4.18)

The calculation of $\underline{\mathbf{K}}^{(0)}$ and $\underline{\mathbf{K}}$ does not give convergence problems, as function $\underline{\Gamma}_k$ tends to the step-like Heaviside function, when t tends a zero:

$$\lim_{t\to 0}\Gamma_k(x,\xi;t)=\sum_{n=1}^{\infty}\frac{2L}{n\pi}\sin\left(\frac{n\pi x}{L}\right)\sin^2\left(\frac{n\pi\xi}{2L}\right)=\frac{L}{2}U(\xi-x)=\frac{L}{2}\begin{cases}1, & x<\xi\\ 0, & x>\xi\end{cases}$$

(4.19)

In the case study reported in Fig. 3.2 and 3.3, the components of vector $\mathbf{i}^{(0)}(x)$ are all equal and $\mathbf{v}^{\mathrm{ext}}(x,\,t)$ is independent of time, so that the solution (4.19) can be further simplified. In fact defining:

$$\Gamma_k^*(x,\xi;t)=\int_0^t\Gamma_k(x,\xi;\tau)\,d\tau=\sum_{n=1}^{\infty}\frac{\lambda_k}{\left[r-\frac{1}{\gamma_k}\left(\frac{n\pi}{L}\right)^2\right]}\left(1-e^{\frac{-t}{\lambda_k}\left[r-\frac{1}{\gamma_k}\left(\frac{n\pi}{L}\right)^2\right]}\right)\sin\left(\frac{n\pi x}{L}\right)\sin\left(\frac{n\pi\xi}{L}\right)$$

(4.20)

with $k = p,\ p-1,\ \ldots,\ 1,\ -1,\ \ldots\ -(p-1)$, and the integration kernel:

$$\mathbf{K}^*(x,\xi,t)=\sum_{\substack{k=-(p-1)\\ k\neq 0}}^{p}\Gamma^*{}_k(x,\xi,t)\frac{\mathbf{b}_k\mathbf{b}_k^T}{\lambda_k}$$

(4.21)

the solution of problem (4.1) can be written in the following form:

$$\mathbf{i}(x,t)=\frac{i_{op}(t)}{\sqrt{N}}\mathbf{b}_0+\frac{2}{L}\int_0^L d\xi\ \mathbf{K}^*(x,\xi,t)\,\mathbf{v}^{ext}(\xi)$$

(4.22)

We have tested the numerical simulations of Boundary Induced Coupling Currents generated in a 16 strand Rutherford cable by a step-like time varying magnetic field reported in Fig. 3.2 and 3.3 comparing them with the analytical solution of the same problem given by (4.22). The comparison between numerical and analytical solution is reported in Fig. 4.1 and 4.2. A very good agreement is obtained between the numerical and analytical solution of the problem. The integral in eq. (4.22) has been performed numerically, with an adaptive gaussian integration. The times required for the integration of (4.21) can in some cases be remarkable due to the space oscillations of vector $\mathbf{v}^{ext}$ in Rutherford cables.

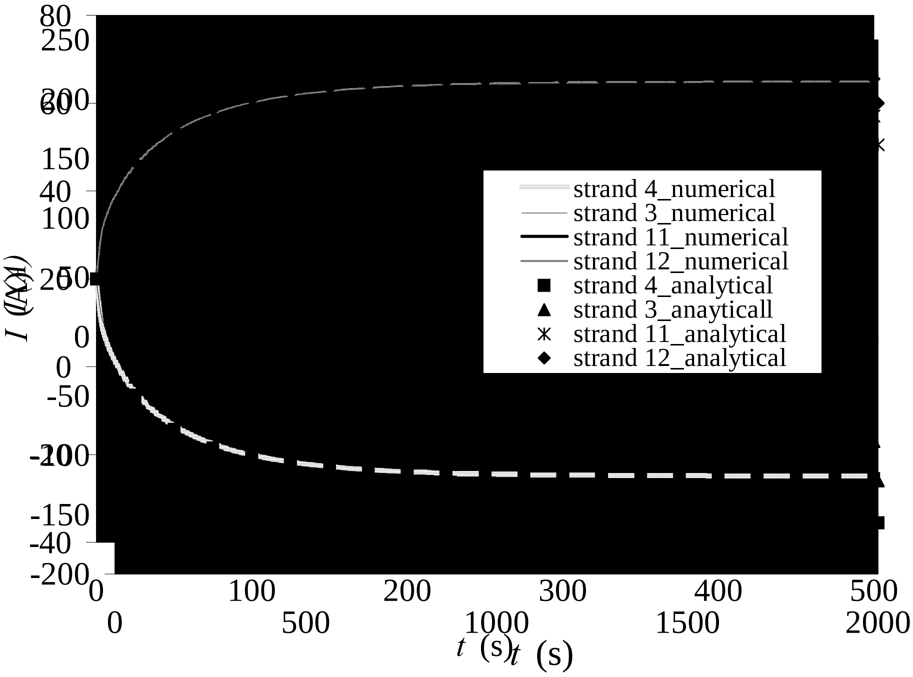

Fig. 4.1 *Comparison between analytical and numerical solution: time dependence of Boundary Induced Coupling Currents in a 16 strands Rutherford cable exposed to a step-like spatial distribution of the magnetic flux density perpendicular to the broad face of the cable. a)* $r_h = 1.54\ 10^{-8}\ \Omega/m$ *b)* $r_h = 1.54\ 10^{-11}\ \Omega/m$. *Data for the simulations are reported in Section 3.3.*

4.2 COMPARISON WITH THE ANALYTICAL SOLUTION OF THE 2-STRAND MODEL

It has been shown in Section 3.1.4 that the equations of free current diffusion in a two strand cable derived in [10] can be obtained from equations (4.1) given the appropriate relation between the parameters of the two models.

In this section the analytical solution given in [10] for the 2-strand model is derived from the analytical solution of the general system 4.12. In order to compare the two solutions we introduce the same assumptions assumed in [10]:

- $i_{op}(t) = 0$;
- $r = 0$
- The cable length is multiple of an even number of twist pitches
- $\mathbf{i}^{(0)}(x) = 0$
- The external field excitation is independent of time and is limited to a short interval of length δ in the middle of the cable.

Under these assumptions we can write:

$$\mathbf{v}^{ext}(\xi) = \frac{\dot{\Phi}/2}{\delta} U\left(\xi - \frac{L}{2} - \frac{\delta}{2}\right) U\left(\frac{L}{2} + \frac{\delta}{2} - \xi\right) \begin{bmatrix} +1 \\ -1 \end{bmatrix}$$

(4.23)

where U is the Heaviside function, and $\dot{\Phi}$ the time derivative of the magnetic flux linked to the two strands along the length δ. In the case considered, N=2, p=1; so that matrices **l** and **g** can be written as follows:

$$\mathbf{l} = \begin{bmatrix} l_{11} & l_{12} \\ l_{12} & l_{11} \end{bmatrix} \qquad\qquad \mathbf{g} = \begin{bmatrix} -g_{12} & +g_{12} \\ +g_{12} & -g_{12} \end{bmatrix}$$

(4.24)

The eigenvalues of **l** are positive and given by:

$$\lambda_0 = l_{11} + l_{12} \qquad\qquad \lambda_1 = l_{11} - l_{12}$$

(4.25)

The eigenvalues of **g** are negative (except for γ_0 which is nil) and can be written as:

$$\gamma_0 = 0 \qquad \text{and} \qquad \gamma_1 = -2g_{12}$$

(4.26)

The base $\mathbf{b}_k$, with k = 1, 0, is common to both matrices:

$$\mathbf{b}_0^{\mathrm{T}} = \left\{ \frac{1}{\sqrt{2}}, \frac{1}{\sqrt{2}} \right\} \qquad \mathbf{b}_1^{\mathrm{T}} = \left\{ \frac{1}{\sqrt{2}}, -\frac{1}{\sqrt{2}} \right\}$$

(4.27)

As shown in Section 3.1.4 the following relations hold for the main parameters of the two models:

$$L_1 = 2\,(l_{11} - l_{12}),\ \ G_1 = g_{12} \tag{4.28}$$

Moreover, we introduce the following parameters defined accordingly to [10]:

$$\mathrm{L} = 2\mathrm{w} + \delta \qquad \alpha = \pi\,\mathrm{w}/(2\mathrm{w} + \delta) \qquad I_m = \frac{w\dot{\Phi}G_1}{2}$$

(4.29)

The following relations hold, which are useful for the calculations:

$$(\pi\delta / 2\mathrm{L}) + \alpha = \pi / 2 \qquad \pi / \mathrm{L} = \alpha / \mathrm{w}$$

(4.30)

We can then write:

$$\mathbf{v}^{ext}(\xi) = \frac{\dot{\Phi}}{2\delta} U\left(\xi - \frac{L}{2} - \frac{\delta}{2}\right) U\left(\frac{L}{2} + \frac{\delta}{2} - \xi\right) \mathbf{b}_1 \sqrt{2}$$

(4.31)

Applying equation (4.20) we obtain:

$$\Gamma_1^*(x,\xi;t) = \sum_{n=1}^{\infty} \frac{\lambda_1}{\left[-\frac{1}{\gamma_1}\left(\frac{n\pi}{L}\right)^2\right]} \left(1 - e^{\frac{-t}{\lambda_1}\left[-\frac{1}{\gamma_1}\left(\frac{n\pi}{L}\right)^2\right]}\right) \sin\left(\frac{n\pi\ x}{L}\right) \sin\left(\frac{n\pi\xi}{L}\right) =$$

$$= \frac{2g_{12}\lambda_1 L^2}{\pi^2} \sum_{n=1}^{\infty} \frac{1}{n^2} \left(1 - e^{-tn^2/\tau}\right) \sin\left(\frac{n\pi\ x}{L}\right) \sin\left(\frac{n\pi\xi}{L}\right)$$

(4.32)

To obtain (4.32) the following relation has been considered:

$$\frac{1}{\lambda_1}\left[-\frac{1}{\gamma_1}\left(\frac{n\pi}{L}\right)^2\right]=\frac{1}{l_{11}-l_{12}}\left[\frac{1}{2g_{12}}\left(\frac{n\pi}{L}\right)^2\right]=$$
$$\frac{1}{L_1G_1}\frac{\pi^2}{(2w+\delta)^2}=\frac{\pi^2}{4}\frac{1}{L_1G_1}\left(\frac{2}{2w+\delta}\right)^2=\frac{1}{\tau}$$

(4.33)

The following equation holds for the integration kernel :

$$\mathbf{K}^*(x,\xi,t)=\Gamma_k^*(x,\xi,t)\frac{\mathbf{b}_1\mathbf{b}_1^T}{\lambda_1}=\frac{\Gamma_k^*(x,\xi,t)}{\lambda_1}\begin{bmatrix}\frac{1}{\sqrt{2}}\\-\frac{1}{\sqrt{2}}\end{bmatrix}\begin{bmatrix}\frac{1}{\sqrt{2}} & -\frac{1}{\sqrt{2}}\end{bmatrix}=$$
$$=\frac{\Gamma_k^*(x,\xi,t)}{\lambda_1}\begin{bmatrix}+1/2 & -1/2\\-1/2 & +1/2\end{bmatrix}=\frac{\Gamma_k^*(x,\xi,t)}{2\lambda_1}\begin{bmatrix}+1 & -1\\-1 & +1\end{bmatrix}=$$
$$=\frac{g_{12}L^2}{\pi^2}\sum_{n=1}^{\infty}\frac{1}{n^2}\left(1-e^{-tn^2/\tau}\right)sin\left(\frac{n\pi\, x}{L}\right)sin\left(\frac{n\pi\xi}{L}\right)\begin{bmatrix}+1 & -1\\-1 & +1\end{bmatrix}$$

(4.34)

The solution can be written as follows:

$$\mathbf{i}(x,t)=\frac{2}{L}\int_0^L d\xi\ \mathbf{K}^*(x,\xi,t)\,\mathbf{v}^{ext}(\xi)=$$
$$=\frac{2g_{12}L}{\pi^2}\sum_{n=1}^{\infty}\frac{1}{n^2}\left(1-e^{-tn^2/\tau}\right)sin\left(\frac{n\pi\, x}{L}\right)\int_0^L d\xi\ sin\left(\frac{n\pi\xi}{L}\right)\begin{bmatrix}+1 & -1\\-1 & +1\end{bmatrix}\mathbf{v}^{ext}(\xi)=$$
$$=\frac{\dot{\Phi}g_{12}L}{\pi^2\delta}\sum_{n=1}^{\infty}\frac{1}{n^2}\left(1-e^{-tn^2/\tau}\right)sin\left(\frac{n\pi\, x}{L}\right)\int_{(L-\delta)/2}^{(L+\delta)/2}d\xi\ sin\left(\frac{n\pi\xi}{L}\right)\begin{bmatrix}+1 & -1\\-1 & +1\end{bmatrix}\begin{bmatrix}+1\\-1\end{bmatrix}=$$
$$\frac{\dot{\Phi}g_{12}L}{\pi^2\delta}\sum_{n=1}^{\infty}\frac{1}{n^2}\left(1-e^{-tn^2/\tau}\right)sin\left(\frac{n\pi\, x}{L}\right)\int_{(L-\delta)/2}^{(L+\delta)/2}d\xi\ sin\left(\frac{n\pi\xi}{L}\right)\begin{bmatrix}+2\\-2\end{bmatrix}$$

(4.35)

In this case i_{op} = 0, so that $i_1 = -i_2$; considering only $i_1(x, t)$, we get:

$$i_1(x,t)=\frac{2\dot{\Phi}G_1L}{\pi^2\delta}\sum_{n=1}^{\infty}\frac{1}{n^2}\left(1-e^{-tn^2/\tau}\right)sin\left(\frac{n\pi\ x}{L}\right)\int_{(L-\delta)/2}^{(L+\delta)/2}d\xi\ sin\left(\frac{n\pi\xi}{L}\right)=$$

$$=\frac{4I_mL}{\pi^2w\delta}\sum_{n=1}^{\infty}\frac{1}{n^2}\left(1-e^{-tn^2/\tau}\right)sin\left(\frac{n\alpha\ x}{w}\right)\int_{(L-\delta)/2}^{(L+\delta)/2}d\xi\ sin\left(\frac{n\pi\xi}{L}\right)=$$

$$=\frac{4}{\pi\alpha}I_m\sum_{n=1}^{\infty}\frac{1}{n^2}\left(1-e^{-tn^2/\tau}\right)sin\left(\frac{n\alpha\ x}{w}\right)\frac{1}{\delta}\int_{(L-\delta)/2}^{(L+\delta)/2}d\xi\ sin\left(\frac{n\pi\xi}{L}\right)$$

(4.36)

In order to further simplify the solution, we can write:

$$\frac{1}{\delta}\int_{(L-\delta)/2}^{(L+\delta)/2}d\xi\ \sin\left(\frac{n\pi\xi}{L}\right)=\frac{L}{n\pi\delta}\left[\cos\left(n\pi\frac{L-\delta}{2L}\right)-\cos\left(n\pi\frac{L+\delta}{2L}\right)\right]=$$

$$=\frac{2L}{n\pi\delta}\sin\left(\frac{n\pi}{2}\right)\sin\left(\frac{n\pi\delta}{2L}\right)$$

(4.37)

As sin ($n\pi/2$) = 0 for n even, we can calculate the sum in (4.36) with only uneven values of n. We can also note that:

$$\sin\left(\frac{n\pi}{2}\right)=\sin\left(\frac{n\pi\delta}{2L}+n\alpha\right)=\sin\left(\frac{n\pi\delta}{2L}\right)\cos(n\alpha)+\cos\left(\frac{n\pi\delta}{2L}\right)\sin(n\alpha)$$

(4.38)

Assuming $\delta \ll L$, we get:

$$\frac{1}{\delta}\int_{(L-\delta)/2}^{(L+\delta)/2}d\xi\ \sin\left(\frac{n\pi\xi}{L}\right)=\frac{\sin\left(\frac{n\pi\delta}{2L}\right)}{\left(\frac{n\pi\delta}{2L}\right)}\left[\sin\left(\frac{n\pi\delta}{2L}\right)\cos(n\alpha)+\cos\left(\frac{n\pi\delta}{2L}\right)\sin(n\alpha)\right]\cong\sin(n\alpha)$$

(4.39)

This is equivalent to directly approximate the integral in (4.37):

$$\frac{1}{\delta}\int_{(L-\delta)/2}^{(L+\delta)/2}d\xi\ \sin\left(\frac{n\pi\xi}{L}\right)=\frac{1}{\delta}\int_{w}^{w+\delta}d\xi\ \sin\left(\frac{n\pi\xi}{2w+\delta}\right)\cong\frac{1}{\delta}\sin\left(\frac{n\pi w}{2w+\delta}\right)\delta=\sin(n\alpha)$$

(4.40)

Defining $\tau_n = \tau / n^2$, we finally obtain the analytical solution for current i_1 which is identical to that reported in [10], eq. (29):

$$i_1(x,t) = \frac{4}{\pi\alpha} I_m \sum_{\substack{n=1 \\ n \text{ uneven}}}^{\infty} \frac{1}{n^2}\left(1-e^{-t/\tau_n}\right)\sin\left(\frac{n\alpha\, x}{w}\right)\sin\left(n\alpha\right)$$

(4.41)

If the external field ramp is stopped at time t_1 and the field is kept constant, the supercurrents start decaying. Each component under the sum in (4.41) decays with its correspondent time constant [10]:

$$i_1(x,t) = \frac{4}{\pi\alpha} I_m \sum_{\substack{n=1 \\ n \text{ uneven}}}^{\infty} \frac{1}{n^2}\left(1-e^{-t_1/\tau_n}\right)\sin\left(\frac{n\alpha\, x}{w}\right)\sin\left(n\alpha\right)e^{-(t-t_1)/\tau_n}$$

(4.42)

4.3 THE REGIME SOLUTION

Due to its definition, Γ_k can cause convergence problems, because the series is made of oscillating terms:

$$\begin{aligned}\Gamma_k(x,\xi;t) &= \sum_{n=1}^{\infty} e^{\frac{-t}{\lambda_k}\left[r-\frac{1}{\gamma_k}\left(\frac{n\pi}{L}\right)^2\right]}\sin\left(\frac{n\pi\, x}{L}\right)\sin\left(\frac{n\pi\xi}{L}\right)= \\ &= \frac{e^{\frac{-rt}{\lambda_k}}}{2}\sum_{n=1}^{\infty} e^{\frac{tn^2}{\lambda_k\gamma_k}\left(\frac{\pi}{L}\right)^2}\cos\left(\frac{n\pi(x-\xi)}{L}\right)-\frac{e^{\frac{-rt}{\lambda_k}}}{2}\sum_{n=1}^{\infty} e^{\frac{tn^2}{\lambda_k\gamma_k}\left(\frac{\pi}{L}\right)^2}\cos\left(\frac{n\pi(x+\xi)}{L}\right) \\ &= \frac{e^{\frac{-rt}{\lambda_k}}}{4}\left[\vartheta_3\left(\pi\frac{x-\xi}{2L}, e^{\frac{t}{\lambda_k\gamma_k}\left(\frac{\pi}{L}\right)^2}\right)-\vartheta_3\left(\pi\frac{x+\xi}{2L}, e^{\frac{t}{\lambda_k\gamma_k}\left(\frac{\pi}{L}\right)^2}\right)\right]\end{aligned}$$

(4.42)

It can be shown [63] that the elliptic function ϑ_3 admits the following representation, with non oscillating terms:

$$\vartheta_3\left(u, e^{-s}\right) = \sum_{n=-\infty}^{\infty} e^{-n^2 s}\cos 2nu = \sqrt{\frac{\pi}{s}}\sum_{n=-\infty}^{\infty} e^{-\frac{(u-n\pi)^2}{s}}$$

(4.43)

The function Γ_k admits the following alternative representation:

$$\begin{aligned}
\Gamma_k(x,\xi;t) &= \frac{e^{\frac{-rt}{\lambda_k}}}{4}\left[\vartheta_3\left(\pi\frac{x-\xi}{2L}, e^{\frac{t}{\lambda_k\gamma_k}\left(\frac{\pi}{L}\right)^2}\right) - \vartheta_3\left(\pi\frac{x+\xi}{2L}, e^{\frac{t}{\lambda_k\gamma_k}\left(\frac{\pi}{L}\right)^2}\right)\right] = \\
&= L\frac{e^{\frac{-rt}{\lambda_k}}}{4}\sqrt{-\frac{\lambda_k\gamma_k}{\pi t}}\sum_{n=-\infty}^{\infty}\left[e^{L^2\frac{\lambda_k\gamma_k}{\pi^2 t}\left(\pi\frac{x-\xi}{2L}-n\pi\right)^2} - e^{L^2\frac{\lambda_k\gamma_k}{\pi^2 t}\left(\pi\frac{x+\xi}{2L}-n\pi\right)^2}\right] = \\
&= L\frac{e^{\frac{-rt}{\lambda_k}}}{4}\sqrt{-\frac{\lambda_k\gamma_k}{\pi t}}\sum_{n=-\infty}^{\infty}\left[e^{\frac{\lambda_k\gamma_k}{t}\left(\frac{x-\xi}{2}-nL\right)^2} - e^{\frac{\lambda_k\gamma_k}{t}\left(\frac{x+\xi}{2}-nL\right)^2}\right] = \\
&= \frac{L}{4}\sqrt{-\frac{\lambda_k\gamma_k}{\pi t}}\sum_{n=-\infty}^{\infty}\left[e^{\frac{-rt}{\lambda_k}+\frac{\lambda_k\gamma_k}{t}\left(\frac{x-\xi}{2}-nL\right)^2} - e^{\frac{-rt}{\lambda_k}+\frac{\lambda_k\gamma_k}{t}\left(\frac{x+\xi}{2}-nL\right)^2}\right]
\end{aligned} \qquad (4.44)$$

Finally, defining $\theta = \sqrt{\tau} \quad \Rightarrow 2d\theta = \frac{d\tau}{\sqrt{\tau}}$, we obtain for Γ_k^* the following expression:

$$\begin{aligned}
&\Gamma_k^*(x,\xi;t) = \int_0^t \Gamma_k(x,\xi;\tau)\, d\tau = \\
&\int_0^t \frac{L}{4}\sqrt{-\frac{\lambda_k\gamma_k}{\pi\tau}}\sum_{n=-\infty}^{\infty}\left[e^{\frac{-r\tau}{\lambda_k}+\frac{\lambda_k\gamma_k}{\tau}\left(\frac{x-\xi}{2}-nL\right)^2} - e^{\frac{-r\tau}{\lambda_k}+\frac{\lambda_k\gamma_k}{\tau}\left(\frac{x+\xi}{2}-nL\right)^2}\right] d\tau = \\
&= \frac{L}{2}\sqrt{-\frac{\lambda_k\gamma_k}{\pi}}\int_0^{\sqrt{t}} d\theta \sum_{n=-\infty}^{\infty}\left[e^{\frac{-r\theta^2}{\lambda_k}+\frac{\lambda_k\gamma_k}{\theta^2}\left(\frac{x-\xi}{2}-nL\right)^2} - e^{\frac{-r\theta^2}{\lambda_k}+\frac{\lambda_k\gamma_k}{\theta^2}\left(\frac{x+\xi}{2}-nL\right)^2}\right] = \\
&= \sum_{n=-\infty}^{\infty}\left[\frac{L}{2}\sqrt{-\frac{\lambda_k\gamma_k}{\pi}}\int_0^{\sqrt{t}} e^{\frac{-r\theta^2}{\lambda_k}+\frac{\lambda_k\gamma_k}{\theta^2}\left(\frac{x-\xi}{2}-nL\right)^2} d\theta - \frac{L}{2}\sqrt{-\frac{\lambda_k\gamma_k}{\pi}}\int_0^{\sqrt{t}} e^{\frac{-r\theta^2}{\lambda_k}+\frac{\lambda_k\gamma_k}{\theta^2}\left(\frac{x+\xi}{2}-nL\right)^2} d\theta\right]
\end{aligned} \qquad (4.45)$$

Defining $Q = \frac{x-\xi}{2} - nL$, the single term of the series can be written as:

$$\frac{L}{2}\sqrt{-\frac{\lambda_k\gamma_k}{\pi}}\int_0^{\sqrt{t}} e^{\frac{-r\theta^2}{\lambda_k}+\frac{\lambda_k\gamma_k}{\theta^2}Q^2}\,d\theta = \frac{L}{2}\sqrt{-\frac{\lambda_k\gamma_k}{\pi}}e^{-2|Q|\sqrt{-r\gamma_k}}\int_0^{\sqrt{t}} e^{-\left[\theta\sqrt{\frac{r}{\lambda_k}}-\frac{\sqrt{-\lambda_k\gamma_k}}{\theta}|Q|\right]^2}d\theta$$

(4.46)

Defining $y=\theta\sqrt{\frac{r}{\lambda_k}}-\sqrt{-\lambda_k\gamma_k}\frac{|Q|}{\theta} \quad \Rightarrow \quad \theta=\frac{y}{2}\sqrt{\frac{\lambda_k}{r}}+\sqrt{\frac{y^2}{4}\frac{\lambda_k}{r}+\lambda_k|Q|\sqrt{\frac{-\gamma_k}{r}}}$ we get:

$$d\theta=\frac{1}{2}\sqrt{\frac{\lambda_k}{r}}\left(1+\frac{y}{\sqrt{y^2+4|Q|\sqrt{-r\gamma_k}}}\right)dy$$

(4.47)

We obtain:

$$\frac{L}{2}\sqrt{-\frac{\lambda_k\gamma_k}{\pi}}\int_0^{\sqrt{t}} e^{\frac{-r\theta^2}{\lambda_k}+\frac{\lambda_k\gamma_k}{\theta^2}Q^2}\,d\theta =$$
$$\frac{L\lambda_k}{4}\sqrt{-\frac{\gamma_k}{\pi r}}e^{-2|Q|\sqrt{-r\gamma_k}}\int_{-\infty}^{\sqrt{\frac{rt}{\lambda_k}}-\sqrt{\frac{-\lambda_k\gamma_k}{t}}|Q|} e^{-y^2}\left(1+\frac{y}{\sqrt{y^2+4|Q|\sqrt{-r\gamma_k}}}\right)dy$$

(4.48)

Defining the error function $erf(x)=\frac{2}{\sqrt{\pi}}\int_0^x e^{-y^2}dy$ and erfc (x) = 1 − erf (x), we get:

$$\frac{L}{2}\sqrt{-\frac{\lambda_k\gamma_k}{\pi}}\int_0^{\sqrt{t}} e^{\frac{-r\theta^2}{\lambda_k}+\frac{\lambda_k\gamma_k}{\theta^2}Q^2}\,d\theta =$$
$$\frac{L\lambda_k}{4}\sqrt{-\frac{\gamma_k}{\pi r}}e^{-2|Q|\sqrt{-r\gamma_k}}\left[-\frac{\sqrt{\pi}}{2}erf(-\infty)+\frac{\sqrt{\pi}}{2}erf\left(\sqrt{\frac{rt}{\lambda_k}}-\sqrt{\frac{-\lambda_k\gamma_k}{t}}|Q|\right)+\right. \qquad (4.49)$$
$$\left.-\int_0^{-\infty}\frac{ye^{-y^2}}{\sqrt{y^2+4|Q|\sqrt{-r\gamma_k}}}dy+\int_0^{\sqrt{\frac{rt}{\lambda_k}}-\sqrt{\frac{-\lambda_k\gamma_k}{t}}|Q|}\frac{ye^{-y^2}}{\sqrt{y^2+4|Q|\sqrt{-r\gamma_k}}}dy\right]$$

Setting $w^2=y^2+4|Q|\sqrt{-r\gamma_k} \quad \Rightarrow \quad wdw=ydy$ we obtain:

$$\int_0^X \frac{ye^{-y^2}}{\sqrt{y^2+4|Q|\sqrt{-r\gamma_k}}}dy = e^{4|Q|\sqrt{-r\gamma_k}} \int_{\sqrt{4|Q|\sqrt{-r\gamma_k}}}^{\sqrt{X^2+4|Q|\sqrt{-r\gamma_k}}} e^{-w^2}dw = \tag{4.52}$$

$$= \frac{\sqrt{\pi}}{2}\left[erf\left(\sqrt{X^2+4|Q|\sqrt{-r\gamma_k}}\right) - erf\left(\sqrt{4|Q|\sqrt{-r\gamma_k}}\right)\right]$$

(4.50)

and finally:

$$\Gamma_k^*(x,\xi;t) = \Gamma_k^*(x,\xi;\infty) + \frac{L\lambda_k}{8}\sqrt{-\frac{\gamma_k}{r}}\sum_{n=-\infty}^{\infty}$$

$$\left[-e^{-|x-\xi-2nL|\sqrt{-r\gamma_k}}\, erfc\left(\sqrt{\frac{rt}{\lambda_k}} - \sqrt{\frac{-\lambda_k\gamma_k}{t}}\left|\frac{x-\xi}{2}-nL\right|\right) - e^{|x-\xi-2nL|\sqrt{-r\gamma_k}}\, erfc\left(\sqrt{\frac{rt}{\lambda_k}} + \sqrt{\frac{-\lambda_k\gamma_k}{t}}\left|\frac{x-\xi}{2}-nL\right|\right) + \right.$$

$$\left. + e^{-|x+\xi-2nL|\sqrt{-r\gamma_k}}\, erfc\left(\sqrt{\frac{rt}{\lambda_k}} - \sqrt{\frac{-\lambda_k\gamma_k}{t}}\left|\frac{x+\xi}{2}-nL\right|\right) + e^{|x+\xi-2nL|\sqrt{-r\gamma_k}}\, erfc\left(\sqrt{\frac{rt}{\lambda_k}} + \sqrt{\frac{-\lambda_k\gamma_k}{t}}\left|\frac{x+\xi}{2}-nL\right|\right)\right]$$

The first two terms in the sum are independent of time and represent the regime solution. We can write:

$$\Gamma_k^*(x,\xi;t) = \frac{L\lambda_k}{8}\sqrt{-\frac{\gamma_k}{r}}\sum_{n=-\infty}^{\infty}\left[2e^{-|x-\xi-2nL|\sqrt{-r\gamma_k}} - 2e^{-|x+\xi-2nL|\sqrt{-r\gamma_k}} + \right.$$

$$- e^{-|x-\xi-2nL|\sqrt{-r\gamma_k}}\, erfc\left(\sqrt{\frac{rt}{\lambda_k}} - \sqrt{\frac{-\lambda_k\gamma_k}{t}}\left|\frac{x-\xi}{2}-nL\right|\right) - e^{|x-\xi-2nL|\sqrt{-r\gamma_k}}\, erfc\left(\sqrt{\frac{rt}{\lambda_k}} + \sqrt{\frac{-\lambda_k\gamma_k}{t}}\left|\frac{x-\xi}{2}-nL\right|\right) + \tag{4.51}$$

$$\left. + e^{-|x+\xi-2nL|\sqrt{-r\gamma_k}}\, erfc\left(\sqrt{\frac{rt}{\lambda_k}} - \sqrt{\frac{-\lambda_k\gamma_k}{t}}\left|\frac{x+\xi}{2}-nL\right|\right) + e^{|x+\xi-2nL|\sqrt{-r\gamma_k}}\, erfc\left(\sqrt{\frac{rt}{\lambda_k}} + \sqrt{\frac{-\lambda_k\gamma_k}{t}}\left|\frac{x+\xi}{2}-nL\right|\right)\right]$$

It is worth noting that $\lim_{t\to 0}\Gamma_k^*(x,\xi;t) = 0$ and that it is possibile to evaluate in a simple way the regime value of Γ_k^*. We have in fact:

$$\Gamma_k*(x,\xi;\infty)=\int_0^\infty \frac{L}{4}\sqrt{-\frac{\lambda_k\gamma_k}{\pi\tau}}\sum_{n=-\infty}^{\infty}\left[e^{\frac{-r\tau}{\lambda_k}+\frac{\lambda_k\gamma_k}{\tau}\left(\frac{x-\xi}{2}-nL\right)^2}-e^{\frac{-r\tau}{\lambda_k}+\frac{\lambda_k\gamma_k}{\tau}\left(\frac{x+\xi}{2}-nL\right)^2}\right]d\tau=$$

$$=\frac{L}{4}\sqrt{-\frac{\lambda_k\gamma_k}{\pi}}\sum_{n=-\infty}^{\infty}\left[\int_0^\infty \frac{e^{\frac{-r\tau}{\lambda_k}+\frac{\lambda_k\gamma_k}{\tau}\left(\frac{x-\xi}{2}-nL\right)^2}}{\sqrt{\tau}}d\tau-\int_0^\infty \frac{e^{\frac{-r\tau}{\lambda_k}+\frac{\lambda_k\gamma_k}{\tau}\left(\frac{x+\xi}{2}-nL\right)^2}}{\sqrt{\tau}}d\tau\right]=$$

$$=\frac{L}{4}\sqrt{-\frac{\lambda_k\gamma_k}{\pi}}\sum_{n=-\infty}^{\infty}\left[\mathrm{L}_{s=\frac{-r}{\lambda_k}}\left\{\frac{e^{\frac{\lambda_k\gamma_k}{t}\left(\frac{x-\xi}{2}-nL\right)^2}}{\sqrt{t}}\right\}-\mathrm{L}_{s=\frac{-r}{\lambda_k}}\left\{\frac{e^{\frac{\lambda_k\gamma_k}{t}\left(\frac{x+\xi}{2}-nL\right)^2}}{\sqrt{t}}\right\}\right]$$

(4.53)

Considering that $\mathrm{L}_s\left\{\frac{e^{-a/4t}}{\sqrt{t}}\right\}=\sqrt{\frac{\pi}{s}}\;e^{-\sqrt{as}}$ [63], we can write:

$$\Gamma_k*(x,\xi;\infty)=\frac{L}{4}\sqrt{-\frac{\lambda_k\gamma_k}{\pi}}\sum_{n=-\infty}^{\infty}\left[\mathrm{L}_{s=\frac{-r}{\lambda_k}}\left\{\frac{e^{\frac{\lambda_k\gamma_k}{t}\left(\frac{x-\xi}{2}-nL\right)^2}}{\sqrt{t}}\right\}-\mathrm{L}_{s=\frac{-r}{\lambda_k}}\left\{\frac{e^{\frac{\lambda_k\gamma_k}{t}\left(\frac{x+\xi}{2}-nL\right)^2}}{\sqrt{t}}\right\}\right]=$$

$$=\frac{L\lambda_k}{4}\sqrt{-\frac{\gamma_k}{r}}\sum_{n=-\infty}^{\infty}\left[e^{-2\sqrt{-r\gamma_k}\left|\frac{x-\xi}{2}-nL\right|}-e^{-2\sqrt{-r\gamma_k}\left|\frac{x+\xi}{2}-nL\right|}\right]$$

(4.54)

As we have $0 < x < L$ and $0 < \xi < L$, decomposing the series in positive and negative values, we get:

$$\Gamma_k^*(x,\xi;\infty)=\frac{L\lambda_k}{4}\sqrt{-\frac{\gamma_k}{r}}\left\{\sum_{n=-\infty}^{-1}e^{-2\sqrt{-r\gamma_k}\left(\frac{x-\xi}{2}-nL\right)}-\sum_{n=-\infty}^{-1}e^{-2\sqrt{-r\gamma_k}\left(\frac{x+\xi}{2}-nL\right)}\right.$$

$$\left.+e^{-2\sqrt{-r\gamma_k}\left|\frac{x-\xi}{2}\right|}-e^{-2\sqrt{-r\gamma_k}\left(\frac{x+\xi}{2}\right)}+\sum_{n=1}^{\infty}e^{2\sqrt{-r\gamma_k}\left(\frac{x-\xi}{2}-nL\right)}-\sum_{n=1}^{\infty}e^{2\sqrt{-r\gamma_k}\left(\frac{x+\xi}{2}-nL\right)}\right\}=$$

$$=\frac{L\lambda_k}{4}\sqrt{-\frac{\gamma_k}{r}}\left\{e^{-(x-\xi)\sqrt{-r\gamma_k}}\sum_{n=1}^{\infty}\left(e^{-2L\sqrt{-r\gamma_k}}\right)^n-e^{-(x+\xi)\sqrt{-r\gamma_k}}\sum_{n=1}^{\infty}\left(e^{-2L\sqrt{-r\gamma_k}}\right)^n\right.$$

$$\left.+e^{-|x-\xi|\sqrt{-r\gamma_k}}-e^{-(x+\xi)\sqrt{-r\gamma_k}}+e^{-(x-\xi)\sqrt{-r\gamma_k}}\sum_{n=1}^{\infty}\left(e^{-2L\sqrt{-r\gamma_k}}\right)^n-e^{-(x+\xi)\sqrt{-r\gamma_k}}\sum_{n=1}^{\infty}\left(e^{-2L\sqrt{-r\gamma_k}}\right)^n\right\}=$$

$$=\frac{L\lambda_k}{2}\sqrt{-\frac{\gamma_k}{r}}\left\{\frac{\cosh(x-\xi)\sqrt{-r\gamma_k}-\cosh(x+\xi)\sqrt{-r\gamma_k}}{e^{2L\sqrt{-r\gamma_k}}-1}+\frac{e^{-|x-\xi|\sqrt{-r\gamma_k}}-e^{-(x+\xi)\sqrt{-r\gamma_k}}}{2}\right\}$$

(4.55)

where we have used the formula: $\sum_{n=1}^{\infty}q^n=\frac{1}{\frac{1}{q}-1}$. Finally, we can write:

$$\boxed{\Gamma_k^*(x,\xi;\infty)=L\lambda_k\sqrt{-\frac{\gamma_k}{r}}\left\{\frac{e^{-|x-\xi|\sqrt{-r\gamma_k}}-e^{-(x+\xi)\sqrt{-r\gamma_k}}}{4}-\frac{\sinh\left(x\sqrt{-r\gamma_k}\right)\sinh\left(\xi\sqrt{-r\gamma_k}\right)}{e^{2L\sqrt{-r\gamma_k}}-1}\right\}}$$

(4.56)

These regime values (4.56) can be directly inserted into eq.(4.21) obtaining:

$$\mathbf{K}^*(x,\xi,\infty)=\sum_{\substack{k=-(p-1)\\k\neq 0}}^{p}\Gamma^*{}_k(x,\xi,\infty)\frac{\mathbf{b}_k\mathbf{b}_k^T}{\lambda_k}$$

(4.57)

The regime solution is finally given by (4.22), with the appropriate kernel **K***:

$$\mathbf{i}(x,t)=\frac{i_{op}(t)}{\sqrt{N}}\mathbf{b}_0+\frac{2}{L}\int_0^L d\xi\ \mathbf{K}^*(x,\xi,\infty)\,\mathbf{v}^{ext}(\xi)$$

(4.58)

We have checked the regime solution for the evaluation of BICC's in a 16 strand Rutherford cable, for the same case study reported in Figs. 4.1. The comparison bewteen analytical and numerical results is shown in Fig. 4.2. The two curves are not distinguishable in both the regimes studied, due to a very good agreement with the numerical results relative to the steady state currents obtained at the end of the long transients.

Fig. 4.2 Comparison between analytical and numerical solution: regime solution of Boundary Induced Coupling Currents in a 16 strands Rutherford cable exposed to a step-like spatial distribution of the magnetic flux density perpendicular t[illegible]a for the simulations are reported in [illegible]